PROCESS ANALYSIS AND ASPEN PLUS SIMULATION OF NUCLEAR-BASED HYDROGEN PRODUCTION WITH A COPPER-CHLORINE CYCLE

by

Cletus Chukwu

A Thesis Submitted in Partial Fulfillment
of the Requirements for the Degree of

Master of Applied Science

in

The Faculty of Engineering and Applied Science

Mechanical Engineering Program

University of Ontario Institute of Technology

August, 2008

CERTIFICATE OF APPROVAL

Submitted by: Cletus Chukwu Student #: 100333501
First Name, Last Name

In partial fulfillment of the requirements for the degree of:

Master of Applied Science in Mechanical Engineering
Degree Name in full (e.g. Master of Applied Science) Name of Program

Date of Defense (if applicable): _____

Thesis Title:
Process Analysis and Aspen Plus Simulation of Nuclear-Based Hydrogen Production with a Copper-Chlorine Cycle

The undersigned certify that they recommend this thesis to the Office of Graduate Studies for acceptance:

Chair of Examining Committee	Signature	Date (yyyy/mm/dd)
External Examiner	Signature	Date (yyyy/mm/dd)
Member of Examining Committee	Signature	Date (yyyy/mm/dd)
Member of Examining Committee	Signature	Date (yyyy/mm/dd)

As research supervisor for the above student, I certify that I have read the following defended thesis, have approved changes required by the final examiners, and recommend it to the Office of Graduate Studies for acceptance:

Name of Research Supervisor	Signature of Research Supervisor	Date (yyyy/mm/dd)
Name of Research Co-Supervisor	Signature of Research Co-Supervisor	Date (yyyy/mm/dd)

ABSTRACT

Thermochemical processes for hydrogen production driven by nuclear energy are promising alternatives to existing technologies for large-scale commercial production of hydrogen, without dependence on fossil fuels. In the Copper-Chlorine (Cu-Cl) cycle, water is decomposed in a sequence of intermediate processes with a net input of water and heat, while hydrogen and oxygen gases are generated as the products. The Super Critical Water-cooled Reactor (SCWR) has been identified as a promising source of heat for these processes. In this thesis, the process analysis and simulation models are developed using the Aspen Plus^{TM} chemical process simulation package, based on experimental work conducted at the Argonne National Laboratory (ANL) and Atomic Energy of Canada Limited (AECL). A successful simulation is performed with an Electrolyte Non Random Two Liquid (ElecNRTL) model of Aspen Plus. The efficiency of the cycle based on three and four step process routes is examined in this thesis. The thermal efficiency of the four step thermochemical process is calculated as 45%, while the three step hybrid thermochemical cycle is 42%, based on the lower heating value (LHV) of hydrogen. Sensitivity analyses are performed to study the effects of various operating parameters on the efficiency, yield, and thermodynamic properties. Possible efficiency improvements are discussed. The results will assist the development of a lab-scale cycle which is currently being conducted at the University of Ontario Institute of Technology (UOIT), in collaboration with its partners.

ACKNOWLEDGMENTS

I wish to express my profound gratitude to my co-supervisors; Dr Greg Naterer and Dr Marc Rosen. I sincerely appreciate their financial support, advice, and guidance throughout my graduate study at UOIT. Their contributions to my research are invaluable.

I would like to acknowledge the financial support provided for this research by the Ontario Research Excellence Fund, Atomic Energy of Canada Limited, the Natural Sciences and Engineering Research Council of Canada, and the Province of Ontario's Ministry of Research and Innovation. I am deeply grateful to Dr Michele Lewis for her assistance during this thesis research. She provided me with updates in hydrogen production with Cu-Cl cycle research at Argonne National Laboratory and guided me in process simulations of these cycles. I also wish to thank the faculty and staff of the Faculty of Engineering and Applied Science at UOIT for providing me with quality education and creating an enabling environment during my research that led to this thesis.

I extend my heartfelt thanks to Dr Emmanuel Ogedengbe and family, Mr Lamide Olubuyide and family, and Dr Dayo Adeeko and family for their moral and spiritual support. My special appreciation goes to Mr Victor Odili, Mr Tony Crosta, and Ms Emma Klingstedt for being good friends.

Lastly I wish to express my indebtedness to my family for their support throughout my study period. To my mom, Mrs Esther Chukwu for her love and care. My story will never be complete without mentioning the contributions of my brother Mr Larry O. C. Chukwu in my life. He gave me the opportunity to attend university and also

orchestrated my studying overseas. I wish to express my deepest gratitude to my siblings; Pastor Sunday Chukwu, Mr Cajethan Chukwu, Ms Chijioke Chukwu, Mr Nnamdi Chukwu, Ms Christiana Chukwu, and Mrs. Grace Okoli. Finally to my cousin brother, Mr Nicholas Uzor, thank you for being there for me always.

TABLE OF CONTENTS

LIST OF FIGURES

LIST OF TABLES

NOMENCLATURE

Roman Letters	Definitions
a	Equation of state energy parameter
b	Equation of state co-volume
C_p	Specific Heat capacity
f	Fugacity
G	Gibbs energy
H	Enthalpy
k	Equation of state binary parameter
K	Chemical equilibrium constant
n	Mole number
p	Pressure
R	Universal gas constant
S	Entropy
T	Temperature
V	Volume
x,y	Mole fraction
Z	Compressibility factor

Greek Letters	Definitions
γ	Activity coefficient

φ	Fugacity coefficient
μ	Thermodynamic potential

Superscripts	**Definitions**
c	Combustion property
i	Component index
f	Formation property
m	Molar property
vap	Vaporization property
r	Reaction property
ref	Reference state property
*	Pure component property, asymmetric convention
∞	At infinite dilution
a	Apparent property
E	Excess property
ig	Ideal gas property
l	Liquid property
s	Solid property
t	True property
v	Vapour property

CHAPTER 1

INTRODUCTION

1.1 Background

As many think world oil and gas reserves are approaching a peak production capacity and environmental concerns such as climatic change increase, there is an urgent need to develop sustainable energy sources that will power the economies of the world. Hydrogen is a promising and clean energy carrier. It can help facilitate the use of alternative resources to meet present and future energy requirements of society and industry. Hydrogen has several inherent advantages compared to other energy carriers, due to its energy density and environmentally benign nature. At present, tens of millions of tons of bulk industrial hydrogen are produced annually by steam-methane reforming (SMR), in a market valued estimated at over $300 billion worldwide [1].

The SMR process involves methane reacting with steam at 750-800°C [2] to produce a synthesis gas, which is a mixture primarily made up of hydrogen and carbon monoxide. In the second step, a water gas shift reaction, the carbon monoxide produced in the first reaction is reacted with steam over a catalyst to form hydrogen and carbon dioxide. This process occurs in two stages, consisting of a high temperature shift at 350ºC and a low temperature shift at about 210ºC. There are several advantages associated with steam-methane reforming. The SMR process is an efficient and widely used process for hydrogen production. The efficiency of SMR is about 65% to 75%, among the highest of

commercially available production methods. Natural gas is relatively easy to handle, and it is a feedstock with a relatively high hydrogen-to-carbon ratio.

The cost of hydrogen produced by SMR is strongly dependant on natural gas prices. It is the least expensive among bulk hydrogen production technologies at present. There is also a well-developed natural gas infrastructure already in existence. However, SMR produces about eleven tons of carbon dioxide for every ton of hydrogen produced [1], so it generates large amount of greenhouse gases that many think lead to global warming.

To avoid emission of CO_2 into the atmosphere, it can be concentrated, captured, and sequestered. Sequestration technologies are relatively new and there is no demonstrated evidence to prove that these technologies will be commercially successful. Sequestration in oceans is controversial because of the possible adverse impact on the aquatic environment, due to reduction of ocean water pH.

SMR is a mature technology, which makes it a practical beginning in the transition to a hydrogen energy economy. But a problem with SMR is it operates near its theoretical limits; the hydrogen produced is still expensive compared to the cost targets for producing hydrogen for future automobiles and other applications [2]. Although it has high efficiency and a well-established process, in the future it may not be economical due to escalating costs of natural gas.

Rather than natural gas as the feedstock for hydrogen, water consists of hydrogen and oxygen bonded together, which can be decomposed to produce hydrogen. Direct thermal decomposition of water into hydrogen and oxygen at present is infeasible because of material requirements to withstand high temperatures and pressures over

2000^{o}C and up to 30 bars, respectively, and also the problem of separation of constituent gases to avoid recombination among other drawbacks. Electrolytic hydrogen production from electricity is a commercial technology. Hydrogen is produced via electrolysis by passing electricity through two electrodes in water. The water molecule is split and it produces oxygen at the anode and hydrogen at the cathode.

There are different types of industrial electrolysis units presently used. One type involves an aqueous solution of potassium hydroxide, used for its high conductivity [3]. These types of electrolysis units are called alkaline electrolyzers. They can be either unipolar or bipolar. The unipolar electrolyzer resembles a tank and it has electrodes connected in parallel. A membrane is placed between the cathode and anode, which separates the hydrogen and oxygen as the gases are produced, while allowing the transfer of ions. The bipolar design resembles a filter press. Electrolysis cells are connected in series, and hydrogen is produced on one side of the cell, with oxygen on the other. A membrane separates the electrodes.

Another type of electrolysis unit is a Solid Polymer Electrolyte (SPE) electrolyzer. These systems are also called Proton Exchange Membrane (PEM) electrolyzers. In this unit, the electrolyte is a solid ion conducting membrane, as opposed to the aqueous solution in the alkaline electrolyzers. The membrane allows the hydrogen ion to transfer from the anode side of the membrane to the cathode side, where it forms hydrogen. The SPE membrane also serves to separate the hydrogen and oxygen gases. Oxygen is produced at the anode on one side of the membrane and hydrogen is produced on the opposite side of the membrane.

Regardless of the technology, the overall electrolysis reaction is the same:

$$H_2O(l) \rightarrow \frac{1}{2} O_2(g) + H_2(g) \quad (1.1)$$

The reaction at each electrode differs between PEM and alkaline systems. In a PEM system, the reactions at the electrodes are:

$$2 H^+ + 2e^- \rightarrow H_2(g) \text{ (PEM Hydrogen Production at the Cathode)} \quad (1.2)$$

$$H_2O(l) \rightarrow \frac{1}{2} O_2(g) + 2 H^+ + 2e^- \text{ (PEM Oxygen Production at the Anode)} \quad (1.3)$$

In an alkaline system, the reactions at each electrode are:

$$2 H_2O(g) + 2e^- \rightarrow H_2(g) + 2OH^- \text{ (Alkaline Hydrogen Production at the Cathode)} \quad (1.4)$$

$$2OH^- \rightarrow \frac{1}{2} O_2(g) + H_2O(l) + 2e^- \text{ (Alkaline Oxygen Production at the Anode)} \quad (1.5)$$

These processes have high conversion efficiency, but the overall system including the production of electricity used in electrolysis has an efficiency below 30%. As a result, only a small fraction of worldwide hydrogen production (about 2-3%) is attributed to electrolysis, generally only when high purity hydrogen is needed.

1.2 Literature Survey

In Canada, hydrogen has an increasingly significant role in the future overall energy mix of the country, not only as a transportation fuel but also for the oil and gas industry. For instance, hydrogen is heavily used (about a million tons per year) in the Alberta oil sands for upgrading bitumen to synthetic crude oil. Hydrogen is also the fuel of choice for fuel cells, which are expected to become increasingly important in the automotive sector.

Due to the shortcomings of present technology (i.e., electrolysis and direct thermal splitting of water to produce hydrogen) several alternative processes have been identified, including efforts to split water at lower temperatures. The net inputs for such processes are water and heat, while hydrogen and oxygen are produced, and other components are recycled. There are no emissions to the environment. These processes usually require lower temperatures compared to direct water thermolysis.

Steinfeld [4], Tamaura et al. [5] and Abanades et al. [6] have proposed solar-driven thermochemical processes for hydrogen production. These processes use a solar concentrator to absorb high temperature heat, which is utilized in various steps of thermochemical hydrogen production, by supplying the required heat at temperatures up to 800^{o}C. The major drawbacks are the intermittent and unpredictable nature of available sunlight and requirements for heat storage.

Many researchers have examined nuclear power as a promising steady supply of high-temperature heat in large capacities. Although many analyzed nuclear energy as the source of process heat for the reactions, other alternatives are also being investigated. Mathias and Brown [7], Wu and Onuki [8] and Brown et al. [9] have investigated the Sulfur-Iodine cycle. This involves a 3-step thermochemical process of sulfuric acid generation and decomposition, chemical recycling, and hydrogen iodide formation and decomposition. The first and last steps generate oxygen and hydrogen, respectively. All of the individual steps have been experimentally demonstrated. One of the steps in the cycle requires heat at temperatures up to 850^{o}C, which would be provided by the next generation of high temperature nuclear reactors.

Ryland et al. [10] examined high temperature hybrid steam electrolysis with electrical and thermal energy, using solid oxide electrolytic cells. This setup can exchange free energy of the reaction with electrical energy at constant temperature and pressure. Ryland et al. [10] have shown that electrolysis of water at elevated temperatures reduces the electrical energy requirement and increases the thermal efficiency of the cycle. This process requires heat at a temperature of about 850^{o}C, which is expected to be provided from either high temperature helium cooled reactor, or the next generation CANDU reactors with an external heat supplement. The process has a heat to hydrogen efficiency of about 34%. Gooding [11] has proposed a hybrid chlorine cycle that involves a reverse deacon reaction of chlorine and water, and subsequent electrolysis of the hydrochloric acid. This will require a maximum temperature of about 850^{o}C, which again would be provided by high temperature gas cooled reactors. The electrolysis step is the limiting process requiring a cell voltage up to 2.0 Volts and about 385 kJ of electrical energy. The thermal efficiency for this cycle is about 30%.

Rosen [12] performed a thermodynamic analysis of hydrogen production by thermochemical water decomposition using the Ispra Mark-10 cycle. Granovskii et al. [13] conducted a thermodynamic analysis of a chemical heat pump to link a Super Critical Water-cooled Reactor (SCWR) and a thermochemical water splitting cycle for hydrogen production. This process will convert synthesis gas to methane through an exothermic reaction and at lower temperature convert methane back to hydrogen and carbon dioxide (synthesis gas) in an endothermic reaction. These two reactions proceed simultaneously in a water shift reaction. The chemical heat pump is expected to absorb heat at a low temperature and release it at a higher temperature, thereby increasing the

temperature of the SCWR steam high enough to be deployed for thermochemical hydrogen production. The cycle requires a higher temperature than produced by the SCWR. This additional modification can increase the thermal efficiency of the cycle up to 2%. Rosen and Scott [14] have performed a comparative efficiency assessment for different hydrogen production processes and Yildiz and Kazimi [15] have investigated the efficiency of hydrogen production systems using nuclear energy technologies.

Teo et al. [16] and Sakurai et al. [17] have studied a UT-3 cycle, developed at the University of Tokyo by Kameyama and Yoshida [18]. This cycle involves a gas-solid reaction process, requiring four steps with calcium, bromine and iron. This process requires heat at up to 750^{o}C in one of the steps. It will be linked with the proposed high temperature gas cooled reactors.

The University of Ontario Institute of Technology (UOIT), Atomic Energy of Canada Ltd. (AECL), Argonne National Laboratory (ANL), partner universities across Ontario and abroad, and other collaborators are investigating a low temperature cycle for thermochemical production of hydrogen, based on the copper-chlorine (Cu-Cl) cycle. Two alternative routes in this process are being investigated: one requires a four-step process and another requires a three-step process. This cycle has numerous advantages over other thermochemical cycles, including the requirement for lower temperatures, lower cost materials, and ability to utilize waste heat. The highest temperature needed by the copper-chlorine thermochemical cycle is about 550^{o}C.

Several past studies have examined the copper-chlorine cycle. Lewis et al. [19-24] have investigated the four-step process at ANL proposed by Carty et al. [25] These steps include an exothermic hydrogen generation reaction, a hydrolysis reaction, an oxy-

decomposition reaction, and an electrowinning process. There is also an intermediate spray drying process in this cycle. ANL has experimentally verified with laboratory proof-of-principle demonstrations all of the steps [19-23] and a UOIT-led team is currently developing a lab-scale demonstration at higher flow capacities [26-28]. AECL, ANL, UOIT, and other partners are also investigating a hybrid process route that will combine two of the four steps [29-31]. This would eliminate solids handling, as the hydrogen would be generated by an electrolysis process. Past AECL studies have successfully combined the first two steps of the cycle in a high-temperature electrolytic process, which eliminates solids handling and drying of copper powder, where particle size is crucial. Proof-of-principle demonstrations have been made at a small scale [29]. AECL is also investigating the membrane material, which is critical for this hybrid process route.

1.3 Objectives of Thesis

This thesis aims to predict thermal efficiencies of two variations of the Cu-Cl cycle. By analyzing different scenarios and configurations, high efficiency and realistic layout can be established. The second chapter provides a detailed explanation of thermochemical processes of water decomposition. In the third chapter, thermodynamic models and property calculations are presented for the Cu-Cl cycle. Then process simulations for different configurations are outlined in chapter 4. Finally, conclusions and recommendations for future research are presented in chapters 5 and 6, respectively.

CHAPTER 2

THERMOCHEMICAL PROCESS OF HYDROGEN PRODUCTION

2.1 Overview of Thermochemical Cycles

Hydrogen can be produced by thermochemical water-splitting in a series of reactions with a net input of heat and water, and net output products of hydrogen and oxygen. The temperature requirement for direct thermal decomposition of water is over 2000^{o}C, to obtain a significant hydrogen conversion yield. Even at this high temperature, the hydrogen yield from water thermolysis is only about 10% [32]. A thermochemical cycle to split water can operate at much lower temperatures, with the same overall water decomposition (separation of hydrogen and oxygen is obtained, since they are produced in separate reactions). In a hybrid process, electricity is used, in addition to heat for the processes. The other chemicals and reagents are recycled in a closed loop. Heat can be supplied by nuclear energy, using an advanced high-temperature nuclear reactor, or other suitable sources of heat. Thermochemical water splitting using nuclear energy is believed by many to be environmentally benign, since no fossil fuels are required.

Although several hundred thermochemical cycles have been identified [25], research demonstrating technical feasibility and viability has been reported for only a few cycles. A selection of the most promising cycles was done based on certain factors that affect the feasibility of commercial hydrogen production. For this commercial viability, the following screening criteria were adopted based on a study by Abanades et al. [33]

(i) Process temperature

Cycles that require a heat input temperature in any of the steps that exceed 900°C are discarded. Not only will it be very difficult to achieve this high temperature for a commercial application, there is a serious challenge with materials and separation of chemicals above this temperature. Based on this criterion [33], the following metal oxide cycles were eliminated:

- Mo/MoO_2 cycle

$$MoO_2(s) \rightarrow Mo(s) + O_2(g) \qquad (3713^oC) \qquad (2.1)$$

$$Mo(s) + 2H_2O(g) \rightarrow MoO_2(s) + 2H_2(g) \qquad (1543^oC) \qquad (2.2)$$

- SiO_2/SiO cycle

$$SiO_2(s) \rightarrow SiO(g) + \frac{1}{2}O_2(g) \qquad (2977^oC) \qquad (2.3)$$

$$SiO(g) + H_2O(g) \rightarrow SiO_2(s) + H_2(g) \qquad (2656^oC) \qquad (2.4)$$

- W/WO_3 cycle

$$WO_3(s) \rightarrow W(s) + \frac{3}{2}O_2(g) \qquad (3910^oC) \qquad (2.5)$$

$$W(s) + 3H_2O(g) \rightarrow WO_3(s) + 3H_2(g) \qquad (884^oC) \qquad (2.6)$$

(ii) Process safety and environmental impact

Some process cycles are viable, but discarded due to the toxicity or highly corrosive nature of the components [33]. These cycles are potentially dangerous to the environment and considered not suitable for further investigation. Such cycles that contain cadmium, mercury and bromine compounds at high ratios are grouped in this category. Although some of these cycles were identified to be feasible and viable at lower

temperatures, they were eliminated based on this criterion. These include the following cycles.

- HgO/Hg cycle

$$Hg(g) + H_2O(g) \rightarrow HgO(s) + H_2(g) \quad (360^oC) \quad (2.7)$$

$$HgO(s) \rightarrow Hg(s) + \frac{1}{2}O_2(g) \quad (600^oC) \quad (2.8)$$

- CdO/Cd cycle

$$Cd(s) + H_2O(aq) \rightarrow CdO(s) + H_2(g) \quad (25^oC) \quad (2.9)$$

$$CdO(s) \rightarrow Cd(s) + \frac{1}{2}O_2(g) \quad (1400^oC) \quad (2.10)$$

- $FeBr_2$ cycle

$$3FeBr_2(l) + 4H_2O(g) \rightarrow Fe_3O_4(s) + 6HBr(g) + H_2(g) \quad (850^oC) \quad (2.11)$$

$$Fe_3O_4(s) + 8HBr(g) \rightarrow 3FeBr_2(s) + 4H_2O(g) + Br_2(g) \quad (250^oC) \quad (2.12)$$

$$H_2O(g) + Br_2(g) \rightarrow 2HBr(g) + \frac{1}{2}O_2(g) \quad (650^oC) \quad (2.13)$$

- Al_2O_3 cycle

$$2Al_2O_3(s) + 6Br_2(g) \rightarrow 4AlBr_3(s) + 3O_2(g) \quad (700^oC) \quad (2.14)$$

$$4AlBr_3(s) + 6WO_3(s) \rightarrow 2Al_2O_3(s) + 6Br_2(g) + 6WO_2(s) \quad (1500^oC) \quad (2.15)$$

$$6WO_2(s) + 6H_2O(g) \rightarrow 6H_2(g) + 6WO_3(s) \quad (150^oC) \quad (2.16)$$

- Sc_2O_3 cycle

$$Sc_2O_3(s) + 3Br_2(g) \rightarrow 2ScBr_3(s) + \frac{3}{2}O_2(s) \quad (400^oC) \quad (2.17)$$

$$2ScBr_3(s) + 3WO_3(s) \rightarrow Sc_2O_3(s) + 3Br_2(g) + 3WO_2(s) \quad (1600^oC) \quad (2.18)$$

$$3WO_2(s) + 3H_2O(g) \rightarrow 3WO_3(s) + 3H_2(g) \quad (150^oC) \quad (2.19)$$

- KOH cycle

$$2KOH(aq) + 2K(s) \rightarrow 2K_2O(s) + H_2(g) \qquad (750^oC) \qquad (2.20)$$

$$2K_2O(s) \rightarrow K_2O_2(s) + 2K(s) \qquad (825^oC) \qquad (2.21)$$

$$K_2O_2(s) + H_2O(g) \rightarrow 2KOH(aq) + \frac{1}{2}O_2(g) \qquad (125^oC) \qquad (2.22)$$

(iii) Process complexity

Some process cycles seem thermodynamically promising, but were eliminated due to the high complexity of one or more process steps [33]. Processes that involve a number of difficult and complicated gas separation steps were eliminated. These cycles are considered economically infeasible due to lack of suitable technologies for membrane separation. Also, cycles that include carbon compounds were eliminated, due to the problem of separation to obtain pure hydrogen, free of carbon contamination. These include the following cycles.

- CO/CO_2 cycle

$$CO(g) + H_2O(g) \rightarrow CO_2(g) + H_2(g) \qquad (700^oC) \qquad (2.23)$$

$$CO_2(g) \rightarrow CO(g) + \frac{1}{2}O_2(g) \qquad (1700^oC) \qquad (2.24)$$

- Schulten C/S cycle

$$CO(g) + H_2O(g) \rightarrow CO_2(g) + H_2(g) \qquad (550^oC) \qquad (2.25)$$

$$CO_2(g) + H_2O(g) + SO_2(g) \rightarrow CO(g) + H_2SO_4(aq) \qquad (500^oC) \qquad (2.26)$$

$$H_2SO_4(aq) \rightarrow H_2O(g) + SO_2(g) + \frac{1}{2}O_2(g) \qquad (900^oC) \qquad (2.27)$$

- Carbon-Iron Cycle

$$C(s) + H_2O(g) \rightarrow CO(g) + H_2(g) \quad (700^oC) \quad (2.28)$$

$$CO(g) + 2Fe_3O_4(s) \rightarrow C(s) + 3Fe_2O_3(s) \quad (250^oC) \quad (2.29)$$

$$3Fe_2O_3(s) \rightarrow 2Fe_3O_4(s) + \frac{1}{2}O_2(g) \quad (1400^oC) \quad (2.30)$$

- Hitachi cycle

$$2NH_4I(s) \rightarrow 2NH_3(g) + I_2(g) + H_2(g) \quad (500^oC) \quad (2.31)$$

$$2NaI(s) + 2NH_3(g) + CO_2(g) + H_2O(aq) \rightarrow Na_2CO_3(aq) + 2NH_4I(s) \quad (25^oC) \quad (2.32)$$

$$Na_2CO_3(aq) + I_2(g) \rightarrow 2NaI(s) + CO_2(g) + \frac{1}{2}O_2(g) \quad (700^oC) \quad (2.33)$$

- Osaka 75 cycle

$$2NH_4I(s) \rightarrow 2NH_3(g) + I_2(g) + H_2(g) \quad (500^oC) \quad (2.34)$$

$$BaCO_3(s) + I_2(g) \rightarrow BaI_2(s) + CO_2(g) + \frac{1}{2}O_2(g) \quad (800^oC) \quad (2.35)$$

$$BaI_2(s) + 2NH_3(g) + CO_2(g) + H_2O(aq) \rightarrow BaCO_3(s) + 2NH_4I(s) \quad (50^oC) \quad (2.36)$$

- Cu-I-N cycle

$$2NH_4I(s) \rightarrow 2NH_3(g) + I_2(g) + H_2(g) \quad (500^oC) \quad (2.37)$$

$$2CuO(s) + I_2(g) \rightarrow 2CuI(s) + \frac{1}{2}O_2(g) \quad (850^oC) \quad (2.38)$$

$$2CuI(s) + NH_3(g) + H_2O(g) \rightarrow 2CuO(s) + 2NH_4I(s) \quad (200^oC) \quad (2.39)$$

- Miura cycle

$$Sb_2O_3(s) + 2I_2(g) + 2H_2O(aq) \rightarrow Sb_2O_5(s) + 4HI(aq) \quad (20^oC) \quad (2.40)$$

$$4HI(aq) \rightarrow 2I_2(g) + 2H_2(g) \qquad (550^oC) \qquad (2.41)$$

$$Sb_2O_5(s) \rightarrow Sb_2O_3(s) + 4O_2(g) \qquad (1000^oC) \qquad (2.42)$$

- Yokohama Mark 3

$$2FeSO_4(s) + I_2(g) + 2H_2O(aq) \rightarrow 2Fe(OH)SO_4(aq) + 2HI(aq) \qquad (20^oC) \qquad (2.43)$$

$$2HI(aq) \rightarrow I_2(g) + H_2(g) \qquad (450^oC) \qquad (2.44)$$

$$2Fe(OH)SO_4(aq) \rightarrow 2FeSO_4(s) + H_2O(aq) + \frac{1}{2}O_2(g) \qquad (100^oC) \qquad (2.45)$$

(iv) Process economics

These are process cycles that seem feasible even with a lower temperature requirement, but were discarded due to the scarcity of components [33]. These cycles contain elements that are not abundant in the crust of the earth, the oceans, or the atmosphere. The required ratio of the reactants to hydrogen produced would not be practically feasible, so they are eliminated. Usually the elements are very heavy, which hampers transfer of solids. The cycles included are listed below.

- Eu-Sr Cycle

$$2EuO(s) + H_2O(aq) \rightarrow Eu_2O_3(aq) + H_2(g) \qquad (20^oC) \qquad (2.46)$$

$$I_2(g) + SrO(s) \rightarrow SrI_2(s) + \frac{1}{2}O_2(g) \qquad (227^oC) \qquad (2.47)$$

$$Eu_2O_3(s) + SrI_2(s) \rightarrow 2EuO(s) + I_2(g) + SrO(s) \qquad (700^oC) \qquad (2.48)$$

- Mg-I-U cycle

$$I_2 + Mg(OH)_2(s) + U_3O_8(s) \rightarrow MgI_2(s) + 3UO_3(s) + H_2O(aq) \qquad (20^oC) \qquad (2.49)$$

$$MgI_2(s) + H_2O(g) \rightarrow Mg(OH)_2(s) + I_2(g) + H_2(g) \quad (227^oC) \quad (2.50)$$

$$3UO_3(s) \rightarrow U_3O_8(s) + \frac{1}{2}O_2(g) \quad (700^oC) \quad (2.51)$$

- Sr-U cycle

$$Sr_3U_2O_8(s) + 3Sr(OH)_2(aq) \rightarrow 2Sr_3UO_6(s) + H_2(g) + 2H_2O\ (g) \quad (600^oC) \quad (2.52)$$

$$2Sr_3UO_6(s) + 3H_2O(aq) \rightarrow Sr_3U_2O_9(s) + 3Sr(OH)_2(aq) \quad (90^oC) \quad (2.53)$$

$$Sr_3U_2O_9(s) + 3H_2O(g) \rightarrow + Sr_3U_2O_8(s) + 2O_2(g) + 3H_2 \quad (600^oC) \quad (2.54)$$

Using the previous criteria and others [33], the number of cycles for consideration was reduced. In previous studies, the thermochemical process evaluation and screening were generally conducted with respect to a linkage with an advanced high-temperature nuclear reactor such as a SCWR, a helium gas cooled reactor, or solar energy as the primary energy source. This thesis will focus on those cycles that can derive the source of heat from nuclear energy only. The maximum cycle temperature for an advanced high-temperature nuclear reactor is about 850^{o}C. Hence, the range selected for the optimum maximum temperature was 550–850^{o}C. Processes requiring higher temperatures than available from nuclear power plants were not considered.

Three cycles for generation of hydrogen using nuclear energy remained after others were eliminated based on the previous selection criteria. These cycles are the S-I cycle [7-9], the UT-3 [16-18] and the Cu-Cl cycle [19-31]. These three cycles have several advantages, due to their ability to be linked with the next generation of high temperature nuclear power plants.

2.2 Sulfur-Iodine (S-I) Cycle

The S-I cycle consists of the following three main steps.

$$H_2SO_4(aq) \rightarrow SO_2(g) + H_2O(g) + \frac{1}{2}O_2(g) \qquad (850^oC) \qquad (2.55)$$

$$I_2(g) + SO_2(g) + 2H_2O(g) \rightarrow 2HI(s) + H_2SO_4(aq) \qquad (120^oC) \qquad (2.56)$$

$$2HI(s) \rightarrow I_2(g) + H_2(g) \qquad (400^oC) \qquad (2.57)$$

The first step of the cycle involves sulfuric acid decomposition. It is an endothermic reaction at about 850^{o}C; this step also generates oxygen gas. The second step involves recycling of sulfuric acid and hydrogen iodide, also called a Bunsen reaction. This reaction is exothermic at about 120^{o}C. The final step is the generation of hydrogen through hydrogen iodide decomposition. This reaction step occurs at about 400^{o}C.

This cycle has a thermal efficiency of about 47% and potentially up to 60% with co-generation of hydrogen and electricity [34]. The process is proven at a laboratory scale. An integrated cycle for large-scale production is complicated due to heat and material requirements, and the presence of fuming sulfuric acid. For example, the Bunsen reaction step poses challenges in terms of separation of the mixture constituents. A distillation process would result in a reverse reaction between sulfuric acid and hydrogen iodide. Also hydrogen iodide/iodine/water forms an azeotropic mixture in the separation. The processing of hydrogen iodide is also problematic due to hydrogen iodide binding with iodine in a poly-iodine type, for which it is difficult to break the linkages. Another alternative for separating the sulfur iodine is an electrodialysis concentration of hydrogen

iodide/iodine/water mixture, and a subsequent decomposition of hydrogen iodide in a membrane reactor. The following side reactions are also observed in this cycle.

- Sulfur formation

$$6HI(s) + H_2SO_4(aq) \rightarrow 3I_2(g) + S(s) + 4H_2O(g) \quad (2.59)$$

- Hydrogen Sulfide formation

$$8HI(s) + H_2SO_4(aq) \rightarrow 4I_2(g) + H_2S(g) + 4H_2O(g) \quad (2.60)$$

A schematic of the S-I cycle, identifying all process steps, is shown in figure 1, while the process cycle with the Gibbs free energy and enthalpy of reactions are shown in figure 2.

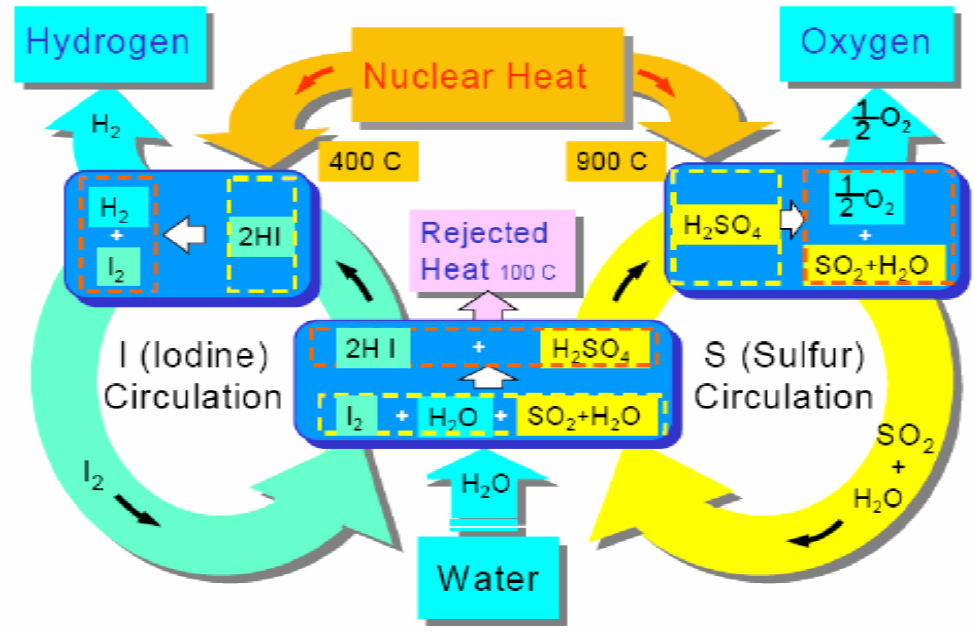

Figure 1: Sulfur-Iodine cycle (Ref. [7]).

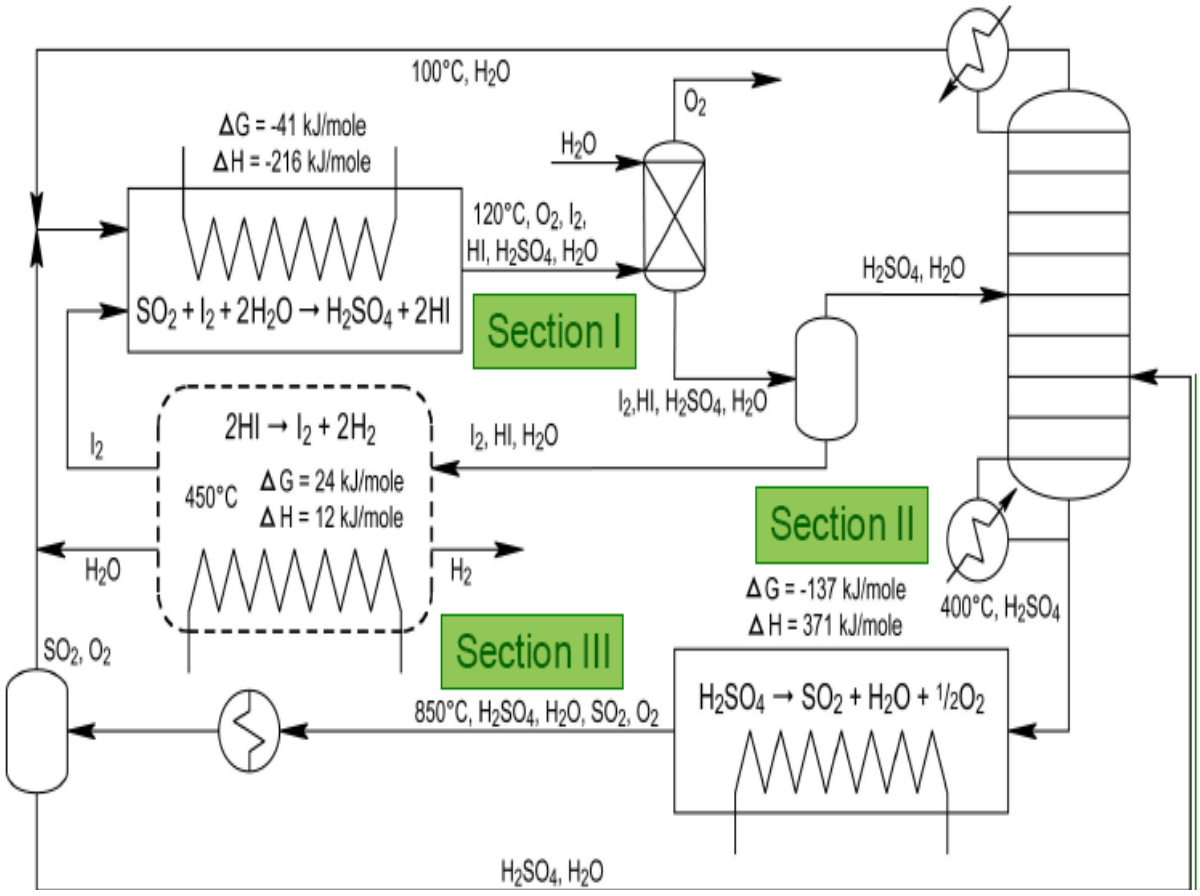

Figure 2: Sulfur-Iodine thermodynamic cycle (Ref. [7]).

Suppiah et al. [34] have proposed a different alternative, through the use of electrical energy to supplement the heat. This would allow the cycle to be linked with the next generation nuclear power plants. They proposed the decomposition of sulfuric acid using electrical energy through electro-resistive heating in the presence of a ferric oxide catalyst. Past experimental data on this method using a platinum based catalyst have yielded 100% conversion. Platinum supported on titanium oxide was identified as a promising catalyst for this decomposition.

The Savannah River National Laboratory (SRNL) [35] is also investigating a hybrid S-I cycle that will combine electricity and thermal energy to enable the generation of hydrogen according to the equations below:

1 $$H_2SO_4(aq) \xrightarrow{850\,^oC} SO_2(g) + H_2O(g) + \frac{1}{2}O_2(g) \text{ (Thermochemical)} \quad (2.61)$$

2 $$SO_2(g) + 2H_2O(aq) \xrightarrow{80\,^oC} H_2SO_4(aq) + H_2(g) \text{ (Electrochemical)} \quad (2.62)$$

The process steps for this cycle are shown in figure 3.

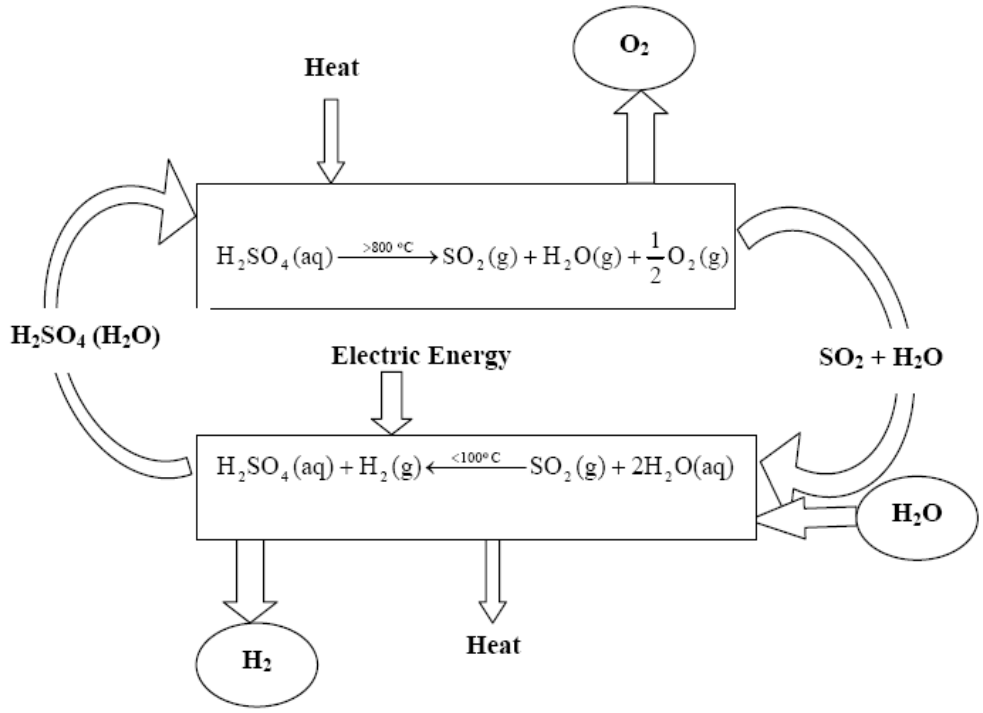

Figure 3: Hybrid S-I cycle of thermochemical hydrogen production (adapted from Ref. [35]).

The electrical cost of producing hydrogen using the hybrid cycle is proportional to the cell potential. A major drawback with the hybrid cycle is low current density. It is very difficult to keep the current density high and simultaneously maintain low voltage.

Another major drawback of this cycle is the design of an efficient membrane for the gas separation.

2.3 UT-3 Thermochemical Cycle

The UT-3 or Br-Ca-Fe thermochemical cycle of hydrogen production is a four-step process initially developed at the University of Tokyo [16-18]. This cycle involves only solid and gas components and it has a maximum temperature of about 750^{o}C. The reactions are performed in fixed bed reactors. The process steps for the UT-3 cycle are shown below.

$$CaO(s) + Br_2(g) \xrightarrow{600\,^{o}C} CaBr_2(s) + \frac{1}{2}O_2(g) \tag{2.63}$$

$$CaBr_2(s) + H_2O(g) \xrightarrow{750\,^{o}C} CaO(s) + 2HBr(g) \tag{2.64}$$

$$Fe_3O_4(s) + 8HBr(g) \xrightarrow{250\,^{o}C} 3FeBr_2(s) + Br_2(g) + 4H_2O(g) \tag{2.65}$$

$$3FeBr_2(s) + 4H_2O(g) \xrightarrow{560\,^{o}C} Fe_3O_4(s) + 6HBr(g) + H_2(g) \tag{2.66}$$

The UT-3 process comprises the following units:

- Calcium reactor unit;
- Two reactors alternating between bromination of calcium oxide and hydrolysis of calcium bromide
- Iron reactor unit;
- Two reactors alternating between bromination of magnetite and hydrolysis of ferrous bromide;
- Hydrogen separation unit;
- Oxygen separation unit.

The reactants cycle between oxide and bromide forms as given below:

$$CaBr_2(s) \Leftrightarrow CaO(s) \tag{2.67}$$

$$FeBr_2(s) \Leftrightarrow Fe_3O_4(s) \tag{2.68}$$

The reaction steps of the UT-3 cycle are shown in figure 4.

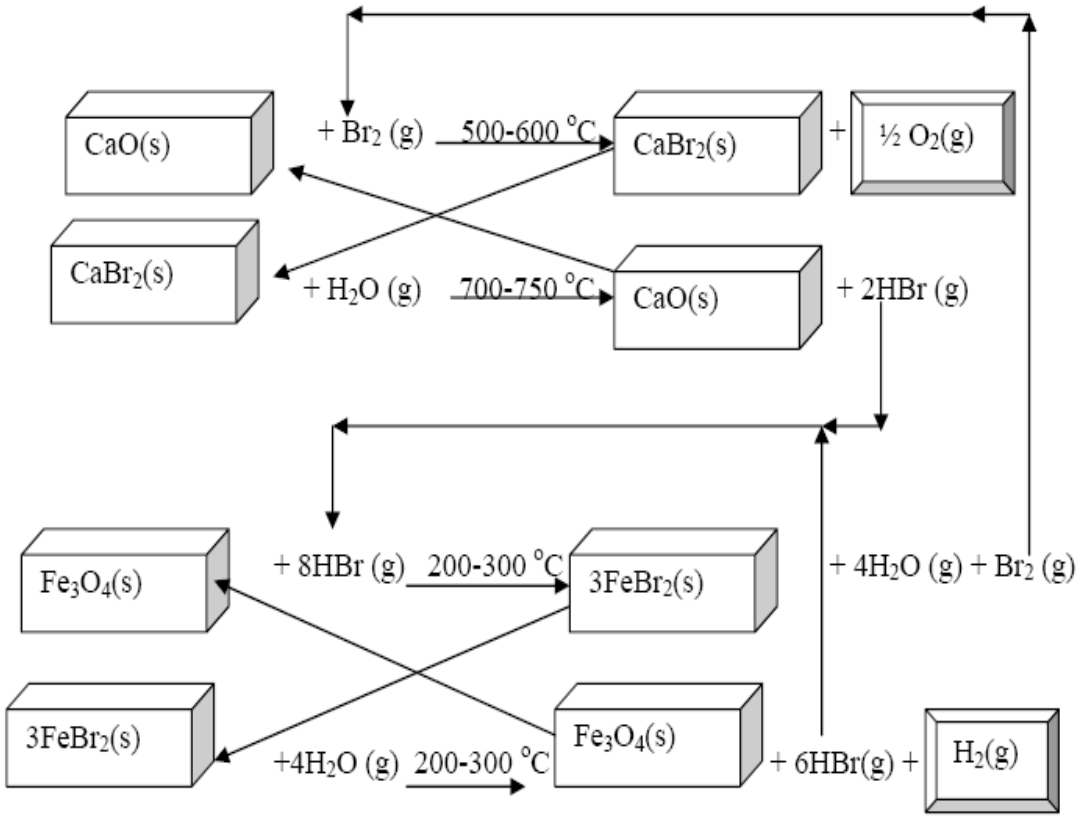

Figure 4: Process cycle of the UT-3 thermochemical hydrogen production (adapted from Ref. [18]).

The molar volumes are different for the oxide and bromide forms, leading to loss of reactive surface. The predicted efficiency of the adiabatic UT-3 cycle varies between 35% and 50% [18], depending upon the efficiency of the membrane separators, and whether electricity is co-generated along with hydrogen. A 10% overall efficiency

increase is projected with co-generation [16]. The UT-3 cycle has an inherent advantage of changing the direction of flow of gas components, with the solid components remaining fixed, thereby performing both the endothermic and exothermic reactions intermittently in one reactor. This can eliminate the drawbacks of solids handling as the solids remain in the fixed bed reactor. The UT-3 cycle however faces a number of challenges that limit its commercial application:

- Complexity in handling both exothermic and endothermic reactions in one reactor in a sequence requiring both heating and cooling heat exchangers linked together.
- The time to attain steady state after the transient, from one reaction form to the other. This affects the thermal efficiency adversely, solid reactants and catalyst attrition occurs within this period of time.
- Reactions are thermodynamically unfavorable as the free energies for the four reactions are slightly positive.
- The hydrogen and oxygen generated are carried by the high temperature steam where they constitute a very low mole fraction, so separation of these gases requires a very high efficiency membrane, which adds to the cost of the plant.
- The desired separation scheme will not involve condensation of water, due to the energy requirements and corrosion.
- Less costly palladium membranes cannot be used in the separation of the constituent gases, since they are attacked by halogen acids.
- Alumina supported silica membranes are effective in separating hydrogen from hydrogen bromide and water, but they are vulnerable to performance deterioration.

2.4 Copper-Chlorine Thermochemical Cycle

The copper-chlorine cycle is a lower temperature cycle of thermochemical hydrogen production examined by Carty et al. [25] and ANL [19-24], among others. This cycle is more promising than the existing cycles due to its advantages:

- The maximum cycle temperature for any of the steps is less than 550^{o}C. Thus the cycle is more compatible with nuclear power plants.
- The intermediate chemical steps are relatively safe and all materials are readily available.
- There is little solid handling, thereby allowing the cycle to operate smoothly.
- All individual steps have been investigated and experimentally proven with no significant side reactions.
- One of the sub-steps could be performed at a much lower temperature, with low grade waste heat from the nuclear or other sources.

The sequence of steps ensures that all chemicals components are recycled with addition of only heat and water.

Two process routes will be examined in this thesis: one that requires four steps and another process combining two of the four steps and reducing the cycle to three process steps. The following list shows the steps involved in the four step process cycle.

1 $2Cu(s)+2HCl(g) \xrightarrow{450\ ^{o}C} 2CuCl(l)+H_2(g)$ (2.69)

2a $4CuCl(aq) \xrightarrow{25\ ^{o}C} 2CuCl_2(aq)+2Cu(s)$ (2.70)

2b $2CuCl_2(aq) \xrightarrow{90\ ^{o}C} 2CuCl_2(s)$ (2.71)

3 $2CuCl_2(s)+H_2O(g) \xrightarrow{450\ ^{o}C} Cu_2OCl_2(s)+2HCl(g)$ (2.72)

4 $$Cu_2OCl_2(s) \xrightarrow{500\,^{o}C} 2CuCl(s) + \frac{1}{2}O_2(g) \quad (2.73)$$

The four-step cycle is illustrated in figure 5.

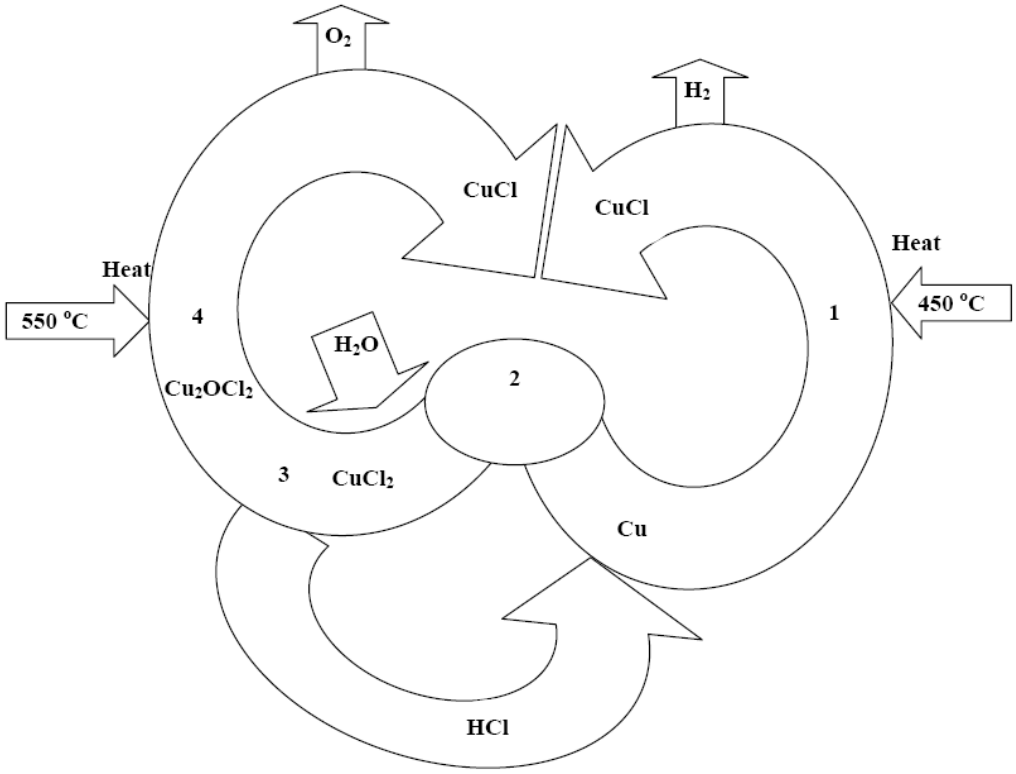

Figure 5: Four-step Cu-Cl process cycle of thermochemical hydrogen production.

The cycle shown in figure 5 comprises a hydrolysis reaction, an oxy-decomposition reaction, an electrolysis reaction, and a hydrogen generation reaction. It also requires an intermediate spray dying process that prepares the reactants to the required state and form. The cycle involves sequences of both exothermic and endothermic reactions, with the highest temperature of the cycle below 550^{o}C. Waste heat from nuclear processes at temperatures below 100^{o}C and other sources could be used for the spray drying process. This additional step can improve the efficiency of the cycle by up to 3%. The steps involved in this cycle are discussed below.

Step 1; Hydrogen generation step: $2Cu(s)+HCl(g) \xrightarrow{450\ ^oC} 2CuCl(l)+H_2(g)$

This is an exothermic reaction that has been experimentally proven at ANL to be feasible [19]. It will proceed spontaneously at 350°C with hydrogen production. However, because the CuCl is preferred in liquid form for ease of transfer, and because better reaction kinetics are attained at a higher temperature, the reaction temperature is increased to 450°C [30]. This is 20°C above the melting point of CuCl and it helps to stabilize the reaction between hydrochloric acid and copper. This reaction also requires the copper as a very fine powder, for a higher reaction yield of hydrogen.

Step 2A; Electrolysis of CuCl: $4CuCl(aq) \xrightarrow{25\ ^oC} 2CuCl_2(aq)+2Cu(s)$

This process takes place at ambient temperature using an electrochemical cell. CuCl is sparingly soluble in water and therefore some HCl is added to dissolve the CuCl for electrolysis. Solid copper particles are deposited and transferred using a screw propeller or other solid conveyer. A water slurry containing HCl and $CuCl_2$ is also separated. This process is energy intensive, in terms of electrical power for electrolysis and there is ongoing research [29-31] to reduce this energy requirement.

Step 2B; Drying of $CuCl_2$: $2CuCl_2(aq) \xrightarrow{90\ ^oC} 2CuCl_2(s)$

The $CuCl_2$ product from the electrochemical process must be separated and prepared by vaporization of water in the aqueous reagent. This process is performed at a temperature of 90°C or possibly lower temperature in a flash dryer. There is ongoing research at UOIT to vaporize the water using a new method that pressurizes the liquid stream sufficiently to atomize droplets through a pressure-reducing nozzle in the spray

system, at a reduced temperature of below 70°C [27]. This use of spray drying at reduced temperatures will add to the benefits of this cycle since low grade waste heat from the nuclear plant could be used for the process.

Step 3; Hydrolysis reaction: $2CuCl_2(s)+H_2O(g) \xrightarrow{450\,^oC} Cu_2OCl_2(s)+2HCl(g)$

The solid $CuCl_2$ from step 2B reacts with high temperature steam at 450°C in a fluidized bed. This process must be controlled, in order to prevent azeotrope between the steam and HCl. The particle size must be taken into consideration and the products must be continuously removed, as they are formed by an efficient separator, since Cu_2OCl_2 is sparingly soluble in dense steam. Excess water is required to achieve a significant yield of the product, which unfortunately increases the cost and size of the plant.

Step 4; Oxy-decomposition reaction: $Cu_2OCl_2(s) \xrightarrow{500\,^oC} 2CuCl(s) + \frac{1}{2}O_2(g)$

The oxy-decomposition of Cu_2OCl_2 has the highest temperature requirement. The heat for this process step would be supplied by the SCWR or other high temperature nuclear reactors. Though this reaction was proven experimentally to be feasible, there are some challenges in this step. For example the thermodynamic properties of the reactant are not fully understood.

This cycle has the following main advantages over other cycles:

- The maximum temperature for any of the steps in the cycle is 550°C. This renders it more compatible to be integrated with heat sources.
- The intermediate components are readily available and inexpensive and pose little or no hazardous material problems.

- All of the process steps, unlike those for many other cycles, have been proven experimentally, including the reaction yields, with no inhibiting reactions.
- There is minimal solid handling as compared to other proposed cycles.

The drawbacks of this cycle are summarized below:

- There is a high energy requirement for the electrochemical step.
- The particle size for the hydrogen generation step is affected by the spray drying and precipitation of the copper powder.
- Some solid handling of the reactants is required.

Rosen et al. [26] have developed a conceptual layout of the four-step copper-chlorine process cycle indicating various steps and processes taking place including their valid phases. The layout of this plant is shown in figure 6.

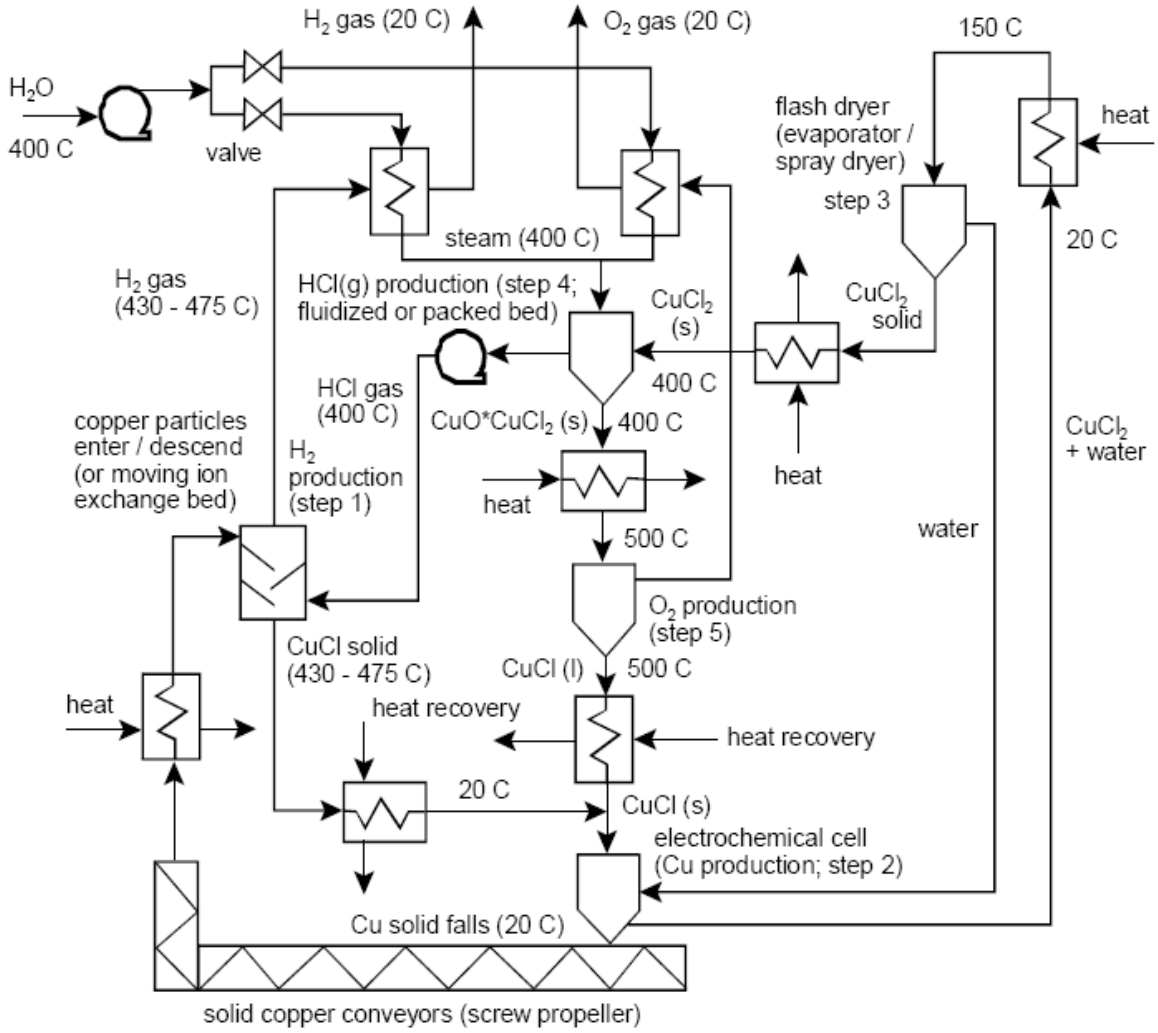

Figure 6: Conceptual layout of four-step copper-chlorine cycle (Ref. [26]).

The three-step Copper-Chlorine cycle is another promising alternative for hydrogen production. This hybrid cycle reduces solid handling by combining equations (2.69)-(2.71) into equation (2.74). The enthalpies and Gibbs free energies of formation for the components at standard temperature and pressure are shown in table 1.

1) $2CuCl(aq) + 2HCl(aq) \rightarrow 2CuCl_2(s) + H_2(g)$ (electrochemical) (100°C) (2.74)

2) $2CuCl_2(s) + H_2O(g) \rightarrow Cu_2OCl_2(s) + 2HCl(g)$ (vacuum) (400°C) (2.75)

$$3)\ Cu_2OCl_2(s) \xrightarrow{500\,^oC} 2CuCl(s) + \frac{1}{2}O_2(g) \qquad (2.76)$$

Table 1: Thermodynamic properties of Cu-Cl cycle components

Compound	ΔH_F^o **(kJ/mol)**	ΔG_F^o **(kJ/mol)**
$CuCl_2(s)$	-217.4	-173.6
$CuCl(s)$	-137.0	-120.0
$CuO(s)$	-162.0	-129.4
$Cu(s)$	0.0	0.0
$Cu_2OCl_2(s)$	-381.3	-310.5

In table 1, the variables in the second and third columns are defined as

ΔH_F^o = Enthalpy of formation at 298.15 K and 1 bar

ΔG_F^o = Gibbs free energy of formation at 298.15 K and 1 bar

All reactions have been experimentally demonstrated. Past studies [19-23,31] indicated particular challenges in the hydrolysis (2.75) and electrolysis reactions (2.74). The two thermal reactions, hydrolysis of $CuCl_2$ (2.75) and the decomposition of Cu_2OCl_2 (2.76), have been demonstrated at ANL [19,31]. In bench scale experiments, all of the oxygen was recovered at 530ºC from reaction (2.76). The electrolytic process (2.74) has been demonstrated successfully at the AECL [16]. The process schematic of this version of Cu-Cl cycle is shown in figure 7.

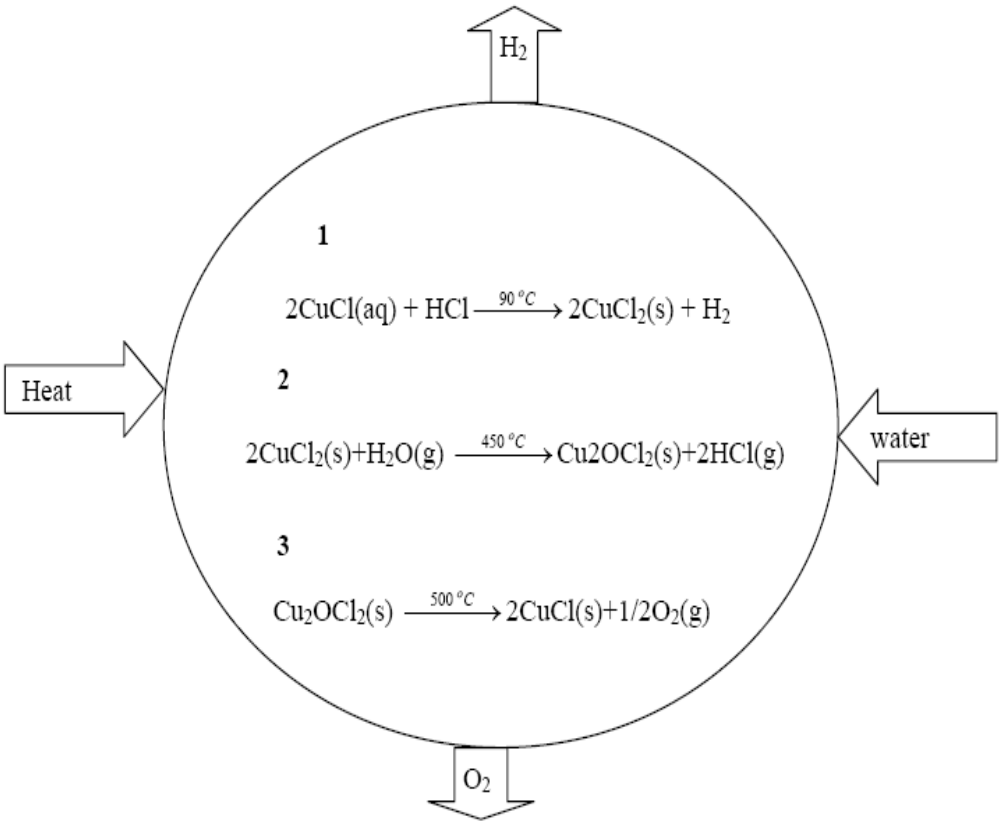

Figure 7: Three step process route of hydrogen production using Cu-Cl cycle.

The hydrolysis reaction is a challenging because of two factors: (i) competing reaction of $CuCl_2$ and Cl_2, and (ii) the need for excess water.

The competing reaction is the thermal decomposition of $CuCl_2$:

$$2CuCl_2\ (s) \Leftrightarrow 2CuCl\ (s) + Cl_2\ (g) \qquad (2.77)$$

This competing reaction can be minimized by the choice of operating conditions and the reactor design. A sensitivity study and experimental results [34] indicate that steam must be supplied in excess for high yields of the desired Cu_2OCl_2 and HCl. The excess steam increases the capital costs significantly because of the larger number of vessels required.

Step 1 involves the generation of hydrogen using an electrochemical cell. This step by far is the most challenging task in the cycle. There is a need to design an efficient membrane that can separate the gas generated. This process faces challenges in terms of energy requirements. There is also a need to keep the current density high while simultaneously operating at a low cell potential. Step 2 can be performed in a vacuum, thereby eliminating the effects of fuming hydrochloric gas. Though limited data are available for the properties of copper oxochlorate, ANL has estimated its properties using equimolar volume of copper(ii)oxide and copper(ii)chloride.

This hybrid process has been demonstrated at AECL to be feasible and the hydrogen yield is encouraging. A platinum catalyst was used in the electrochemical cell, although new and more efficient polymer membranes are being investigated for the process. The cell potential for this electrochemical process is still high, but better designs are being investigated to reduce the cell potential without compromising the current density.

CHAPTER 3

PROCESS MODELING OF COPPER-CHLORINE CYCLE

3.1 Aspen Plus Process Simulation Software

This chapter focuses on the copper-chlorine thermochemical cycle under development by UOIT and other partners. The objective is to simulate nuclear-based hydrogen production using the copper-chlorine thermochemical cycle, to improve the understanding of the cycle and enable scale-up to larger flow capacities. Simulation will be conducted with the Aspen Plus chemical process simulation software.

Aspen Plus is a process simulator that predicts the behavior of chemical reactions and steps using standard engineering relationships, such as mass and energy balances, rate correlations, as well as phase and chemical equilibrium data. By choosing the appropriate unit operations and thermodynamic models, reliable thermodynamic data and realistic operating conditions, Aspen Plus uses mathematical models to predict the performance of the cycle and actual plant behavior [36].

Aspen Plus can handle very complex processes, including multiple-column separation systems, chemical reactors, distillation of chemically reactive compounds, and even electrolyte solutions like mineral acids. Aspen Plus can help to design better plants, reduce plant design time, and increase profitability in existing plants by improving on current processes. Aspen Plus can interactively change specifications, such as the flowsheet configuration, operating conditions, and feed compositions, to predict new

cases and analyze alternatives. The software can analyze results, and generate plots, reports, process flow diagram (PFD)-style drawings, and spreadsheet files.

Aspen Plus predicts the cycle performance and performs a wide range of additional tasks such as:

- Perform sensitivity analyses and case studies;
- Generate custom graphical and tabular output;
- Estimate and regress physical properties;
- Fit simulation models to plant data;
- Optimize processes;
- Interface results to spreadsheets and other compatible packages;
- Share input and results among other Windows applications using object linking and embedding (OLE).

Aspen Plus contains data, properties, unit operation models, built-in defaults, reports, and other features and capabilities developed for specific industrial applications. The chemical template is suitable for a wide range of chemical (non-electrolyte) applications. There are also templates for electrolytes, solid and organic compounds, and mixtures. It is also useful for petrochemical and energy simulation applications. Two solution techniques can be adopted with Aspen Plus: Sequential Modular (SM) approach and the Equation Oriented (EO) approach. With the SM approach, equations and constraints are collected for each process unit into a separate computational subroutine, wherein each module or unit operation calculates its outlet stream values for the given input conditions and parameters, using a given thermodynamic model specified for that process unit, irrespective of the source of input information. The SM approach calculates the stream

output, sequentially from one module to the other, starting with the feed stream until the final products are obtained [37]. The recycle loops must be specified in the flowsheet. In complex processes, it is more desirable to use SM. The SM approach is illustrated in figure 8.

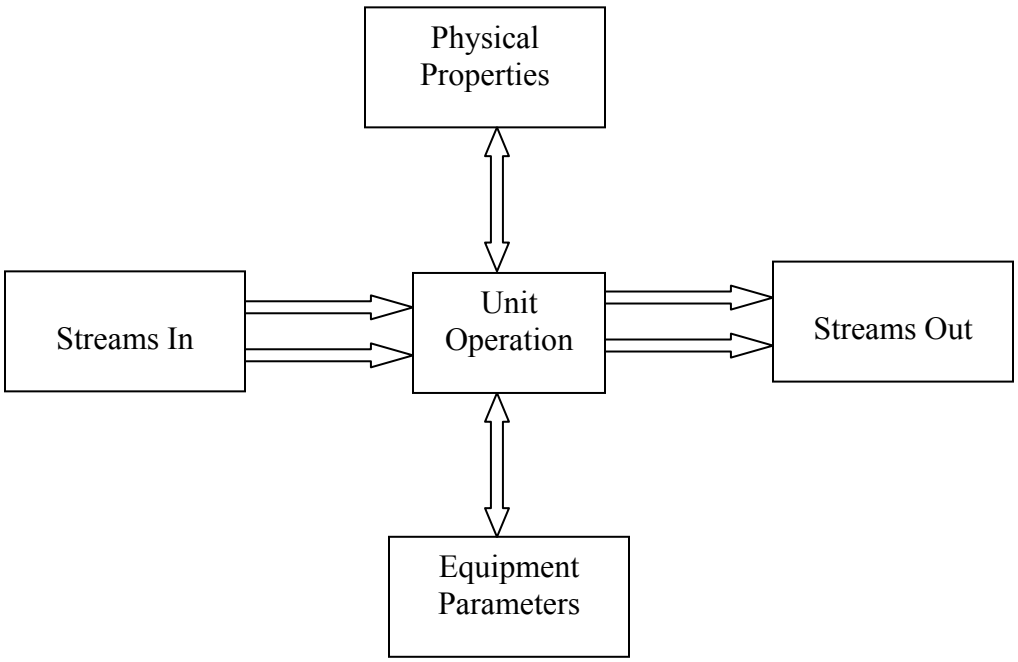

Figure 8: Sequential Modular approach (adapted from Ref. [37]).

In contrast, the EO gathers and solves all equations simultaneously. This reduces computer time, although a good starting point is required, in order to adopt the EO approach. Good knowledge of the process and accurate predictions are needed in order to adopt EO in a PFD, which may be difficult for a complex process and new design, without existing knowledge of the behaviour. A more robust simulation can be achieved by combining these two approaches into a single simulation. This can be accomplished by using the SM approach to initialize, and afterwards using the EO approach to solve the

flowsheet more precisely, by using the result from the SM approach, or using them as the initial points. Alternatively, the flowsheet can be analyzed by SM and then EO for optimization or model tuning. Using Aspen Plus, a successful simulation can be carried out by performing the following steps.

- Selecting and defining unit operation models for the simulation and placing them onto the flowsheet. This includes labeling the unit blocks from the Aspen Plus library, including user defined blocks.
- Linking the unit operations together using labeled streams. All material and energy streams must be identified, including the input and output streams.
- Specifying the global setup. This includes units of measurement, run type, input, mode, flow conditions, and so forth.
- Specifying all components that are involved in the process and identifying all Henry components. This can be performed from the Aspen Plus component database, and non-database components.
- Specifying thermodynamic models for all unit blocks to represent the physical properties of the components and mixtures in the process, including properties that are not given in the Aspen Plus database.
- Specifying flow rate and thermodynamic conditions of all feed streams.
- Specifying the operating conditions of all unit operations.
- Performing the simulation; normal, automatic, troubleshooting, or on-demand case.
- Performing model analyses, flowsheeting options, or calculator blocks for sensitivity analyses.

In an Aspen Plus simulation, thermodynamic processes are carried out in blocks that could be reactors, heat exchangers, pressure changers, mixers/splitters, separators, or even user defined models among others. These are called unit operations and they perform specific functions based on feed input, thermodynamic models and operating conditions. The reactants, products or energy transfer across the unit operations and interactions with the external environment take place through the material and energy streams. The following blocks will be used for simulations in this thesis.

1. Stoichiometry reactor (RStoic): This can handle reactions that occur independently, in a series of reactors, and perform selectivity and heat of reaction calculations. RStoic unit operations are used in the following cases:

- Reaction kinetics of the major components are unknown or unimportant;
- The stoichiometry of the reactions is known;
- User can specify the extent of a reaction or conversion.

In Aspen Plus, RStoic is set up by specifying operating conditions, reactions, reference conditions for heat of reaction calculations, product and reactant components for selectivity calculations, particle size distribution, and component attributes.

2. Equilibrium reactor (REquil): This is used when some or all reactions in the process reach equilibrium. REquil can calculate single phase chemical equilibrium, or simultaneous phase and chemical equilibra. It can also calculate equilibrium by solving stoichiometric chemical and phase equilibrium equations. This model is set up in Aspen

Plus by specifying reactor operating conditions, valid phases, reactions, convergence parameters, and solid and liquid entrainment in the vapour stream(s).

3. Gibbs reactor (RGibbs): This model uses Gibbs free energy minimization with phase splitting to calculate the equilibrium in a chemical reaction. RGibbs does not require the specification of the reaction stoichiometry. RGibbs can also calculate the chemical equilibria between any number of conventional solid components and fluid phases. RGibbs also allows restricted equilibrium specifications for systems that do not reach complete equilibrium. RGibbs is used to model reactors with:

- Single phase (vapour or liquid) chemical equilibrium
- Phase equilibrium for vapour and any number of liquid phases with no chemical reactions
- Phase and/or chemical equilibrium with solid solution phases
- Simultaneous phase and chemical equilibrium

In Aspen Plus, this model is set up by specifying reactor operating conditions and phases in equilibrium calculations, possible products, phases of outlet streams, inert components, and equilibrium restrictions.

4. Yield Reactor (RYield): RYield is used to model processes under the following conditions:

- Reaction stoichiometry is unknown or unimportant
- Reaction kinetics are unknown or unimportant

- Yield distribution is known

RYield requires the specification of the yields per mass of total feed, excluding any inert components for the products, or else calculates them in a user-supplied FORTRAN subroutine. RYield normalizes the yields to maintain a mass balance. This reactor can model single or multiphase reactors. They are set up in Aspen Plus by specifying reactor operating conditions, component yields, inert components, convergence parameters, particle size distribution, and component attributes for the outlet stream(s).

5. Separators (Sep): This refers to two phase (Sep2) or three phase (Sep3) separators. They combine inlet streams and separate the resulting stream into two or more streams, according to splits that are specified for each component. One can also specify the splits for each component in each sub-stream. The separator model can be used to represent component separation operations, such as a stoichiometry reactor when vapour-liquid equilibrium is achieved or known, but the details of the reactor energy balance are unknown or unimportant. In Aspen Plus, separators are set up by entering split specifications, flash specifications, and convergence parameters for the mixed inlet and each outlet stream. Flash is a variant of separators that performs rigorous two (vapour-liquid) or three (vapour-liquid-liquid) phase equilibrium calculations. This produces one vapour outlet stream, one liquid outlet stream, and an optional water decant stream. In Flash, a user can optionally specify a percentage of the liquid phase to be entrained in the vapour stream. This is accomplished by entering the flash specifications, convergence parameters, and entrainment specifications in the input form.

6. Mixers: These combine material streams, heat streams or, work streams into a single stream. A single mixer block cannot mix streams of different types; for example, material, heat, and work. When mixing material streams, one can specify either the outlet pressure or pressure drop. If the pressure drop is specified, the mixer determines the minimum of the inlet stream pressures, and it applies the pressure drop to the minimum inlet stream pressure to compute the outlet pressure. If the outlet pressure or pressure drop is not specified, the mixer uses the minimum pressure from the inlet streams for the outlet pressure. When mixing heat or work streams, the mixer does not require any specifications. The mixer performs an adiabatic calculation on the product to determine the outlet temperature, unless a "Mass Balance Only Calculation" is specified on the mixer for the set up simulation options sheet.

7. Splitters: These are divided into two: Stream Splitter (FSplit) or Sub-stream Splitter (SSplit). FSplit combines streams of the same type and divides the resulting stream into two or more streams of the same type. All outlet streams have the same composition and conditions as the mixed inlet. This is used to model flow splitters, such as bleed valves. FSplit cannot split a stream into different types. For example, FSplit cannot split a material stream into a heat stream and a material stream. This is accomplished in Aspen Plus by entering split specifications, flash conditions, calculation options, and key components associated with split specifications. On the other hand, SSplit combines material streams and divides the resulting stream into two or more streams. This is used to simulate a splitter when the split of each sub-stream among the outlet streams is different. Sub-streams of the outlet streams have the same composition,

temperature, and pressure as the corresponding sub-streams in the mixed inlet stream. Only the sub-stream flow rates differ. In Aspen Plus, this is accomplished by entering split specifications, flash conditions, calculation options, and key components associated with split specifications. To simulate a splitter when the composition and properties of sub-streams in the output streams are different, a separator is used.

8. Heat Exchangers: these determine the thermal and phase conditions of a mixture with one or more inlet streams. Heaters perform the following single phase or multiphase calculations:

- Determine bubble or dew points;
- Add or remove any amount of user specified heat flow;
- Match degrees of superheating or sub-cooling.

Heaters determine the heating or cooling duty required to achieve a certain vapour fraction. A heater produces one outlet stream, with optional water decant stream. The heat duty specification may be provided by a heat stream from another block. Heaters are used to supply the required heat for the thermochemical cycle. They also allow the recovery of heat from exothermic reactions. The heater feature can be used to represent the following components: Heaters, Coolers, Valves, Pumps, and Compressors (whenever work-related results are not needed). It can also be used to set the thermodynamic condition of a stream. When the outlet conditions are specified, Heater determines the thermal and phase conditions of a mixture with one or more inlet streams. In Aspen Plus, inter-stage heaters and coolers can be specified in one of two ways:

- Specifying the duty directly on the input specification sheet;
- Requesting heat transfer coefficient (UA) calculations on the input specification sheet.

If the heater duty is specified directly, a positive duty is entered for heating and a negative duty for cooling. If a heat transfer calculation is requested, the reactor model calculates the duty and outlet temperature of the heating/cooling fluid, simultaneously within the block. To request UA calculations, the heating or cooling fluid component and inlet temperature of the fluid must be specified. The heat capacity of the fluid can be specified directly on the input specification form, or the unit model can compute it from a property method specified for that model. If the heat capacity is needed for the unit model, the pressure and phase of the heating or cooling fluid must also be specified.

9. Streams: These are the connections linking the unit operations to each other and external systems. There are two types of streams in Aspen Plus: Material and energy streams. Material streams connect unit operation models and transfer material. Material streams in Aspen Plus allow the presence of solids that are not in phase equilibrium with fluid phase components. Material streams consist of one or more sub-streams, each of which represents the flow of a different type of material. The sub-streams that make up a stream are not in equilibrium and do not necessarily have the same temperature. All sub-streams, however, must have the same pressure. In Aspen Plus, material streams are specified by defining the stream conditions, including the composition and flow rates. In some cases, the particle size distribution is also specified.

The stream composition can be defined in terms of component flows, fractions, or concentrations. When the component fractions are specified, the total mole, mass, or liquid volume flow rate must also be specified. Component fractions must sum to 1.0. The user can enter both component flows and the total flow. Aspen Plus normalizes the component flows to match the total flow. If the component concentration is specified, the component ID must also be specified for the solvent and total flow. For a stream that has one phase, in addition to specifying the temperature and pressure, a valid phase must also be specified. A stream in a flowsheet can have a "tear" in Aspen Plus. The tear removes a recycle by guessing an initial value for the stream where it enters a block, then allows the solver to progress through the flowsheet. Eventually a result is calculated for the stream, and this is compared with the initial estimate. To resolve the tear, a new guess is made, gradually converging towards the correct value for the stream.

An energy stream in Aspen Plus supplies heat or otherwise removes excess heat from unit operations. This stream is also used to supply work to the blocks. The inlet heat stream supplies heat to a unit operation block. This can be used in two ways as follows:

- For duty specification; in this case, the duty for the heat stream is specified on stream input form. There is no need to specify the duty for the block. For example, if a heat stream is used to supply the heat duty to a heater block, only one specification is needed on the heater input specifications sheet.
- For an overall energy balance; for this purpose, the duty for the destination block is specified, or more than one block specification is defined to calculate the duty. For example, if two specifications on the heater input specifications sheet are given, the block calculates the duty. The duty specified on this form is not used as

A user can manipulate directly any variables that are entered before a simulation. These variables are either read-only or write-read. For variables calculated by Aspen Plus, they should not be overwritten or varied directly, as this would lead to inconsistent results. These variables should be read-only. Accessed variables can be either scalar or vector. Simulation objects can be activated or deactivated. When deactivated, they need to be completely specified to start the problem. Deactivated simulation objects (other than streams) are ignored during a simulation.

In Aspen Plus, deactivating the inlet and outlet streams of a block does not cause the block to be deactivated, even if all streams connected to a block are deactivated, except in the following cases:

- Streams with both source and destination block deactivated or not present are deactivated, and ignored during the simulation.
- Referencing a deactivated block or stream causes a heat exchanger block to be deactivated. The stream disabling logic is then repeated.

- Referencing a deactivated block or stream causes a Cost block, Pressure-Relief block, Calculator block, Transfer block, Design-Specification, Constraint, Optimization, Data-Fit block, Sensitivity block, or Balance block to be deactivated. Targets of a deactivated Calculator or Transfer block will not be deactivated.
- Calculator, Transfer, and other blocks execute before and after the reference deactivated block is deactivated.
- Convergence blocks that reference a deactivated Tear Stream, Tear-Variable, Design-Specification, Constraint, or Optimization are deactivated.
- Sequences that reference deactivated blocks are ignored and revert back to automatic sequencing.
- Deactivated Tear Streams or Tear-Variables are ignored.
- Deactivated Convergence blocks in Convergence-Order are ignored.

Objects that are deactivated by association are listed in the history file. Deactivating items does not change the flowsheet connectivity, other than removing the deactivated items which does not automatically cause any streams to be reinitialized. Some uses of deactivation may require reinitializing the streams that were solved with a different activation.

3.2 Thermodynamic Models for Calculations

In Aspen Plus, all unit operation models need property values to generate the results. The following properties are normally required in the Aspen Plus physical property calculations:

- Fugacity coefficients;
- Enthalpy;
- Entropy;
- Gibbs energy;
- Molar volume;
- Transport properties;
- Thermal conductivity.

These are called major properties and at least one is required to perform energy and mass balances in a unit operation. For simulations that involve both mass and energy balance calculations, a user must supply the following parameters: molecular weight (MW), extended Antoine vapour pressure model (PLXANT), and an ideal gas heat capacity model (CPIG or CPIGDP). Some of these properties are dependent on others. Departure functions are used by Aspen Plus. This refers to the difference between actual values of properties and the corresponding values calculated for ideal gases. Models of these functions, such as the enthalpy departure, entropy departure and Gibbs free energy departure, are used together with the ideal gas properties to calculate the actual properties.

The most frequently used properties are fugacities. Fugacity is a measure of chemical potential in the form of adjusted pressure. It directly relates to the tendency of a substance to prefer one phase (liquid, solid, gas) over another. Fugacities are required for thermodynamic equilibrium, enthalpy, and free energy calculations. In an ideal liquid solution, for example, the liquid fugacity of each component in the mixture is directly proportional to the mole fractions of the components. This occurs because an ideal

solution assumes that all molecules in the liquid are identical in size and randomly distributed. However, a copper-chlorine mixture in this thesis is highly non-uniform in terms of size, shape, and intermolecular interactions between the components. This implies size and energy asymmetry. Energy asymmetry occurs between polar and non-polar molecules and also between different polar molecules.

Another key thermodynamic property that characterized this feature is phase equilibrium. Aspen Plus has interactive tools for analyzing the properties and vapour-liquid equilibrium of chemical systems. The basic relationship for every component, i, in the vapour and liquid phases of a system at equilibrium is given by:

$$f_i^v = f_i^l \tag{3.1}$$

Here, f is the fugacity of the components and v and l denote the vapour and liquid phases respectively. Two thermodynamic property methods will be examined in the following sections: (i) equation of state and (ii) activity coefficient models.

3.2.1 Equation of State Method

An equation of state describes the pressure, volume, and temperature (PVT) behavior of pure components and mixtures. Equations of state have an important role in chemical engineering design and the study of phase equilibria of fluids and fluid mixtures.

Equations of state have been used for mixtures of non-polar and slightly polar compounds [38], as well as more recently for the calculation of phase equilibria in non-polar and polar mixtures. The advantages of equations of state are their applicability over wide ranges of temperature and pressure, for mixtures of diverse components, from light

gases to heavy liquids. They can be used for vapour-liquid, liquid-liquid, and supercritical fluid phase equilibria, and also gas, liquid, and supercritical phases.

Many equations of state have been developed in past studies [39,40] with either an empirical or theoretical basis. The Van der Waals equation of state can predict vapour–liquid co-existence. The Redlich-Kwong equation of state [39] improved the accuracy of the Van der Waals equation by including temperature dependence for the attractive term. Peng and Robinson [40] proposed additional modifications to the Redlich-Kwong equation to more accurately predict the vapor pressure, liquid density, and equilibria ratios. An equation of state is usually written explicitly in terms of pressure. Most equations of state have different terms to represent attractive and repulsive forces between molecules. Any thermodynamic property, such as fugacity coefficients or enthalpies, can be calculated from the equation of state. Equation of state properties are then calculated relative to the ideal gas properties of the same mixture at the same conditions. In the equation of state property method [36], the fugacity of components in the vapour and liquid phase is given by:

$$f_i^v = \varphi_i^v \chi_i P \tag{3.2}$$

$$f_i^l = \varphi_i^l \chi_i P \tag{3.3}$$

where χ denotes the mole fraction of a component and P denotes pressure. The fugacity coefficient φ is expressed as:

$$\ln \varphi_i^\alpha = -1/RT \int_\infty^{V\alpha} \left[\left(\partial P / \partial_{ni} \right)_{T,V,n} - RT/V \right] dV - \ln Z_m^\alpha \tag{3.4}$$

where α denotes the component phase, R denotes the universal gas constant, T denotes temperature, V denotes volume, n denotes number of moles, Z denotes compressibility factor and m denotes molar property.

The excess Gibbs energy in a mixture at any pressure is

$$G_m^E = R\,T\,\ln\,\varphi - \sum_i \chi_i R\,T\,\ln\,\varphi_i^* \tag{3.5}$$

where E denotes excess and * denotes asymmetry.

The equation of state can be related to other properties through the following fundamental thermodynamic equations:

- Enthalpy departure of the mixture:

$$\left(H_m - H_m^{ig}\right) = -\int_{\infty}^{V}\left(p - \frac{RT}{V}\right)dV - RT\ln\left(\frac{V}{V^{ig}}\right) + T\left(S_m - S_m^{ig}\right) + RT\left(Z_m - 1\right) \tag{3.6}$$

where ig denotes ideal gas property.

- Entropy departure of the mixture:

$$\left(S_m - S_m^{ig}\right) = -\int_{\infty}^{V}\left[\left(\frac{\partial P}{\partial T}\right)_V - \frac{R}{V}\right]dV + R\ln\left(\frac{V}{V^{ig}}\right) \tag{3.7}$$

- Gibbs energy departure of the mixture:

$$\left(G_m - G_m^{ig}\right) = -\int_{\infty}^{V}\left(p - \frac{RT}{V}\right)dV - RT\ln\left(\frac{V}{V^{ig}}\right) + RT\left(Z_m - 1\right) \tag{3.8}$$

From a given equation of state, the fugacities are calculated according to equations (3.2) and (3.3). The other thermodynamic properties of a mixture can then be computed from the departure functions as follows:

- Vapour enthalpy of the mixture:

$$H_m^v = H_m^{ig} + \left(H_m^v - H_m^{ig}\right) \tag{3.9}$$

- Liquid enthalpy of the mixture:

$$H_m^l = H_m^{ig} + \left(H_m^l - H_m^{ig}\right) \tag{3.10}$$

- Vapour Gibbs energy of the mixture:

$$G_m^v = G_m^{ig} + \left(G_m^v - G_m^{ig}\right) \tag{3.11}$$

- Liquid Gibbs energy of the mixture:

$$G_m^l = G_m^{ig} + \left(G_m^l - G_m^{ig}\right) \tag{3.12}$$

- Vapour entropy of the mixture

$$S_m^v = S_m^{ig} + \left(S_m^v - S_m^{ig}\right) \tag{3.13}$$

- Liquid entropy of the mixture:

$$S_m^l = S_m^{ig} + \left(S_m^l - S_m^{ig}\right) \tag{3.14}$$

The molar ideal gas enthalpy, entropy and Gibbs free energy are respectively given by:

$$H_m^{ig} = \sum_i y_i \left[\Delta_f H_i^{ig} + \int_{T^{ref}}^{T} C_{p,i}^{ig}(T)dT\right] \tag{3.15}$$

$$S_m^{ig} = \sum_i y_i \left[\Delta_f S_i^{ig} + \int_{T^{ref}}^{T} C_{p,i}^{ig}(T)dT\right] \tag{316}$$

$$G_m^{ig} = \sum_i y_i \left[\Delta_f G_i^{ig} + \int_{T^{ref}}^{T} C_{p,i}^{ig}(T)dT\right] \tag{3.17}$$

In the above equation, $C_{p,i}^{ig}$ denotes the ideal gas heat capacity, $\Delta_f G_i^{ig}$ denotes the standard Gibbs free energy of formation for an ideal gas at 298.15 K and 1 atmosphere, T^{ref} denotes the reference temperature (298.15 K) and y denotes the mole fractions of the components in a gas.

Using the equation of state, the total volume of the mixture is calculated through: $P(T,V_m)$ for V_m. This can also be computed from an empirical correlation [41].

The following two equations of state methods will be used in the Aspen Plus simulation.

(i) Soave-Redlich-Kwong (SRK) method

The SRK method uses the Soave-Redlich-Kwong cubic equation of state for all thermodynamic properties, with an option to improve the liquid molar volume using a volume correction. It has a composition-independent fugacity coefficient for faster convergence. This property method gives reasonable results over a wide range of temperatures and pressures, but it is particularly suitable in high temperature and high pressure regions. The SRK method can be used in the critical region. Unlike the activity coefficient property methods, it does not exhibit anomalous behavior [42].

The SRK equation of state is given by:

$$P = \frac{R\,T}{V_m - b} - \frac{a}{V_m\left(V_m + b\right)} \tag{3.18}$$

where individual variables a and b denote equation of state energy and co-volume parameters respectively. In this study, SRK will be applied in simulation of sensitivity block due to super critical components involved.

(ii) Peng-Robinson (Peng-Rob) method

The Peng-Robinson equation-of-state is the basis for the Peng-Rob property method. The model has been extended to include advanced asymmetric mixing rules, by choosing an additional temperature dependent parameter called the alpha function [43]. The mixing rules, however, do not use more than a single binary interaction parameter, which should be independent of temperature, pressure, and composition. Results are

comparable to those of property methods that use a standard Soave-Redlich-Kwong equation of state. When advanced function and asymmetric mixing rules are used with suitable parameters, the Peng-Robinson model can be used to accurately simulate polar, non-ideal chemical systems, similar to the Soave-Redlich-Kwong model. The standard form of the Peng-Rob equation of state is given by:

$$p = \frac{R\,T}{V_m - b} - \frac{a\,\alpha}{V_m\left(V_m + b\right) + b\left(V_m - b\right)} \tag{3.19}$$

The alpha function, α, in equation (3.19) is temperature dependent.

3.2.2 Activity Coefficient Property Methods

Mixtures containing molecules of similar size and character have less intermolecular interactions between different component molecules. Idealization can also exist between polar molecules, if the interactions cancel each other, but generally there are non-ideal interactions in mixtures of unlike molecules. Either the size and shape, or the intermolecular interactions between components, may be dissimilar. The activity coefficient of a mixture (γ_i) is a factor used in thermodynamics to account for deviations from ideal behavior in a mixture of chemical substances. In an ideal mixture the interactions between each pair of chemical species are the same and the enthalpy of mixing is zero. As a result, the properties of the mixtures can be expressed directly in terms of concentrations or partial pressures of the substances, using ideal mixture laws such as Raoult's law. Deviations from the idealization are accommodated by modifying the concentration by an activity coefficient [36].

The fugacity coefficient therefore can be expressed as:

$$f_i^v = x_i \gamma_i f_i^{*v} \tag{3.20}$$

$$f_i^l = x_i \gamma_i f_i^{*l} \tag{3.21}$$

When γ_i deviates more from unity, more non-ideal characteristics will be exhibited by the mixture. In the majority of mixtures, γ_i is greater than unity. By comparing equations (3.2) and (3.3) with (3.20) and (3.21), a higher fugacity than 1 is observed. The fugacity can also be interpreted as the tendency to vaporize. If compounds vaporize more than an ideal solution, then they increase their average inter-molecular distance. Activity coefficients greater than unity have more repulsion between unlike molecules. If the repulsion is strong, liquid-liquid separation occurs. This is another mechanism that decreases contact between unlike molecules. It is less common for γ_i to be smaller than unity, which suggests a strong attraction between unlike molecules. In this case, liquid-liquid separation does not occur, but instead complexes are formed. The activity coefficient method is the best way to represent highly non-ideal liquid mixtures at low pressures.

Binary parameters are estimated using Aspen Plus tool or experimental data, such as phase equilibrium data. Binary parameters are valid only over the temperature and pressure ranges of the data. Values outside of the valid range should be used with caution, especially in liquid-liquid equilibrium applications. The activity coefficient models are more accurate at low pressures of below 10 atmospheres. Activity coefficient models have lower accuracy for systems containing dissolved gases at low pressures and small concentrations, as well as non-ideal chemical systems at high pressures. Two

activity coefficient models will be used in this thesis: (i) the Non-Random Two Liquid method and (ii) the Electrolyte Non-Random Two Liquid method.

(i) Non-Random Two Liquid (NRTL) method

The NRTL model calculates the liquid activity coefficients for mixtures at a low pressure. It is recommended for highly non-ideal chemical systems, and it can be used for vapour-liquid equilibrium (VLE) and liquid-liquid equilibrium (LLE) applications. The model can also be used for advanced equation-of-state mixing rules [43]. The Aspen Physical Property System has a large number of built-in binary parameters for the NRTL model. The binary parameters have been regressed using VLE and LLE data from the Dortmund Databank [44]. The binary parameters for the VLE applications were regressed using the ideal gas, and Redlich-Kwong equation of state [45]. The distribution of ions in NRTL is shown in figure 8, and the equation for the NRTL model is given by:

$$\ln\gamma_i = \frac{\sum_j \chi_j \tau_{ji} G_{ji}}{\sum_k \chi_k G_{ki}} + \frac{\sum_j \chi_j G_{ij}}{\sum_k \chi_k G_{kj}} \left(\tau_{ij} - \frac{\sum_j \chi_m \tau_{mj} G_{mj}}{\sum_k \chi_k G_{kj}} \right) \tag{3.22}$$

$$G_{ij} = \exp\left(-\alpha_{ij}\tau_{ij}\right) \tag{3.23}$$

$$\tau_{ij} = \alpha_{ij} + \frac{b_{ij}}{T} + e_{ij}\ln T + f_{ij}T \tag{3.24}$$

$$\alpha_{ij} = c_{ij} + d_{ij} + \left(T - 273.15K\right) \tag{3.25}$$

where the NTRL binary parameters in equations $\alpha_{ij}, b_{ij}, c_{ij}, d_{ij}, f_{ij}, \text{and } \tau_{ij}$ are non-symmetrical.

The NRTL property method uses:

- The NRTL activity coefficient model for the liquid phase;
- The ideal gas equation of state for the vapour phase;
- The Rackett model [46] for the liquid molar volume;
- Henry's law for supercritical components.

(ii) Electrolyte Non Random Two Liquid (ElecNRTL) method

In electrolyte solutions a larger degree of interactions and phenomena exist than in non-electrolyte solutions. Thus the NRTL model needs additional modifications to include these interactions. Besides physical and inter-molecular interactions, ionic reactions and molecule-ion and ion-ion interactions occur. ElecNRTL is, therefore, more complicated than non-electrolyte activity coefficient models. The dissociation of electrolytes leads to some components forming many species in a solution. This causes a multitude of interactions between species. The ElecNRTL model is an extension of the molecular NRTL model. The ElecNRTL model was originally proposed by Chen and Evans [47], for aqueous electrolyte systems. It was later extended to mixed solvent electrolyte systems [48]. The model reduces to the molecular NRTL model, when there are no electrolyte concentrations in the mixture. The model is based on two fundamental assumptions, described below:

1) Like-ion repulsion assumption, which states that the local interactions of all cations around other cations is zero. This assumption is also applicable for anions around anions, and assumes that the repulsive forces between ions of like charge are very large. This assumption may be justified on the basis that repulsive forces between ions of the same sign are very strong for neighbouring species.

2) Local electro-neutrality assumption, which states that the distribution of cations and anions around a central molecular species occurs such that the net local ionic charge is zero. The distribution of ions in ElecNRTL is shown in figure 9.

In figure 9, when a central solvent molecule exists at the center with other molecules, cations and anions surrounding it, the principle of local electroneutality is followed. In the case of a central cation (anion) with solvent molecules and an anion (cation) in its immediate vicinity, the principle of like ion repulsion is followed; in that case, no ions of like charge exist near each other whereas oppositely charged ions are very close to each other.

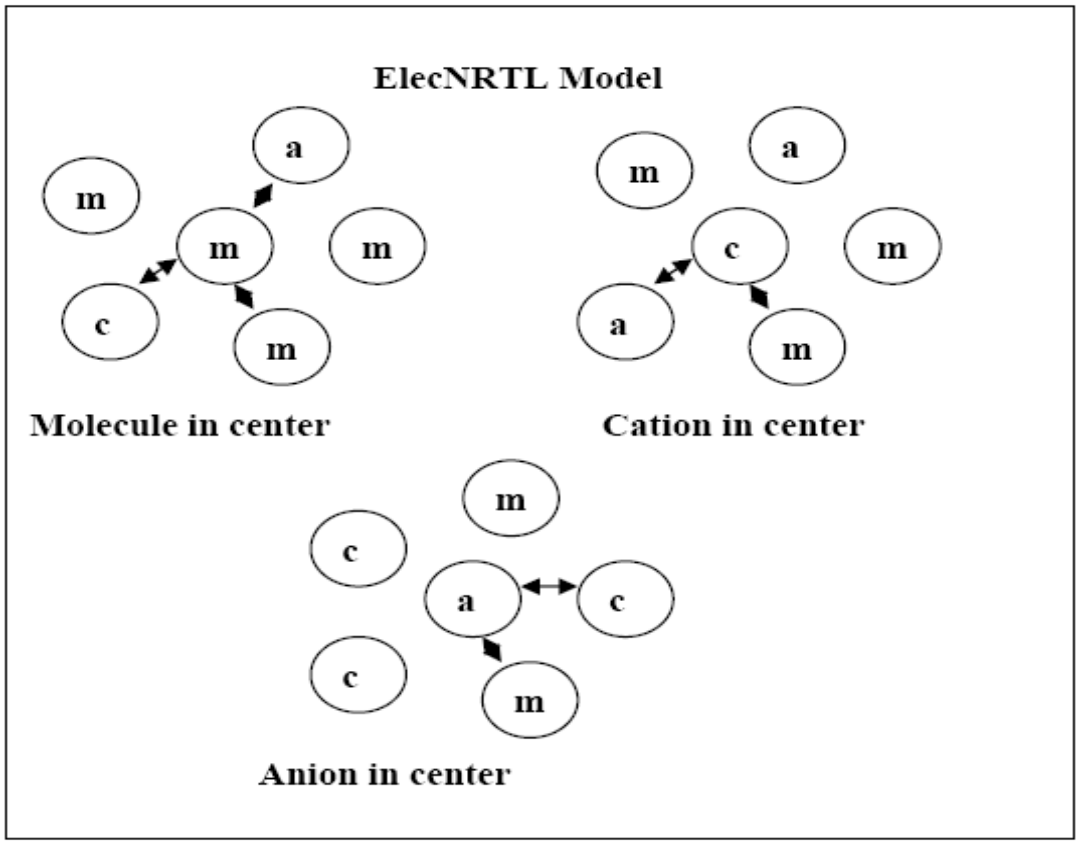

Figure 9: Molecular interactions in the ElecNRTL activity coefficient model.

The extra interactions of ions in ElecNRTL model are due to the local compositions. The ElecNRTL model is a versatile method for the calculation of activity coefficients. It can calculate activity coefficients for ionic species and molecular species in aqueous electrolyte systems, as well as mixed solvent electrolyte systems. ElecNRTL can handle electrolyte solutions of any strength, and it is well suited for solutions with multiple solvents and dissolved gases. The flexibility of the model makes it very suitable for any low-to-moderate pressure application. Using binary and pair parameters, the model can represent aqueous electrolyte systems, as well as mixed solvent electrolyte systems over the entire range of electrolyte concentrations. The electrolyte NRTL model uses an infinite dilute aqueous solution as the reference state for ions. Water must be present in the electrolyte system, in order to compute the transformation of the reference state of ions. Thus, it is necessary to introduce a trace amount of water to use the model for non-aqueous electrolyte systems. The Aspen Plus physical property system uses the ElecNRTL model to calculate the activity coefficients, enthalpies, and Gibbs energies for electrolyte systems. The adjustable parameters for the electrolyte NRTL model include:

- Pure component dielectric constant coefficients needed for molecular species;
- Enthalpy and Gibbs free energy of ions in water;
- Partial molar heat capacity of ions in water;
- Equilibrium constant of reactions from fundamental thermodynamics or curve fitted data;
- NRTL parameters for molecule-molecule, molecule-electrolyte, and electrolyte-electrolyte pairs;
- Born radius of ionic species;

- ElecNRTL pair parameters for ion pairs with molecular species.

In the electrolyte process calculation, the following thermophysical properties are computed at a given temperature, pressure and composition:

- Activity coefficient;
- Enthalpy;
- Reference state Gibbs energy.

These properties are necessary to perform the phase equilibrium, chemical equilibrium, and mass and energy balance calculations. Activity coefficients are the most critical properties for each process calculation. They determine the flow rates, compositions, and stability of phases in the Cu-Cl cycle.

Chen and Evans [47] developed an excess Gibbs energy expression, which contains two contributions: (i) a contribution for the long-range ion-ion interactions that exist beyond the immediate neighborhood of a central ionic species, and (ii) another contribution related to local interactions that exist in the immediate neighborhood of any central species. The non-symmetric Pitzer-Debye-Hückel model will be used to represent the contribution of these long-range ion-ion interactions. The Born equation is used to account for the transformation of the reference state of ions from the infinite dilute mixed solvent solution to the infinite dilute aqueous solution. The local interaction model is developed based on a symmetric model, with reference states of pure solvent and pure dissociated liquid electrolyte. The model is then normalized by infinite dilute activity coefficients, in order to obtain a non-symmetric model.

The NRTL expression for the local interactions, the Pitzer-Debye-Hückel model and the Born equation are combined to give an expression for the excess Gibbs energy of the mixture in the ElecNRTL activity coefficient model [36] leading to

$$\frac{G_m^{*E}}{RT} = \frac{G_m^{*E,PDH}}{RT} + \frac{G_m^{*E,Born}}{RT} + \frac{G_m^{*E,k}}{RT} \tag{3.26}$$

where G_m^{*E} denotes the excess Gibbs energy of the mixture, $G_m^{*E,PDH}$ denotes the excess Gibbs energy from the Pitzer-Debye-Hückel model, $G_m^{*E,Born}$ denotes the excess Gibbs energy from the Born model, and $G_m^{*E,k}$ denotes the excess Gibbs energy due to the local interaction of the ions and solvent.

Taking the appropriate derivative, the activity coefficient of a mixture using the ElecNRTL method can be expressed as follows:

$$\ln \gamma^* = \ln \gamma^{*PDH} + \ln \gamma^{*Born} + \ln \gamma^{*k} \tag{3.27}$$

In order to represent the long-range interaction contribution, the Pitzer-Debye-Hückel model is normalized with a mole fraction of unity for the solvent component and zero for the electrolyte [36], which leads to

$$\frac{G_m^{*E,PDH}}{RT} = -\left(\sum_k \chi_k\right)\left(\frac{1000}{M_B}\right)^{\frac{1}{2}}\left(\frac{4A_\varphi I_x}{\alpha}\right)\ln\left(1+\alpha I_x^{\frac{1}{2}}\right) \tag{3.28}$$

where χ_k denotes the mole fraction of component, k, M_B denotes the molecular weight of the solvent B, I_x denotes the ionic strength (mole fraction scale), A_φ denotes the Debye-Huckel parameter, and α denotes the "closest approach" parameter.

The Debye-Huckel parameter, A_φ, in equation (3.28) is expressed as:

$$A_\varphi = \frac{1}{3}\left(\frac{2\pi N_A \rho}{1000}\right)^{\frac{1}{2}}\left(\frac{Q_e^2}{\varepsilon_w k T}\right)^{\frac{3}{2}} \tag{3.29}$$

where N_A denotes Avogadro's number, ρ denotes the density of the solvent, k denotes the Boltzmann constant, Q_e denotes the electron charge and ε_w denotes the dielectric constant of water.

The ionic strength of the solvent is given by:

$$I_x = \frac{1}{2}\sum_i \chi_i Z_i^2 \tag{3.30}$$

where Z_i represents charge number of ion, i.

The activity coefficient of component i, due to the long range interaction from equation (3.28), can therefore be derived as follows:

$$\ln \gamma_i^{*PDH} = -\left(\frac{1000}{M_B}\right)^{\frac{1}{2}} A_\varphi \left[\left(\frac{2Z_i^2}{\alpha}\right)\ln\left(1+\alpha I_x^{\frac{1}{2}}\right) + \frac{2Z_i^2 - 2I_x^{\frac{3}{2}}}{1+\alpha I_x^{\frac{1}{2}}}\right] \tag{3.31}$$

The excess free energy due to the Born model from equation (3.26) is given by:

$$\frac{G_m^{*E,Born}}{RT} = \frac{Q_e^2}{2kT}\left(\frac{1}{\varepsilon}-\frac{1}{\varepsilon_w}\right)\left(\frac{\sum_i \chi_i Z_i^2}{r_i}\right)10^{-2} \tag{3.32}$$

where r_i denotes the Born radius of component i, and T denotes temperature.

The activity coefficient of component i, due to the transfer of ionic species from the infinite dilute state in a mixed-solvent to the infinite dilute state in the aqueous phase, is given by:

$$\ln \gamma_i^{*Born} = \frac{Q_e^2}{2KT}\left(\frac{1}{\varepsilon} - \frac{1}{\varepsilon_w}\right)\frac{Z_i^2}{r_i}10^{-2} \tag{3.33}$$

The equation for the molar Gibbs energy of an electrolyte mixture using the ElecNRTL model is expressed as:

$$G_m^* = \chi_w \mu_w^* + \sum_k \chi_k \mu_k^\infty + \sum_j \chi_j \ln \chi_j + G_m^{*E} \tag{3.34}$$

where j denotes the component (gas or liquid), k denotes the ion or molecular solute (i) and μ denotes the thermodynamic potential.

The molar Gibbs energy of water, μ_w^*, is calculated from the ideal gas contribution of pure component, μ_w^p, as a function of the ideal gas heat capacity and departure function, which are both available in steam tables. That is,

$$\mu_w^* = \mu_w^{*ig} + \left(\mu_w^p - \mu_w^{*ig}\right) \tag{3.35}$$

where p denotes a pure component and ig denotes ideal gas.

The aqueous infinite dilution Gibbs energy is calculated from Henry's law as follows:

$$\mu_k^\infty = \mu_k^{*ig} + RT \ln\left(\frac{H_{kw}}{P_{ref}}\right) \tag{3.36}$$

where P_{ref} in equation (3.36) represents the reference pressure.

The excess Gibbs energy, G_m^{*E}, is calculated from equation (3.26).

The ElecNRTL enthalpy model is given by:

$$H_m^* = \chi_w H_w^* + \sum_k \chi_k H_k^\infty + H_m^{*E} \tag{3.37}$$

The enthalpy of water, H_w^*, is calculated from the ideal gas model and steam tables.

$$H_w^* = \Delta_f H_w^{*ig} T_{ref} + \int_{T_{ref}}^{T} c_{pk}^{ig} dT + \left(H_w(T,P) - H_w^{ig}(T,P)\right) \tag{3.38}$$

The infinite dilution enthalpy is calculated using the following polynomial model:

$$H_k^\infty = \Delta H_k^{\infty,aq} T_{ref} + \int_{T_{ref}}^{T} c_{p,k}^{\infty,aq} \tag{3.39}$$

3.3 Thermodynamic Properties of Copper-Chlorine Mixtures

In this section, components in the Cu-Cl cycle will be examined and used to predict the behavior of the cycle. Two particular chemical components of the cycle exhibit interesting behaviors. CuCl is an essential component of the cycle that exhibits allotropy and undergoes phase change within the temperatures of interest in the Cu-Cl cycle. ANL [49,50] has experimentally validated some past data from Moscow State University (MSU) [51] that shows the properties of CuCl for certain temperatures. CuCl exists in a simple cubic crystalline (SC) form up to 685 K. Above this temperature, a beta-hexagonal (SB) form occurs up to 696 K, above which it melts to liquid (L). Using the enthalpy and Gibbs free energy of formation of the cubic crystalline CuCl form at the standard temperature of 298.15 K (-137 kJ/mol and -120 kJ/mol, respectively). The enthalpy of fusion for transition from beta-hexagonal solid to liquid at 696 K is 7.08 kJ/mol.

From MSU experiments, a thermodynamic correlation is formed to reflect the three forms of CuCl. The relationship for these three forms of CuCl is shown in figure 10.

From MSU data, the Cu-Cl specific heat dependence on temperature exhibits the relationships in the following equations [51]:

$$c_p(T)=173.778442133+38.206\ \ln x+0.001298\ x^{-2}+0.082339369657\ x^{-1}+191.575\ x \quad (3.40)$$

$(x=T*10^{-4};\ 298.15<T<685\ K)$

$$c_p(T)=277.808151505+79\ \ln x+1.3657\ x^{-1} \quad (3.41)$$

$(x=T*10^{-4};\ 685<T<696K)$

$$c_p(T)=206.987753087+29.319\ \ln x+0.0583185\ x^{-2}-4.11701275112\ x^{-1}+74.09\ x \quad (3.42)$$

$(x=T*10^{-4};\ 696<T<1200K)$

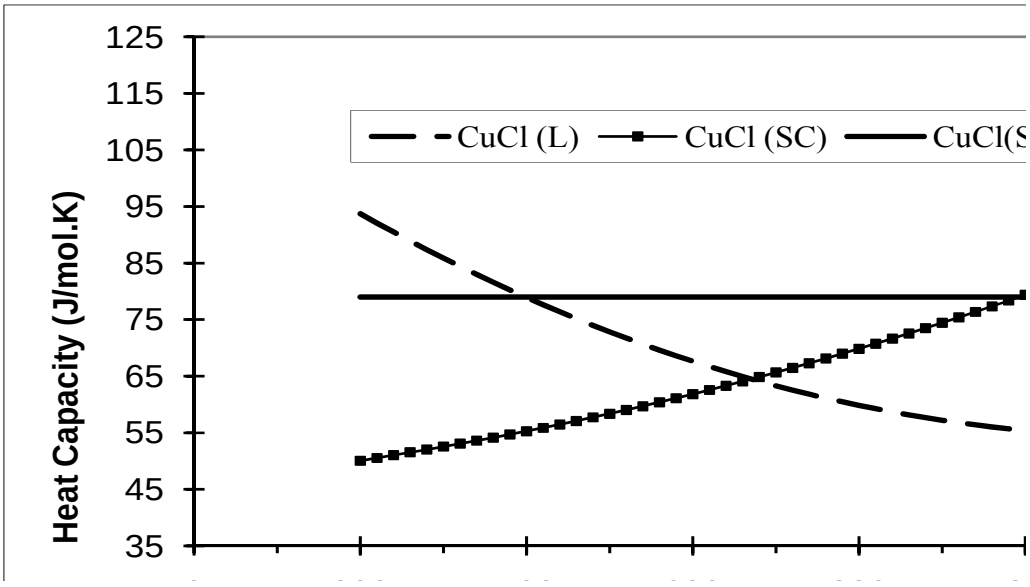

Figure 10: Heat capacities of different CuCl forms (data from Ref. [51]).

The heat capacities of the two solid forms were correlated in Aspen Plus using a vector parameter CPSPO1, which fits a c_P correlation as a function of temperature. The variable c_P of the beta-hexagonal form is kept constant at the value of 80 J/mol.K. The c_P

of the liquid form was correlated by the vector parameter CPIG, which again provides a function of temperature. The valid temperature ranges of each of the three c_P correlations in figure 10 are limited as specified in equations (2.40-2.42), but figure 10 shows their relationships in wide range of temperatures. The correlation for the solid cubic form of CuCl is valid up to the temperature of 685 K; the correlation for beta-hexagonal CuCl is valid from 685 to 696 K; and the range for liquid CuCl lies above 696 K. The parameters for the correlations have been chosen such that correlations will extrapolate reasonably with temperature, so the Aspen Plus simulation will not encounter computational problems.

The values of Gibbs free energy and enthalpy of formation of the cubic form at 298.15 K were set to standard values of -120 kJ/mol and -137 kJ/mol, respectively, since this is the stable form at the standard temperature. The Gibbs free energy and enthalpy values of the other two forms at 298.15 K were set to ensure the correct enthalpy of transition, and continuity in the value of free energy. This was accomplished by the standard-state values of free energy; then enthalpy of the beta-hexagonal form was obtained. The transition enthalpy value of 6.5 kJ/mol was obtained from the solid cubic form at 685 K. Then, continuity in the value of free energy was maintained at the same temperature. The analogous procedure was performed to deduce the standard state values of free energy and enthalpy for the liquid form of CuCl.

Using this approach, the relationships of enthalpies at the reference temperatures are shown in figure 11. This figure shows the temperatures at which the phase transition occurs, and also the enthalpy change associated with the phase transitions.

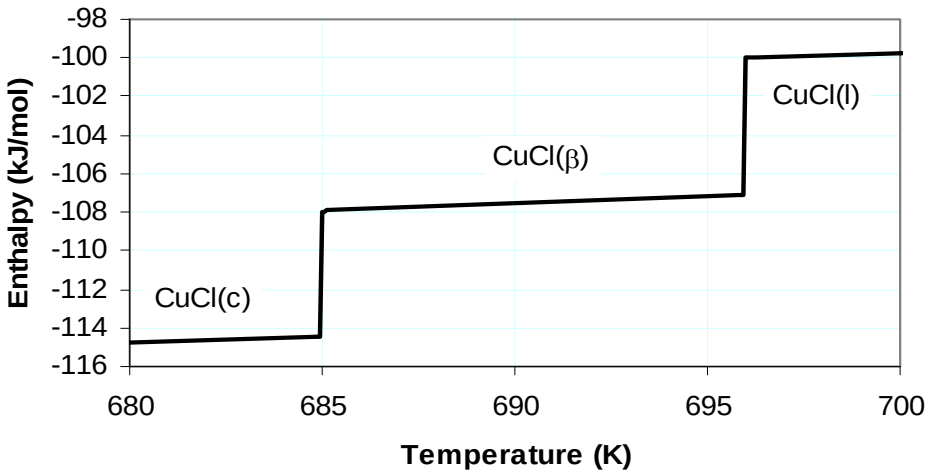

Figure 11: Relationships of different CuCl forms showing their range of existence (Ref. [49]).

The solubility of CuCl is another key property of the components that will be examined. This complex behavior occurs due to the presence of ionic species, which results from the dissociations of $CuCl_2$-CuCl-HCl in the presence of water. CuCl is sparingly soluble in water, but the solubility increases sharply with addition of HCl, whereas $CuCl_2$ is highly soluble in water but the solubility decreases with the addition of HCl, due to a common ion effect. Novikov et al. [52] have experimentally shown the behavior of the $CuCl_2$-CuCl-HCl-H_2O system. Figure 12 shows the relationships involving solubility of CuCl in $CuCl_2$, in the presence of various concentration levels of aqueous HCl at ambient conditions, using data from Novikov et al. [52].

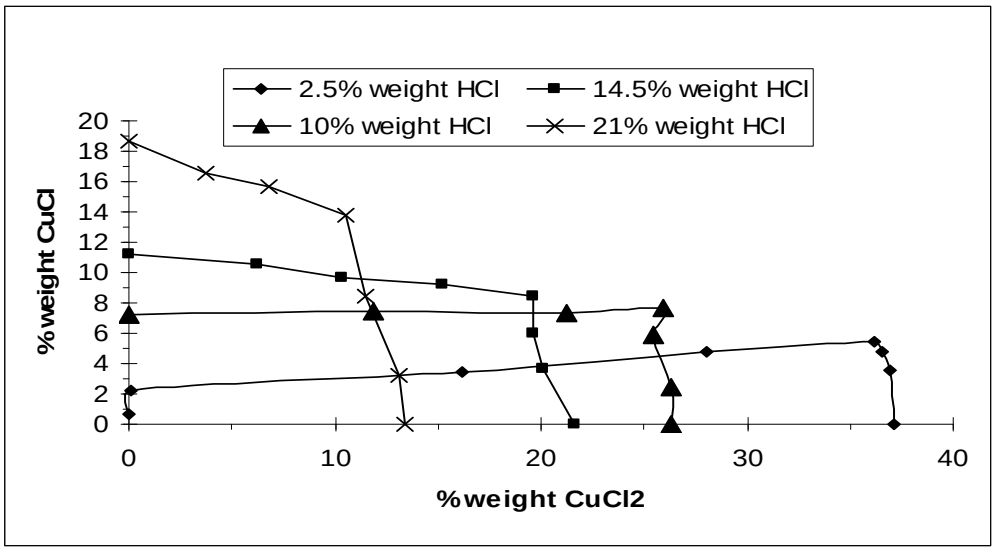

Figure 12: Solubility of CuCl in $CuCl_2$ at various HCl concentration levels (data from Ref. [51]).

The measured data were collected for HCl concentration levels by weight of 2.5%, 10%, 14.5% and 21%. Novikov et al. [52] reported an error margin for the solubility of CuCl in a $CuCl_2$-HCl solution of 1% or less at 25°C, and 4% or less at 40°C. In future research, experimental results will be compared with simulated data and a correction factor may be used. Mathias [49] evaluated and suggested the concentration levels of 4%, 12%, 17% and 26% by weight, so these will be used for the Aspen Plus modeling. The nearly constant horizontal lines in figure 12 indicate that precipitation of CuCl(s) and they were obtained by starting with a fixed aqueous HCl concentration level, and adding CuCl until precipitation starts. The declining vertical lines indicate precipitation of $CuCl_2.H_2O$ and they were calculated by starting with fixed aqueous HCl and adding $CuCl_2$ until precipitation starts. The point at which this sharp change occurs represents the equilibrium point for CuCl and $CuCl_2$. The model provides good insight into the behavior

of this system. Mathias [49] has indicated that the model slightly-over predicts the $CuCl_2$ solubility.

Cu_2OCl_2 is another important component of the Cu-Cl cycle that requires close examination. It is formed from the hydrolysis of $CuCl_2$. Physical properties for this component are not readily available in the Aspen Plus databank. ANL [19,31] has experimentally determined the properties of this component by heating equimolar mixtures of $CuCl_2$ and CuO. This study estimated the thermodynamic properties of this component using an Aspen Plus property estimation tool [36]. The heat capacity of Cu_2OCl_2 at various temperatures based on Aspen Plus estimation data is shown in figure 13. Experimental study obtained by ANL by heating Cu_2OCl_2 up to 530 ^oC has generated oxygen with a high yield. A major issue with this reaction is an undesirable reaction that produces chlorine gas. This chlorine gas would compete with $CuCl_2$ due to a common ion. The quantity of chlorine produced (although little or none) would add to the plant cost, in terms of gas separation and removal.

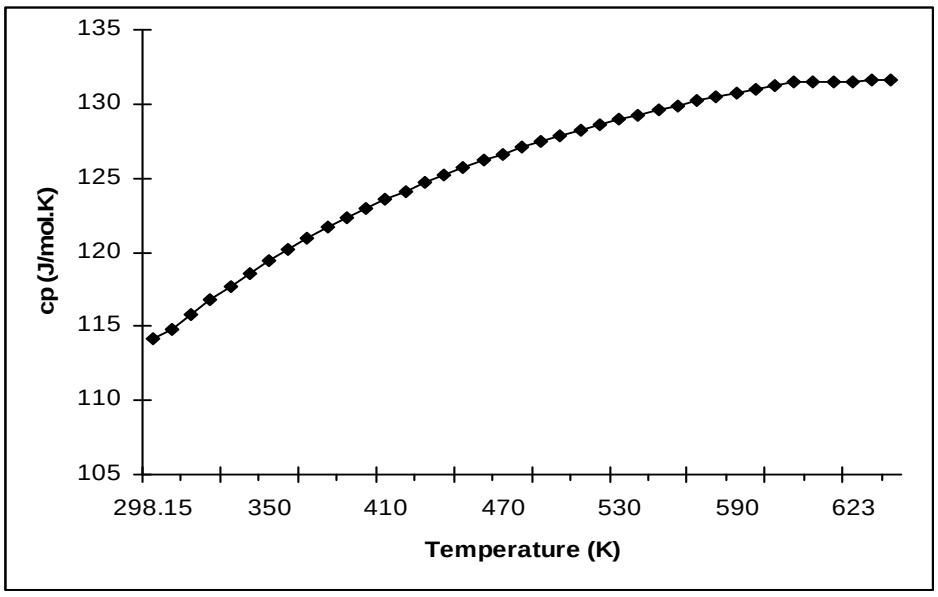

Figure 13: Heat capacity of Cu_2OCl_2 at various temperatures.

Using a thermokinetics approach, Rennels [53] has predicted the behavior of Cu_2OCl_2 using Differential Thermal Analysis (DTA) data. Using advanced numerical techniques, the reactivity of the Cu_2OCl_2 component over a broad temperature range was determined for temperature conditions in which experimental data was unavailable. Using a Freidman analysis [53], it can be shown that

$$\frac{d\alpha}{dt} = A\exp\left(-\frac{E}{RT(t)}\right)f(\alpha) \tag{3.43}$$

where $\frac{d\alpha}{dt}$ denotes the conversion rate of the reaction (J/s), E denotes the activation energy (J), A denotes the pre-exponential factor, $f(\alpha)$ denotes the model function, T denotes temperature (K), and t denotes time (s).

Friedman applied the logarithm of the conversion rate $\frac{d\alpha}{dt}$ as a function of the reciprocal temperature at any conversion α:

$$\frac{d\alpha}{dt} = A(\alpha)\exp\left(-\frac{E(\alpha)}{RT(t)}\right)f(\alpha) \tag{3.44}$$

$$\ln\left(\frac{d\alpha}{dt}\right) = \ln(A(\alpha)) - \frac{E(\alpha)}{RT(t)} + \ln(f(\alpha)) \tag{3.45}$$

Using this expression, the reaction rate of Cu_2OCl_2 can be predicted. Carrying out the thermal decomposition of Cu_2OCl_2 in a 100% oxygen environment will increase the temperature by only 50^oC vs. the reaction at 0% oxygen. The difference between an oxygen environment of 0% and 20% is almost insignificant. This study suggests that the reaction can be performed in air to reduce cost.

CHAPTER 4

PROCESS SIMULATIONS OF THE COPPER-CHLORINE CYCLE

4.1 Thermodynamic Energy Balance of the Copper-Chlorine Cycle

Consider the four-step process cycle given below, which was described earlier:

1 $$2Cu(s)+2HCl(g) \xrightarrow{450\ ^oC} 2CuCl(l)+H_2(g) \quad (4.1)$$

2a $$4CuCl(aq) \xrightarrow{25\ ^oC} 2CuCl_2(aq)+2Cu(s) \quad (4.2)$$

2b $$2CuCl_2(aq) \xrightarrow{90\ ^oC} 2CuCl_2(s) \quad (4.3)$$

3 $$2CuCl_2(s)+H_2O(g) \xrightarrow{450\ ^oC} Cu_2OCl_2(s)+2HCl(g) \quad (4.4)$$

4 $$Cu_2OCl_2(s) \xrightarrow{500\ ^oC} 2CuCl(s)+\frac{1}{2}O_2(g) \quad (4.5)$$

The overall reaction for the process of thermochemical water splitting is shown in figure 14.

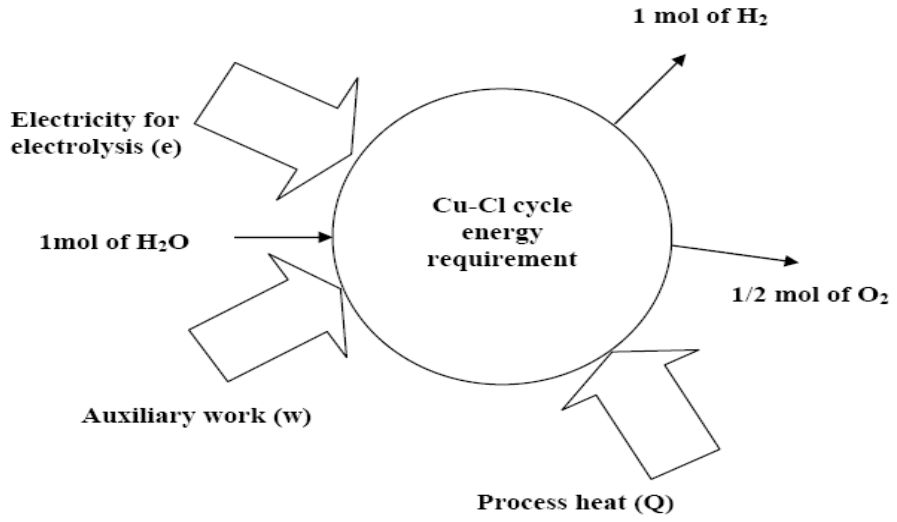

Figure 14: Representation of energy requirements in the Cu-Cl cycle.

The thermodynamic energy balances for the steps in the Cu-Cl cycle are formulated as follows:

Step 1: Hydrogen generation

$$2Cu(s)+HCl(g) \xrightarrow{450\ ^oC} 2CuCl(l)+H_2(g)$$

Heat input

- Heat required in vaporizing moisture from copper metal:

$$H_2O(l, 25\ ^oC) \longrightarrow H_2O\ (g, 100^oC) \tag{4.6}$$

- Heat required to heat copper from 25°C to the reaction temperature of 450°C:

$$Q= \int_{25}^{450} c_{p\,(Cu)}\, dT \tag{4.7}$$

- Heat required to heat hydrochloric acid from room temperature to the reaction temperature:

$$Q= \int_{25}^{450} c_{p\,(HCl)}\, dT \tag{4.8}$$

Heat output

- Heat recovered from recycling water vapor used for drying copper powder:

$$H_2O\ (g, 100^oC) \longrightarrow H_2O(l, 25^oC) \tag{4.9}$$

- Heat recovered from cooling hydrogen that was generated at 450°C:

$$H_2(g, 450^oC) \longrightarrow H_2(g, 25^oC) \tag{4.10}$$

- Heat recovered from cooling copper(I)chloride formed with hydrogen at 450°C:

$$2CuCl\ (l, 450^oC) \longrightarrow 2CuCl(s, 25^oC) \tag{4.11}$$

$$Q= (\Delta H_{CuCl})_{25,solid,C}^{450,liquid} \tag{4.12}$$

Considering the different forms of CuCl, the total heat recovered is calculated as:

$$Q= \begin{matrix}(\Delta H_{CuCl})_{423,liquid}^{450,liquid} + [(\Delta H_{CuCl})_{423,liquid,\beta}^{423,solid} + (\Delta H_{CuCl})_{412,solid,\beta}^{423,solid,\beta} \\ +(\Delta H_{CuCl})_{412,solid,C}^{412,solid,\beta}] + (\Delta H_{CuCl})_{25,solid,C}^{412,solid,C}\end{matrix} \tag{4.13}$$

- Heat of formation of hydrogen at 450°C:

$$Q=\left(\Delta H^{o}_{f_{(H_2)}}\right)^{450\,^{o}C} \tag{4.14}$$

Step 2a: Electrolysis process at ambient temperature

$$4CuCl(aq) \xrightarrow{25\,^{o}C} 2CuCl_2(aq)+2Cu(s)$$

- This step requires electricity input which is expressed as an equivalent heat load for the efficiency conversion.

$$4CuCl(aq) + 4Cl^{-}(aq) \longrightarrow 4CuCl_2^{-}(aq) \tag{4.15}$$

$$4CuCl_2^{-}(aq) \longrightarrow 2CuCl_2(aq) + 4Cl^{-}(aq) + 2Cu(s) \tag{4.16}$$

Step 2b: Drying of copper(II)chloride

- Heat input required to vaporize water from the copper(ii)chloride solution:

$$2CuCl_2(aq, 25^{o}C) \longrightarrow 2CuCl_2(s, 90^{o}C) \tag{4.17}$$

This step will be performed by means of a spray dryer to minimize particle entrainment.

Step 3: Hydrolysis of copper(II)chloride using steam

$$2CuCl_2(s)+H_2O(g) \xrightarrow{450\,^{o}C} Cu_2OCl_2(s)+2HCl(g) \tag{4.18}$$

Heat input:

- Heat required to vaporize water:

$$Q=\left(\Delta H_{H_2O}\right)_{25^{o}C}^{100^{o}C} \tag{4.19}$$

- Heat required to heat copper(II)chloride to reaction temperature:

$$Q=\int_{25}^{400} c_{p(CuCl_2)}\,dT \tag{4.20}$$

- Heat of formation of copper(ii)chloride:

$$Q=\left(\Delta H^{o}_{f_{(CuCl_2)}}\right)^{400\,^{o}C} \quad (4.21)$$

Heat output:

- Heat recycled from water vapor:

$$H_2O\ (g,\ 100\ ^{o}C) \longrightarrow H_2O\ (l,\ 25^{o}C) \quad (4.22)$$

- Heat recovered from the gas product:

$$HCl\ (g,\ 400\ ^{o}C) \longrightarrow HCl\ (aq,\ 25^{o}C) \quad (4.23)$$

Step 4: Oxy-decomposition of copper(II)oxochlorate(I)

$$Cu_2OCl_2(s) \xrightarrow{500\ ^{o}C} 2CuCl(s)+1/2O_2(g) \quad (4.24)$$

Heat input:

- Heat required to raise the temperature to 500^{o}C:

$$Q=\int_{400}^{500} c_{p(Cu_2OCl_2)}\,dT \quad (4.25)$$

- Heat of reaction at 500 ^{o}C:

$$Q=\left(\Delta H^{o}_{f_{(Cu_2OCl_2)}}\right)^{500\ ^{o}C} \quad (4.26)$$

Heat output:

- Heat recovered from oxygen gas:

$$O_2\ (g,\ 500^{o}C) \longrightarrow O_2\ (g,\ 25^{o}C) \quad (4.27)$$

- Heat recovered from copper(I)chloride:

$$CuCl\ (l,\ 500^{o}C) \longrightarrow CuCl\ (l,\ 25^{o}C) \quad (4.28)$$

$$Q=\left(\Delta H_{CuCl}\right)_{25,solid,C}^{500,liquid} \quad (4.29)$$

Considering the phase change of CuCl, the enthalpy change is calculated as follows:

$$Q=\begin{aligned}&(\Delta H_{CuCl})_{423,liquid}^{500,liquid}+[(\Delta H_{CuCl})_{423,liquid,\beta}^{423,solid}+(\Delta H_{CuCl})_{412,solid,\beta}^{423,solid,\beta}\\&+(\Delta H_{CuCl})_{412,solid,C}^{412,solid,\beta}]+(\Delta H_{CuCl})_{25,solid,C}^{412,solid,C}\end{aligned} \quad (4.30)$$

The results of the thermodynamic analysis of the reactions and processes in the Cu-Cl cycle for hydrogen production are shown in table 2. All the exothermic heat is denoted by a negative sign. The basis for the calculations is 1 mol of H_2O to produce 1 mol H_2 and ½ mol of O_2.

Table 2: Thermodynamic data for the Cu-Cl cycle and energy balances

Process Reactions	**T (in)**	**T (out)**	**ΔH**
	^oC	**^oC**	**kJ**
Exothermic Reactions			
H_2(g, 450^{o}C) → H_2(g, 25^{o}C)	450	25	-12.2
½ O_2(g, 500^{o}C) → ½ O_2(g, 25^{o}C)	500	25	-7.3
2Cu(s) + 2HCl(g) → 2CuCl(l) + H_2(g)	450	450	-46.8
2CuCl(l, 450^{o}C) → 2CuCl(s, 25^{o}C)	450	25	-80.8
H_2O (g, 100^{o}C) → H2O(l, 25^{o}C) (from Cu slurry and $CuCl_2$ solution)	100	25	-58.0
2CuCl(l, 500^{o}C) → 2CuCl(s, 25^{o}C)	500	25	-84.8
Total heat released from the process			-290.1
Total theoretical recovered heat (at 70% heat exchanger effectiveness)			-203.1
			Endothermic Reactions
2Cu(s, 25^{o}C) → 2Cu(s, 450^{o}C)	25	450	23.4
H_2O in Cu slurry (l, 25^{o}C) → vapor (g, 100^{o}C)	25	100	29.0
CuO*$CuCl_2$(s) → 2CuCl(l) + ½ O_2(g)	500	500	129.1
2$CuCl_2$(s) + H_2O(g) → CuO*$CuCl_2$(s) + 2HCl(g)	400	400	116.6
2HCl(g, 400^{o}C) → 2HCl(g, 450^{o}C)	400	450	3.0
H_2O(l, 25^{o}C) → H_2O(g, 400^{o}C)	25	400	57.7
2$CuCl_2$(s, 25^{o}C) → 2$CuCl_2$(s, 400^{o}C)	25	400	54.1
2$CuCl_2$(aq, 25^{o}C) → 2$CuCl_2$(s, 25^{o}C) (with spray drying at 90^{o}C)	25	70	83.1
H_2O in $CuCl_2$ solution (l, 25^{o}C) → vapor (g, 100^{o}C)	25	100	29.0
Total endothermic reaction heat required			525.2
Minimum heat required by cycle (ΔH_{net})			322.1

The total heat released by the exothermic reactions is 290.1 kJ per mole of H_2O. Assuming some of the reaction heat has a low quality and temperature, rendering it difficult to recover, a heat exchanger effectiveness of 70% is assumed based on an average effectiveness of cross flow heat exchangers [54]. In this assumption, 203.1 kJ of heat is recovered from the exothermic reaction heat.

The reaction heat for the endothermic processes is about 525.2 kJ, and the net process heat required for the reactions is 322.1 kJ. Since one of the steps involves electrolysis, the electrolytic power requirement is calculated using the expression:

$$\Delta G = -nFE \tag{4.31}$$

where F denotes Faraday's constant (96485), E is the cell potential of the cells and n is the number of transferred electrons. Lewis et al. [21] and Li and Suppiah [29] have shown that a voltage of 0.5 V can be assumed for the electrolysis step, based on a similar process for the Sulfur-Iodine cycle [23]. For the electrochemical cell, it is difficult to maintain a high current density at a low potential. Ongoing research aims to keep the current density as high as possible, with a low voltage, to reduce the energy consumption. The electrochemical energy requirement for the process, assuming a 50% conversion efficiency for heat to electricity based on a similar process [19], is 192.6 kJ.

About 28 kJ of work is assumed for input to the auxiliary equipment [32]. This is the work input required to operate pumps, compressors and so forth. The total theoretical energy required for the process is calculated as the sum of the net process heat, electrical energy (converted to heat) and auxiliary work. This becomes 322.1 kJ + 192.6 kJ + 28 kJ. Thus the total theoretical heat requirement for the cycle will be 542.7 kJ per mole of H_2O. The energy efficiency (η) of this cycle is expressed as the ratio of the energy released by

burning 1 mole of hydrogen to the corresponding energy required to produce 1 mole of the gas. That is,

$$\eta = \frac{\text{LHV}}{Q + e + W} \tag{4.32}$$

where LHV denotes the lower heating value of hydrogen (the energy released by burning hydrogen), Q is the net process heat of the reaction (the difference between the endothermic and exothermic process heat), e is the electrical work required for the reaction (converted electrical energy used for the electrolysis process), and W is the auxiliary work required by pumps, compressors, etc. The efficiency of the cycle using the lower heating value becomes as follows, where the value for LHV of hydrogen used in this calculation is taken from Refs. [7,19]:

$$\eta = \frac{241.83}{322.1 + 192.6 + 28} = \frac{241.83}{542.73} = 45\% \tag{4.33}$$

This efficiency calculation does not include actual heat losses across the heat exchangers. Appropriate heat duty matching and efficiencies for the heat exchangers will be determined by experimentation, and then used to determine the heat exchanger material and type. Consequently, a complete analysis will be undertaken of the heat exchanger networks. The detailed heat exchanger analysis will provide the logarithmic mean temperature differences for the heat exchangers, the approach temperature, and other relevant parameters. Heat exchangers used for processes like this are normally very efficient. This study, nonetheless, assumes a 70% effectiveness. This value seems reasonable based on data reported in the literature [54] for cross flow heat exchangers, which varies between 65% and 85%. However, a sensitivity analysis was carried out and showed that a heat exchanger effectiveness of 50% will reduce the overall efficiency of

the cycle by 5% while an effectiveness of 85% will increase the cycle efficiency by 3.5%. The efficiency calculated in this analysis is not expected to deviate significantly due to the heat exchanger network, because the drying step aims to utilize low grade heat from the moderator and condensers of the nuclear plants, which is expected to offset the inefficiencies in the heat exchangers. The above efficiency calculations yield results fairly close to those obtained for the S-I cycle (as expected) as well as those reported in Refs. [19-23] for other studies, which provide useful verifications of the formulation. This analysis is performed for the four-step cycle only. The three-step cycle is not considered here because research is being carried out presently on the electrochemical cell of the three-step cycle to determine appropriate material, operating conditions etc., making it difficult to carry out an energy balance across the electrolyzer.

4.2 Aspen Plus Simulation of the Four-step Copper-Chlorine Cycle

In this section, an Aspen Plus simulation of the Cu-Cl cycle will be presented based on property values in previous sections and conditions discussed in previous chapters. Aspen Plus has the capability of estimating thermophysical properties for components that are not present in the Aspen Plus database, using a combination of experimental data, structural and molecular formulae. An "Electrolyte Non Random Two Liquid" (ElecNRTL) activity coefficient model is used for the modelling processes in stoichiometry reactors. Also, the Soave-Redlich-Kwong (SRK) cubic equation of state is used to evaluate component properties and phase equilibria in steps that involve vapour-liquid phase change. This method can handle supercritical components of the cycle that

do not form liquid, thereby handling both vapour-liquid phases for large ranges of temperature. The methods determine the critical point for the mixture.

The liquid phase equilibrium in the unit operation has physical property and phase equilibrium calculations. Based on process steps outlined in chapter 2 and the physical property analysis in chapter 3, a process flow diagram (PFD) for this cycle has been developed. This PFD was developed based on a sequential modular simulation. All reactors operate without errors, and hydrogen and oxygen gases are separated using a Sep 2 block. The process flow diagram of the four-step Cu-Cl cycle is shown in figure 15. The process flow diagrams used for this simulation build on past work at ANL [19-21], accessing experimental data from previous works. Unlike past studies, the process flow diagram simulations in this study represent the first completed and closed loop flowsheet simulation of the Cu-Cl cycle. The electrochemical step of the cycle is simulated separately and the results transferred to the whole cycle. This is necessary in order to eliminate recycling in the blocks.

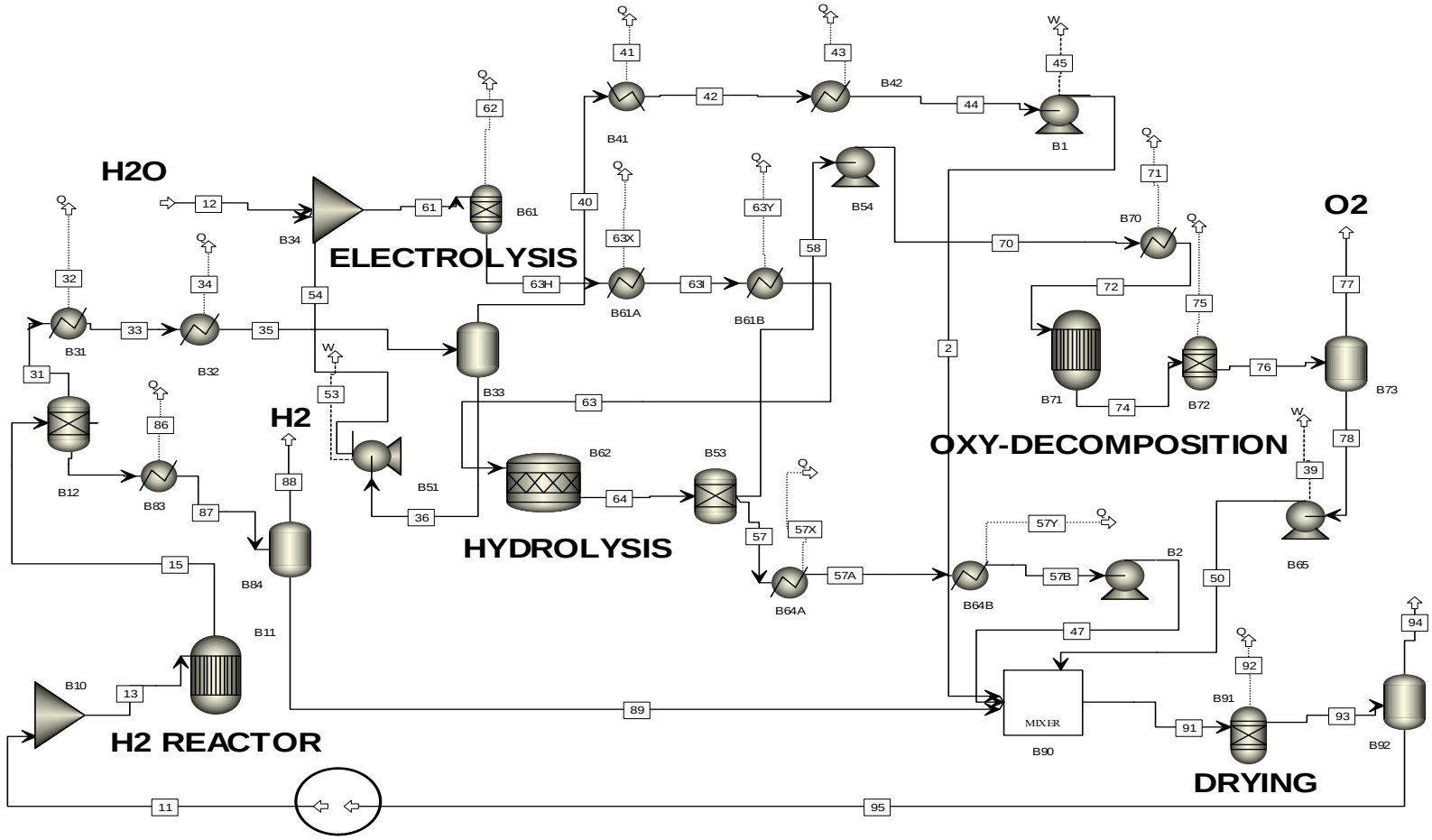

Figure 15: Process flow diagram of four-step thermochemical cycle of hydrogen production with Cu-Cl cycle (Ref. [19]).

In the process flow diagram in figure 15, the stoichiometry reactor B11 performs the hydrogen generation process through the reaction of copper metal and hydrochloric acid. The hydrogen gas generated is separated by the Sep2 unit operation B51 and hydrochloric acid gas is recycled. Hydrolysis occurs in the stoichiometry reactor B62. This reaction takes place in a vacuum, to eliminate the effects of fuming hydrochloric gas. Reactor B71 is used to simulate the oxy-decomposition reaction, where oxygen gas is released and separated using the Sep2 block B73. The drying step of the cycle is performed in the unit operation B91. The electrolysis step is carried out independently and the results are linked back to the entire cycle, to avoid the problem of recycling in the electrolyzer. All reactions go to completion to yield the products, by specifying a conversion rate of 99.99% for the simulation. A brief description of each component in figure 15 is summarized in the appendix.

Heat exchangers are used to supply the required heat at each process step and also recover heat from exothermic processes. Mixers and splitters are used to combine and split the components. High efficiency pumps are used to transfer components from one unit operation to the other, and supplying the required water for each process. Using the thermodynamic methods in the previous sections and specifying the operating conditions from experimental data, the Cu-Cl cycle was simulated successfully. The reactors calculate the heat of reactions at the specified reference conditions, per mole or mass of the reference reactant selected for each reaction. The corresponding energy requirements, input and output temperatures, and other data for the processes at various transfer points are shown in table 3. An input of 100 mol of water yields 100 mol of hydrogen and 50

mol of oxygen. On this mole basis, an energy balance of the cycle and the corresponding efficiency are evaluated.

Table 3: Heat balance results for the four-step process simulation

Heat Exchangers	**Q (kJ)**	**T (in) (^{o}C)**	**T (out) (^{o}C)**
32	7,494.4	25	100
34	24,409.2	100	116
41	-23,186.0	116	105
43	-2,833.6	105	25
57X	-10,736.5	400	90
57Y	32,092.3	90	90
62	-1,552.6	113	90
63X	-9,697.0	90	27
63Y	55,382.1	27	425
71	559.7	425	550
75	-2,718.9	550	25
86	35.1	25	25
92	-17,513.4	117	25
Process heat flow for cycle/100 mol H_2O	51,734.0		
Process heat flow/mol H_2	517.3		
Auxiliary (pump) work	26.4		
Total heat requirement for cycle	543.7		

Using the data in this table, the efficiency of the process cycle can be calculated. The net heat requirement for the cycle per mol of hydrogen is 517.3 kJ. The auxiliary work required to drive pumps is 26.4 kJ. The total heat required to produce 1 mole of hydrogen using the Cu-Cl cycle is therefore 543.7 kJ. The energy efficiency of the cycle is calculated using equation (4.32) as follows:

$$\eta = \frac{241.8}{517.3 + 26.4} = 44.5\% \qquad (4.34)$$

The predicted cycle efficiency agrees well with past results obtained by Lewis [19-21], Rosen and Scott [14] and Yildiz and Kazimi [15].

A drawback of the four-reaction cycle involves the electrolyzer, which produces very finely divided copper powder that is needed for the hydrogen generation reaction. For this simulation, the issues of the form of the components are not a major concern because Aspen Plus is designed to handle solid transfers. Also this simulation is performed with the assumption of minimal entrainment.

4.3 Aspen Plus Simulation of the Three-step Copper-Chlorine Cycle

An alternative process route is being investigated via a three-step cycle that would minimize the solid handling associated with the four-step cycle, The three-step process cycle combines two reaction steps of the four-step cycle (eqns. 4.1 and 4.2). Instead of hydrogen being produced by the reaction of HCl and Cu, and subsequent electrolysis of CuCl to produce Cu, an alternative route is taken. In the three-step process cycle, hydrogen gas is generated through the reaction of CuCl and HCl using an electrochemical cell. This cycle is developed with the objective of minimizing entrainment due to solid handling in the actual plant. Li et al. [29] have experimentally demonstrated the feasibility of this cycle at AECL. A major drawback of this cycle is that presently no material has been conceived that could withstand the highly corrosive hydrochloric acid at high pressure. Also no material has been identified for the design of an efficient membrane for separation of the gases. This study used stoichiometric reactors for the simulation of the cycle. Using the ElecNRTL model, attempts were made to capture all electrolyte components and non-condensable components (Henry's components). The process flow diagram for this process route is shown in figure 16.

The steps of this process route are reiterated below:

Step 1: $2CuCl + 2HCl \rightarrow 2CuCl_2 + H_2$ (100°C) (4.35)

Step 2: $2CuCl_2 + H_2O \leftrightarrow Cu_2OCl_2 + 2HCl$ (430°C) (4.36)

Step 3: $Cu_2OCl_2 \rightarrow 2CuCl + \frac{1}{2} O_2$ (550°C) (4.37)

Hydrogen is generated in an electrochemical cell. Past studies have used mechanistic modelling of the electrolyzer for the hydrogen production step [30]. The Aspen Plus process flow diagram for this process was developed using a stoichiometric reactors. The electrolysis step is performed independently to avoid recycling.

The flowsheet in figure 16 depicts an Aspen Plus model for the three-step cycle. All reactions for the cycle are assumed to go to completion and yield the desired products. The flowsheet uses an input rate of 50 kmol/hr of water, which results in the production of 50 kmol/hr of hydrogen gas and 25 kmol/hr of oxygen gas. The electrolysis process is carried out in block B1. The hydrogen generated is separated in block B3. Hydrolysis takes place in block B22 and hydrochloric gas is separated in block B23. The oxy-decomposition reaction takes place in block B10 and oxygen gas is generated and separated in block B11. All separations in the PFD are implemented as perfect component separators that did not use flash blocks. For both simulations, the efficiencies of the component unit blocks, including pumps, valves, etc., is built into the software and is included in the energy balance calculation of the cycles, thereby allowing the overall efficiency of the cycles to be determined.

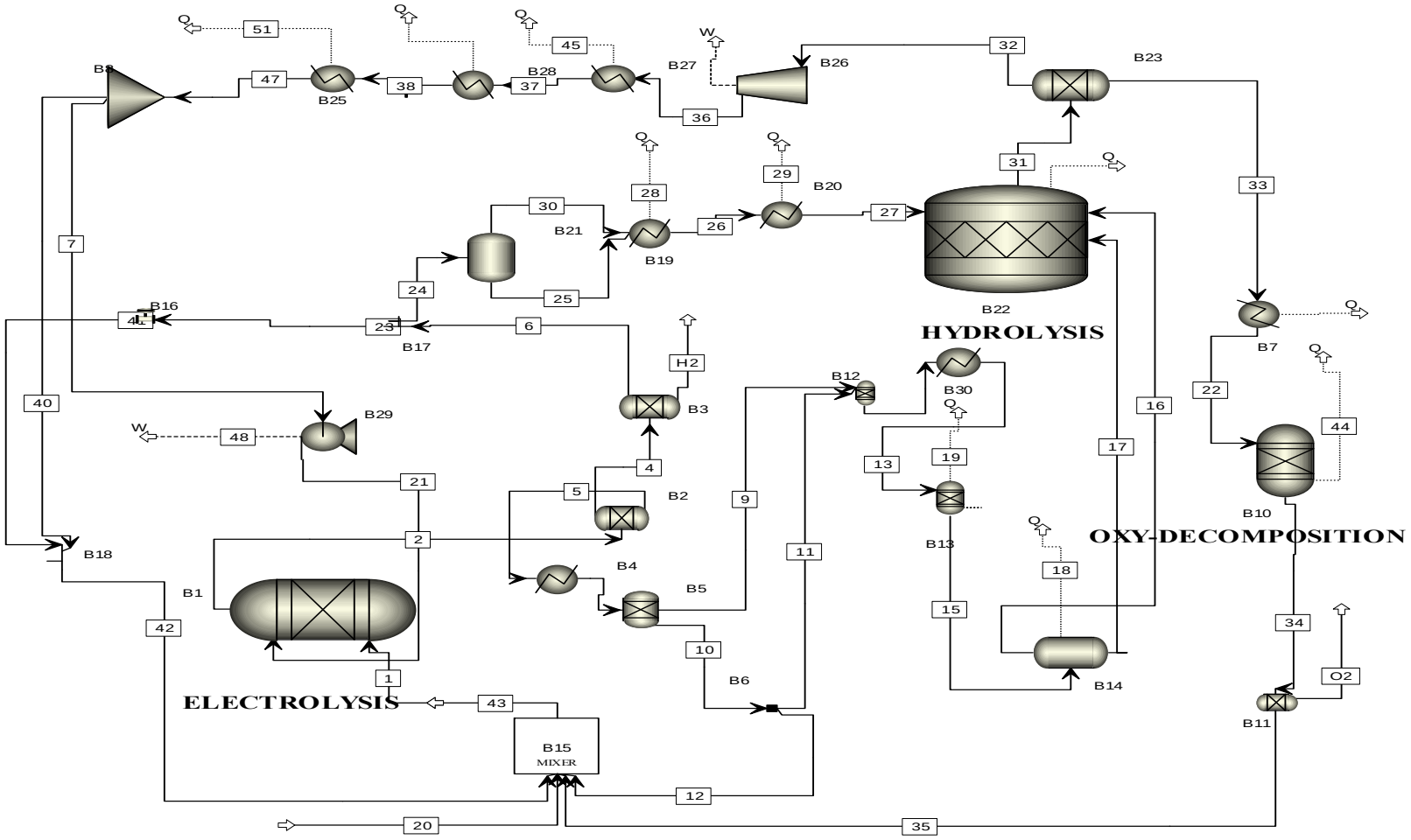

Figure 16: Process simulation of three-step Cu-Cl cycle (Ref. [31]).

Heat integration is accomplished in a systematic way, with high temperature outputs used to warm inputs to the same section. Heat exchange combinations are indicated by dashed lines and their streams are labeled by Q. Hydrogen is generated at 100°C and 23 bars in this simulation and oxygen is produced at 1 bar and 430°C. This temperature can be reduced to a more practical level through further heat integration. Valves and pumps are inserted to produce the desired pressure in each section of the flowsheet. The HCl regeneration step occurs in a vacuum at an absolute pressure of 0.3 bars, while the oxygen generation occurs at atmospheric pressure. The results from the three-step cycle simulation are shown in table 4.

Table 4: Energy balance of three-step process cycle

Heat Exchangers	**T (in) (^{o}C)**	**T (out) (^{o}C)**	**Q (kJ)**
3	400	400	-181.68
18	400	400	0.05
19	400	400	134.14
28	100	100	-1563.68
29	100	400	-414.15
39	400	540	-31.64
44	540	540	-230.51
45	489	116	631.24
46	116	110	2112.82
51	110	105	16.65
72	105	105	-20.12
73	105	22	104.97
Net Heat input			558.09
Work input			22.52
Total Heat requirement			584.73

From this table, the efficiency of the cycle using equation (4.32) is calculated as follows:

$$\eta = \frac{241.83}{558.09 + 22.52} = 41.65\% \tag{4.38}$$

The lower efficiency of this cycle can be attributed to the need for more electricity input as compared to the four-step cycle. This efficiency agrees closely with past studies of Lewis et al. [19-21], Law et al. [30] and Ferrandon et al. [31].

4.4 Model Sensitivity Analyses of Process Steps

Sensitivity analysis is a tool for determining how a process changes with varying key operating and design variables. It will be used to vary one or more flowsheet variables and study the effect of that variation on other flowsheet variables. It is a valuable tool for performing "what if" studies. The flowsheet variables are inputs to the flowsheet. A calculated variable cannot be varied, since otherwise a successful simulation would not be achieved, as either the simulation would ignore the variation, or variables that override a calculated variable would have errors. A sensitivity analysis can be used to verify if the solution to a design specification lies within the range of a manipulated variable. It can also be used to perform a process optimization.

The Sequential Modular simulation approach has advantages over an equation oriented approach. Sequential Modular sensitivity allows a user to perform several simulations with different values for specified input variables. A Sequential Modular sensitivity can perform a full factorial run on sets of values for one or more variables, or vary several variables separately while leaving all others at their base values, or run an arbitrary set of cases with specified values for the manipulated variables in each case. On the other hand, an Equation Oriented analysis calculates a partial Jacobian, providing the partial derivatives of a set of variables indicating their rate of change relative to a set of

manipulated variables. A major advantage of the Sequential Modular sensitivity over the Equation Oriented sensitivity is that the former allows user to investigate individual effect of variations at each step whereas the Equation Oriented approach performs all the sensitivity assessments simultaneously. Therefore, because the Sequential Modular approach solves one block at a time, it is often very straightforward to diagnose solution failures in this strategy. The Equation Oriented approach, on the other hand, solves all the blocks simultaneously and thus it can be difficult to pinpoint the exact cause of a failure. Also because the Equation Oriented sensitivity uses the current value of the Jacobian to calculate the sensitivity, it does not need to re-compute the model solution. However, it may be required to evaluate this for each sensitivity analysis to ensure that the Jacobian is up to date when the sensitivity analysis is performed, which may be too complicated and time consuming for a very large system.

A sensitivity analysis is carried out for the hydrolysis and oxy-decomposition reactors. The effects of operating conditions on the product yields will be analyzed below.

4.4.1 Oxy-decomposition Reactor

A process flow diagram (PFD) for the reactions in this process step is shown in figure 17, using the equation of state property method. A sensitivity block is created with a Sequential Modular sensitivity tool in the data browser. The variables are defined in a consistent manner and all input variables were specified.

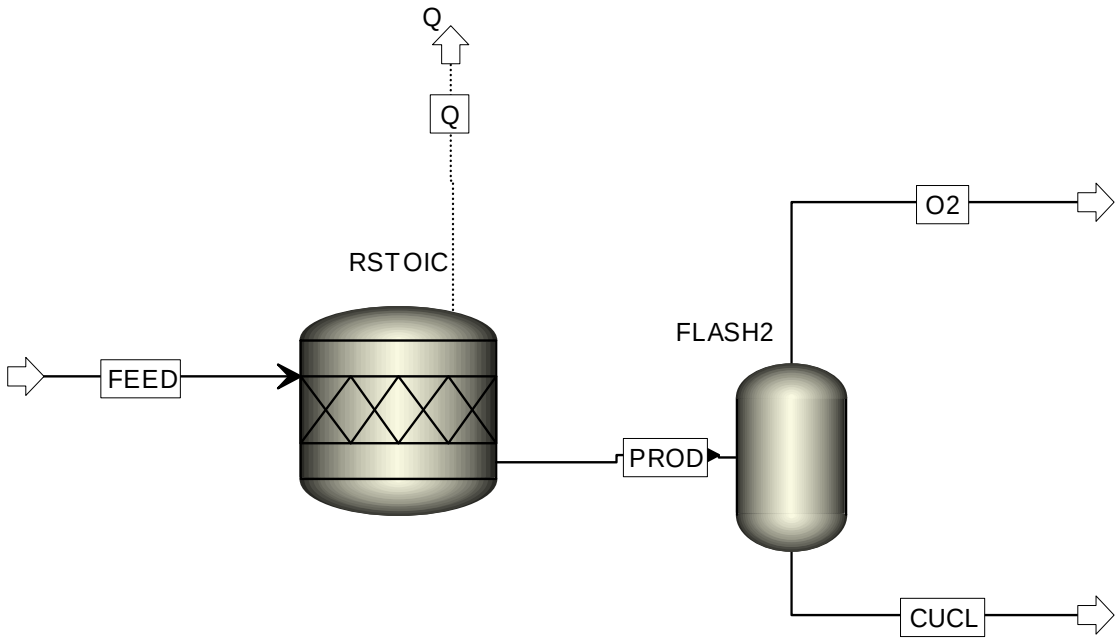

Figure 17: Process flow diagram of the oxy-decomposition reaction step.

Aspen Plus prepares sensitivity blocks automatically and these blocks create loops that are evaluated once for each row of the sensitivity table. A user can also manually arrange a sensitivity block using the Convergence Sequence Specifications sheet. After completing the sensitivity block input specification, the flowsheet is analyzed in Sequential Modular mode to generate tables and/or plots of simulation results, as functions of the feed stream, block input, or other input variables. The sensitivity analysis results are reported in a table on the sensitivity summary sheet. In this section, the simulation results are exported to an Excel spreadsheet. These results are based on the 99.99% conversion rate specified in the simulation. The results of the sensitivity analysis for the oxy-decomposition step are shown in table 5 and figure 18.

Table 5: Sensitivity results for ox-decomposition reactor

Temperature (^oC)	Oxygen Flowrate (kmol/hr)	Chlorine Flowrate (kmol/hr)	Temperature (^oC)	Oxygen Flowrate (kmol/hr)	Chlorine Flowrate (kmol/hr)
320	0.0024	0.0816	460	22.6443	4.7112
330	0.0097	0.1395	470	22.8921	4.2158
340	0.0197	0.2349	480	23.1114	3.7769
350	0.0393	0.3894	490	23.3057	3.3883
360	0.0766	0.6358	500	23.4779	3.0441
370	0.1467	1.0234	510	23.6305	2.7391
380	0.2756	1.6252	520	23.7657	2.4685
390	0.5069	2.0911	530	23.8858	2.2284
400	0.9139	2.3806	540	23.9925	2.0151
410	1.6211	2.6981	550	24.0873	1.8253
420	2.9889	3.1222	560	24.1718	1.6563
430	5.7808	3.6994	570	24.2472	1.5056
440	11.2037	4.3892	580	24.3145	1.3709
450	21.3823	5.1682	590	24.3747	1.2506

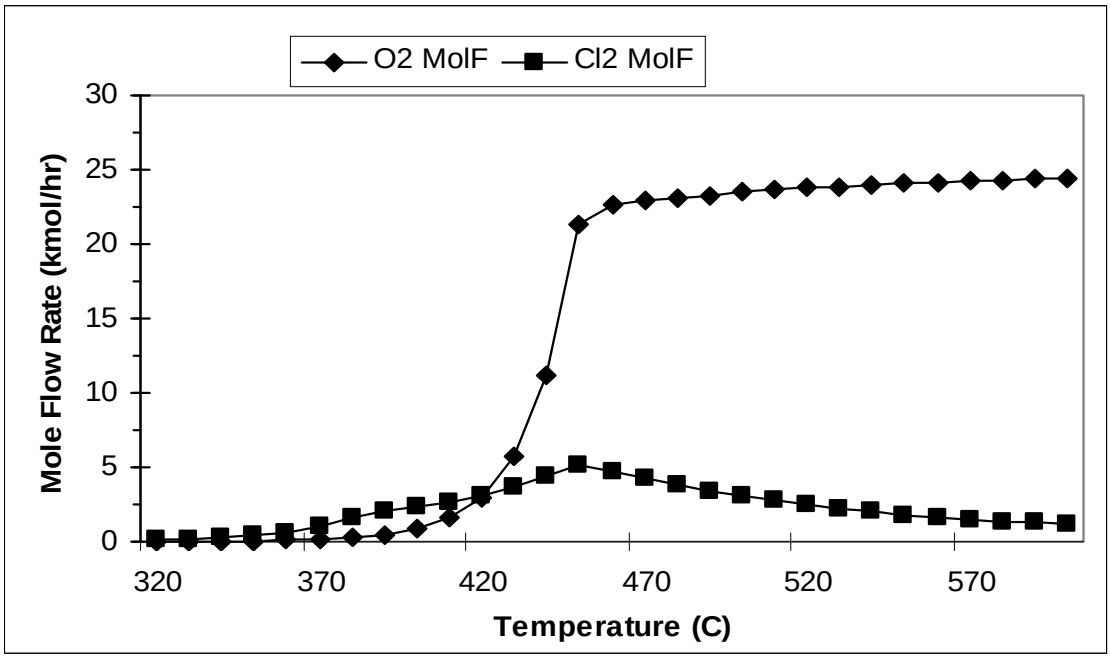

Figure 18: Sensitivity analysis of the oxy-decomposition reaction.

In this analysis, the effect of temperature change on oxygen production is investigated. For 50 kmol/hr of water input, the results show that oxygen generation starts at a temperature as low as 350^{o}C, with a low yield less than 1 kmol/hr. The oxygen yield increases to over 24 kmol/hr at 450^{o}C, and it remains fairly constant with an increase in temperature. This result is consistent with previous yield results that were reported for the complete process simulation of the cycle. Traces of chlorine gas are also observed in this model analysis. The chlorine gas production increases with temperature and peaks at about 450^{o}C, then starts declining as the temperature of the reactor is increased. At a reactor temperature of 550^{o}C, the rate of chlorine gas production is about 2 kmol/hr. At this low production capacity, it is not problematic, but becomes an important issue when the plant is scaled up. There is a need, therefore, to remove this chlorine gas as it would cause some problems if accumulated. In the previous simulation, the loops were open without recycling, to allow for chlorine removal. This undesirable chlorine production can be eliminated by better reactor designs and choice of operating conditions.

4.4.2 Hydrolysis Reactor

Using the same sensitivity procedure, an analysis was carried out for the hydrolysis reactor. An equilibrium reactor is used in this case, since this reaction is expected to reach equilibrium. The process flow diagram for this step is shown in figure 19.

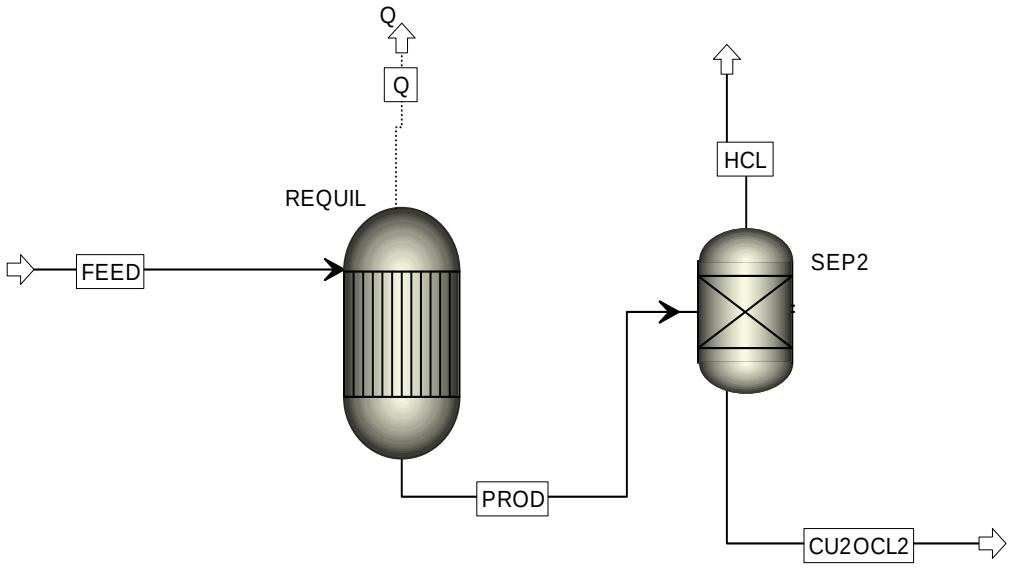

Figure 19: Process flow diagram of the hydrolysis reaction step.

The REquil reactor calculates the vapor liquid equilibrium of the reaction by solving the stoichiometric chemical and phase equilibrium equations. The Soave-Redlich-Kwong cubic equation of state property method is used, due to the presence of critical components at a high pressure. This analysis is performed at a fixed temperature of 430^{o}C. A two-phase separator is used to separate the hydrochloric gas from copper(ii)oxochloride. The results of the model analysis are shown in figures 20 and 21. For a high yield of hydrochloric acid, the water to copper ratio must be high. The current results are consistent with past experimental data of ANL [31]. ANL data have predicted a steam to copper ratio of 17, but this model indicates that a steam to copper ratio of 14 would be sufficient for high yield of the products.

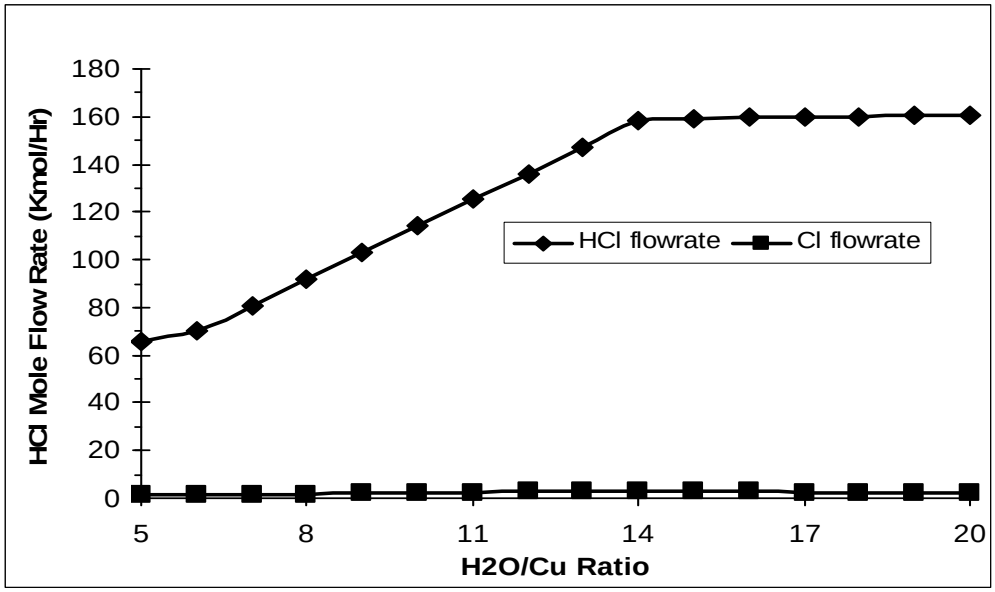

Figure 20: Effects of water/copper ratio on the yield of hydrochloric acid gas.

There are also traces of CuCl vapour and Cl gas production in this reaction. The rate of production of CuCl with temperature increase is shown in figure 21. The presence of CuCl vapour does not constitute a major problem, as it forms part of the components needed in one of the process steps. However, ANL [31] have experimentally demonstrated that the production of CuCl in the hydrolysis reactor would reduce the yield of Cu_2OCl_2. Traces of chlorine gas were present in this analysis as well. In a closed loop, this could poison the catalyst in the membrane of the electrolyzer. This study identified that production of CuCl increases with increased reactor duty due to temperature increase as shown in figure 21. ANL experiments [31] indicated that less CuCl is produced as the temperature decreases below 400^{o}C but the yield of Cu_2OCl_2 decreases as more $CuCl_2$ remained.

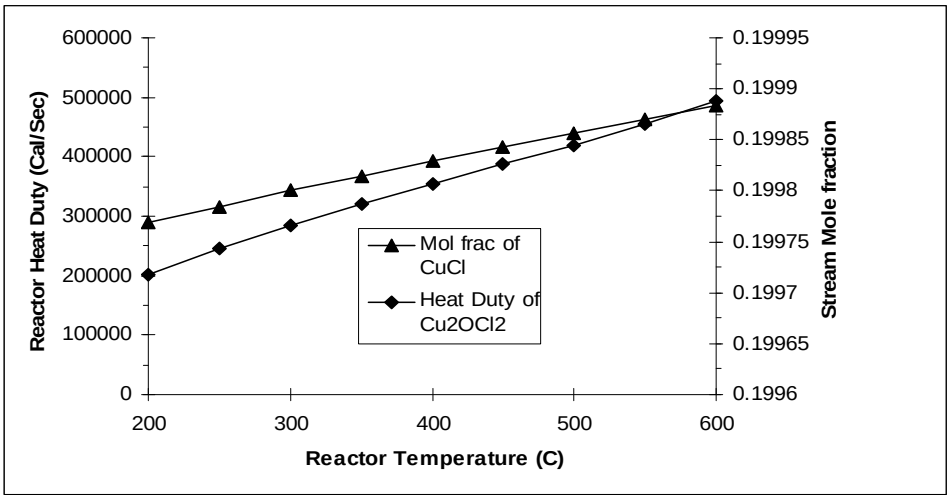

Figure 21: Effects of temperature on oxy-decomposition reaction.

4.4.3 Simultaneous Analysis of Three Reactors

The Calculator block is a user model in Aspen Plus, capable of performing calculations and manipulations of flowsheet variables. The Calculator block allows the specification of sampled and manipulated flowsheet variables. A FORTRAN code or Microsoft Excel spreadsheet can be inserted into the flowsheet computations to define values of the sampled variables and perform user-defined tasks. FORTRAN-based Calculator blocks can also perform other operations, such as writing information to the control panel or history file. When a sequential modular simulator is used to execute one unit operation at a time, a calculator sequence is used to specify when each Calculator block is executed. Before performing a Calculator block, it is pertinent to define which flowsheet variables are imported and exported to Aspen Plus from the Calculator block, and also the position of the Calculator block in the list of unit operation blocks. A FORTRAN subroutine was inserted into the flowsheet to calculate the efficiency of each of the three reactors simultaneously, at each temperature increment step.

A Calculator block was set up in Aspen Plus by the following steps [36]:

1. Creating the Calculator block from the "flowsheeting option" menu tool;
2. Identifying the flowsheet variables that the block samples or manipulates;
3. Entering the FORTRAN code that performs the user defined task;
4. Specifying when the Calculator block is executed;
5. Running and tabulating/plotting results.

For a step-wise increase in the temperature of each reactor, the simultaneous effects on the three reactors can be studied. The FORTRAN calculator performs a heat balance on the three reactors and computes the efficiency.

The results of the model analysis of the effects of temperature change on efficiency of the three reactors are shown in figure 22.

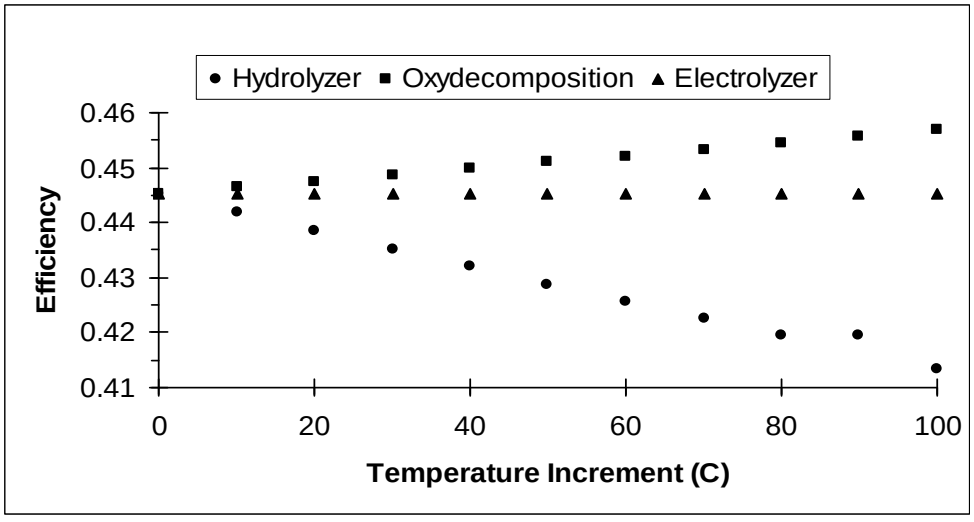

Figure 22: Effects of temperature increments on the efficiency of the reactors.

The results show that a temperature increment does not have a significant effect on the efficiency of the electrolyzer. The efficiency of the oxy-decomposition increases step wise with each temperature increment, while the efficiency of the hydrolyser drops drastically with stepwise temperature increments. This shows there is a need for effective optimization to balance these two trends.

It was discovered during the simulation setup for the two cycles, including the sensitivity simulations, that improper representation of component phases, relationships (chemical and physical) and invalid operating conditions would lead to errors in the simulation. Also simulation with Aspen Plus package does not allow user to manipulate the model equations that govern the simulation methods. Modification or overriding of intermediate stream results to suit inlet conditions of subsequent blocks also led to simulation errors. During the simulation of the Cu-Cl cycles in this study using stoichiometric reactors, a 99.99% conversion rate of the reactants was specified. Conditions that would result in lower yields led to simulation errors, and warnings in the control panel of the simulator.

4.5 Economic Analyses of Thermochemical Cycle for Hydrogen Production

In order to determine the viability of thermochemical hydrogen production with a copper-chlorine cycle, a comparison is made among the costs of hydrogen production using steam methane reforming (SMR), a sulfur-iodine (SI) cycle and a copper-chlorine (Cu-Cl) cycle, including the two process routes for the CuCl cycle described previously. This analysis is based on the cost per kilogram of hydrogen produced. A team of researchers, scientists and industry experts together developed a tool, called Hydrogen

Analysis (H2A) [55], that can be used in the analysis of different hydrogen production processes and their economics. H2A aims to improve the transparency and consistency of analyses, to improve understanding of the differences among analyses, and to seek better validation from industry, thereby providing consistent, transparent and comparable benchmarks in studies [56].

H2A approach uses a discounted cash flow rate of return analysis to determine the minimum hydrogen price required to attain a specified internal rate of return. Using the cash flow approach of H2A, the internal rate of return function calculates the interest rate at which the net present value (NPV) of the cash flow is zero. The H2A cash flow modeling tool is schematically shown in figure 23.

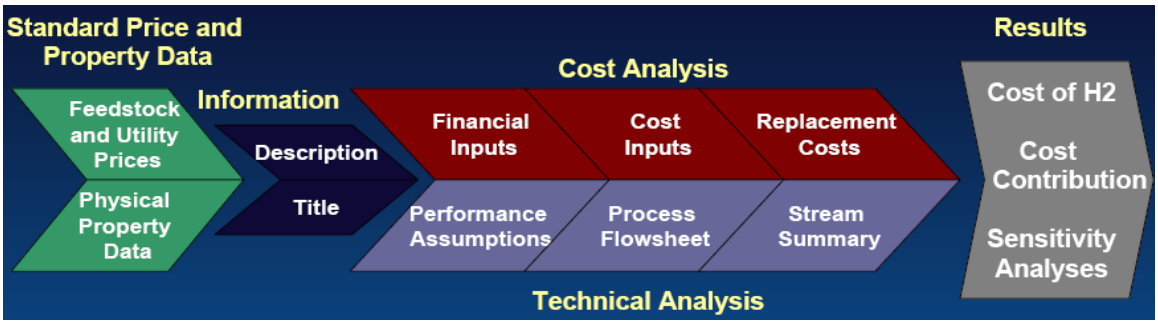

Figure 23: H2A cash flow modeling tool (Ref. [56]).

Williams et al. [57] have performed cost analyses of hydrogen production using steam methane reforming (SMR) technology. The cost of hydrogen production with this technology strongly depends on the cost of natural gas, which is used both as an energy source and a feedstock. At present, the cost of producing hydrogen by SMR varies between US$1.50/kg for large scale production (over 500 tons/day) and US$3.75/kg for small scale production (below 500kg/day), assuming a natural gas price of US$7.00/GJ.

Schultz [58] has estimated an additional US$0.20/kg cost for adding CO_2 sequestration to the SMR process.

Schultz [58] and Brown et al. [59] have reported the estimated cost of hydrogen production using a SI thermochemical cycle. For a hydrogen production plant capacity of 584 tons/day, the cost ranges from US$1.53/kg to US$2.01/kg of hydrogen, based on a 42% production plant efficiency.

Orhan [60] has performed a cost estimation for the four-step Cu-Cl cycle based on energy and exergy analyses of the cycle. That study applies the sixth-tenths-factor rule in determining the fixed capital investment and total production cost for a plant capacity of 5 tons/day hydrogen, based on data for a similar process (the SI cycle). Based on Orhan's analysis [60], the cost of producing hydrogen using the four-step thermochemical Cu-Cl cycle is US$1.68 per kilogram. The energy efficiency of the cycle is not stated for this estimation. This analysis however does not include process flowsheet parameters and actual heat exchanger duties, shaft work, etc.

Ferrandon et al. [31] have performed an extensive cost analysis of a three-step thermochemical hydrogen production via the copper-chlorine cycle, using the H2A analysis tool. Using an Aspen Plus flowsheet for the cycle, a pinch analysis of the heat exchangers provided their logarithmic mean temperature differences. A 10^{o}C approach temperature is assumed for the cycle. Capcost, a software package developed by Turton et al. [61], was used to estimate equipment and installation costs. Capcost generates an equipment list with key design parameters, including costs. Based on a 125 tons/day production capacity and a 40.4% cycle efficiency, the estimated cost of hydrogen production using this cycle will be US$3.30 per kilogram hydrogen.

A comparison of these three hydrogen production processes (SMR, SI, and Cu-Cl) indicates that the cost of thermochemical hydrogen production with the Cu-Cl cycle is competitive with other known large scale production processes, especially with the four-step Cu-Cl process cycle. With ongoing research, especially on the electrolyzer of the three-step Cu-Cl cycle, the cost of hydrogen production is expected to be reduced considerably, in large part due to increases in the efficiency of the cycle. However the three-step Cu-Cl cycle, even at present hydrogen production costs, could be competitive with gasoline and other internal combustion engine fuel for transport applications. One kilogram of hydrogen has approximately the same energy content as 1 US gallon of gasoline. Fuel cells, which are a main intended application for hydrogen in transportation, have twice the efficiency of internal combustion engines [56]. With the present price of gasoline of over US$3.00 per gallon, it is anticipated that hydrogen production via the Cu-Cl cycle, if commercially developed, will be competitive with gasoline for transport applications.

CHAPTER 5

CONCLUSIONS

Thermochemical hydrogen production has not yet reached a commercial viability like steam methane reforming. However, it has a promising potential because it can eliminate greenhouse gas emissions and utilize waste heat from nuclear reactors. Eventually, the process may significantly reduce the costs of hydrogen production, compared to other methods.

This research has involved a thermochemical energy analysis and process simulations that investigated two process routes for thermochemical hydrogen production, using a copper-chlorine cycle. The thesis started with a detailed thermodynamic energy balance of different steps of the copper-chlorine cycle. The enthalpies and Gibbs free energies of these reactions indicated the feasibility of the process steps. All processes except the electrolysis process go to completion without the need for a catalyst.

Preliminary results from the energy balance, together with experimental results from ANL, provide a useful guide during the process simulation. A conceptual design and modelling of two process routes of the cycle were developed and process flow diagrams were produced for both routes. The heat source for the thermochemical processes could be provided by Supercritical Critical Water Reactors (SCWR). Results of physical properties of the cycle components, efficiencies, and sensitivity analysis results were obtained through process simulations. The results give a better understanding of the thermochemical properties of components of this cycle and their behavior within the

cycle operating conditions. Successful comparison between the experimental data from ANL and Aspen Plus simulations was achieved. The reported efficiencies for different process route are above 41% in all cases. Integration of this Cu-Cl cycle with next generation nuclear plants for co-generation of electricity, and hydrogen, or even co-generation of heat, electricity and hydrogen, will be highly efficient and potentially up to 50% efficient.

The results are encouraging and provide evidence of the advantages of the Cu-Cl cycle over other cycles. These results are also helpful in the scale-up endeavors. There are, however, some drawbacks that were noticed during the process simulation of the cycle. For the four-step cycle, there is an issue with solid transfer across the heat exchange due to entrainment. This does not pose problem during simulations, however, due to the Aspen Plus solid handling capability; but this issue is identified as a major issue for an actual plant. The shell and tube heat exchangers were eliminated, due to fouling by solids during transfer from one reactor to the other. There is also an additional challenge of obtaining copper metal from the electrochemical cell as fine powder to increase the reactive surface area and eliminate the formation of passive coatings that could inhibit the continuous reaction of copper and hydrochloric acid. This challenge must be overcome for a high yield of hydrogen. The three-step process route poses challenges in terms of material selection, and the design of the membranes for the separation of the gas. At present, no material has been conceived for the electrochemical cell that would withstand highly corrosive HCl at the high pressure required for hydrogen production. There is also no material identified for the membrane of the electrolyzer. The cycle efficiencies reported in this thesis do not include the separation processes. There is

also a challenge in keeping the voltage low with a high current density up to 500mA/cm^2. For the two process cycles, the sensitivity analysis of the hydrolysis has indicated a need for a large reservoir of water to maintain a high steam to copper ratio. This will add to the cost of the plant and additional space. There is also an issue of the competing reaction between $CuCl_2$ and a by-product chlorine gas, due to the presence of a common ion. The oxy-decomposition reaction kinetics are still under investigation, as the properties used for the simulations are obtained through estimation using an equimolar volume of copper(II)oxide and copper(II)chloride.

CHAPTER 6

RECOMMENDATIONS FOR FUTURE WORK

Several suggestions are made here for future research to improve the efficiency of the cycle. These recommendations will also help eliminate some uncertainties and the need for some assumptions, thereby providing better simulations and a more realistic plant layout for scale-up.

- Perform research in materials and equipment selection, especially heat exchangers and efficient drying methods using low temperature steam for the four-step cycle. The cycle gives a higher efficiency and the steps are less complex.
- There is a need to undertake a detailed pinch analysis of the heat exchangers to determine the best heat matching. This will provide a thorough understanding of the heat recovery system for the cycle.
- The oxy-decomposition step needs to be examined in more detail to determine the best reaction kinetics, including the characteristics of the products from the fluidized bed, and side reactions.
- The electrolyzer design of the three-step process cycle is the most challenging step in this cycle. There is a need to determine a low-cost material for the membrane of the electrolyzer, a good catalyst for the process and a way to reduce the energy requirement by lowering the cell potential.
- A process flowsheet for this cycle needs to be developed using more rigorous and realistic unit operations and thermodynamic models to reflect the actual plant. This will be most useful for obtaining results for a pilot plant.

- There is a need also to determine the best way to site the thermochemical hydrogen plant to effectively utilize heat from a nuclear power plant. The distance between these two plants is crucial and public safety must be taken into consideration.
- There is a need for more experiments on the individual process steps to validate the preliminary results and give better estimations of the thermodynamic properties of the cycle components.

REFERENCES

[1] Larsen, R., Wang, M., Santini, D., Mintz, M., Wu, Y., Vyas, A., "Might Canadian Oil Sands Promote Hydrogen Production Technologies for Transportation? Greenhouse Gas Emission Implication of Oil Sands Recovery and Upgrading", World Resource Review, Vol. 17, 2005, pp. 220-242.

[2] Petri, M.C., Yildiz, B., Klickman, A.E., "US Work on Technical and Economic Aspect Electrolytic, Thermochemical and Hybrid Processes for Hydrogen Production at Temperatures Below 550^{o}C", Int. Journal of Nuclear Production and Application, Vol. 1, 2006, pp. 79-91.

[3] Ivy, J., "Summary of Electrolytic Hydrogen Production", National Renewable Energy Laboratory Milestone Completion Report. Sept. 2004. Colorado, USA.

[4] Steinfeld, A., "Solar Thermochemical Production of Hydrogen", Solar Energy, Vol. 78, 2005, pp. 603-615.

[5] Tamaura, Y., Steinfeld, A., Kuhn, P., Ehrenberger, K., "Production of Solar Hydrogen by a Novel 2-step Water Splitting Thermochemical Cycle", Energy, Vol. 20, 1995, pp. 325-330.

[6] Abanades, S., Charvin, P., Flamant, G., Neveu, P., "Screening of Water-Splitting Thermochemical Cycle Potentially Attractive for Hydrogen Production by Concentrated Solar Energy", Energy, Vol. 31, 2006, pp. 2805-2822.

[7] Mathias, P.M., Brown, L.C., "Thermodynamics of Sulfur-Iodine Cycle for Thermochemical Hydrogen Production", presented at 68th Annual Meeting of Society of Chemical Engineers, 23 March 2003. Tokyo, Japan.

[8] Wu, X., Onuki, K., "Thermochemical Water Splitting for Hydrogen Production Utilizing Nuclear Heat from an HTGR", Tsinghua Science and Technology Journal, Vol. 10, 2005, pp. 270-276.

[9] Brown, L.C., Besenbruch, G.E., Funk, J.E., Marshall, A.C., Pickard, S.K., Showalter, S.K., "High Efficiency Generation of Hydrogen Fuel Using Nuclear Power", Final Technical report for the period Aug. 1, 1999 to Sept. 30, 2002. Sandia National laboratory, Livermore, USA.

[10] Ryland, D.K., Li, H., Sadhankar, R.R., "Electrolytic Hydrogen Generation using CANDU Nuclear Reactors", Proceedings of Second International Green Energy Conference, 25-29 June 2006, Oshawa, Ontario, Canada.

[11] Gooding, C.H., "Economic Analysis of Alternative Flowsheets for the Hybrid Chlorine Cycle", Proceedings of American Institute of Chemical Engineers (AICHE) meeting, 4-9 Nov. 2007, Salt Lake City, Utah, USA.

[12] Rosen, M.A., "Thermodynamic Analysis of Hydrogen Production by Thermochemical Water Decomposition using the Ispra Mark-10 Cycle", Hydrogen Energy Prog. VIII: Proceeding of 8th World Hydrogen Energy Conference, Toronto, 1990, pp. 701-710.

[13] Granovskii, M., Dincer, I., Rosen, M.A., Pioro, I., "Thermodynamic Analysis of the Use of a Chemical Heat Pump to Link a Supercritical Water-Cooled Nuclear Reactor and a Thermochemical Water Splitting Cycle for Hydrogen Production", Proc. 15th Int. Conf. on Nuclear Engineering, 22-26 April 2007, Nagoya, Japan, paper 10350, pp. 1-10.

[14] Rosen, M.A., Scott, D.S., "Comparative Efficiency Assessment for a Range of Hydrogen Production Processes", Int. Journal of Hydrogen Energy, Vol. 23, No. 8, 1998, pp. 653-659.

[15] Yildiz, B., Kazimi, M., "Efficiency of Hydrogen Production Systems using Alternative Nuclear Energy Technologies", Int. Journal of Hydrogen Energy, Vol. 31, 2006, pp. 77-92.

[16] Teo, E.D., Brandon, N.P., Vos, E., Kramer, G.J., "A Critical Pathway Energy Efficiency Analysis of Thermochemical UT-3 cycle", Int. Journal of Hydrogen Energy, Vol. 30, 2005, pp. 559-564.

[17] Sakurai, M., Bilgen, E., Tsutsunmi, A., Yoshida, K., "Adiabatic UT-3 Thermochemical Process for Hydrogen Production", Int. J. Hydrogen Energy, Vol. 21, 1996, pp. 865-870,

[18] Kameyama, H., Yoshida, K., "Br-Ca-Fe Water Decomposition Cycle for Hydrogen Production", Proceedings of 2nd World Hydrogen Energy Conference (WHEC), 1978, pp. 829-850, Zurich, Switzerland.

[19] Lewis, M.A., Masin, J.G., Vilim, R.B., "Development of the Low Temperature Cu-Cl Thermochemical Cycle", Proceedings of International Congress on Advances in Nuclear Power Plants (ICAPP '05), 15-19 May 2005, Seoul, Korea.

[20] Lewis, M.A., "Recent Advances in the Cu-Cl Cycle's Development at Argonne National Laboratory", Presentation at ORF Workshop, 28 May 2007, University of Ontario Institute of Technology, Oshawa, Ontario, Canada.

[21] Lewis, M.A., Masin, J., Taylor, A., "Evaluation of Alternative Thermochemical Cycle", Presentation at AICHE Annual Meeting, 12-17 November 2006, San Francisco, California, USA.

[22] Lewis, M.A., Serban, M., Basco, J.K., "Hydrogen Production at <550^{o}C Using a Low Temperature Thermochemical Cycle", ANS/ENS Exposition, November 2003. New Orleans, USA.

[23] Lewis, M.A., Serban, M., Basco, J.K., "Kinetic Study of the Hydrogen and Oxygen Production Reactions in the Copper-Chloride Thermo-chemical Cycle," Conference Proceedings of AIChE Spring National Meeting, pp. 2690-2698, 25-29 April 2004, New Orleans, USA.

[24] Lewis, M.A., "An Assessment of the Efficiency of the Hybrid Copper-Chloride Thermochemical Cycle", Conference Proceedings of AIChE annual meeting Oct. 30- Nov. 4, 2005. Cincinnati, Ohio, USA.

[25] Carty, R.H., Mazumder, M.M., Schreider, J.D., Panborn, J.B., "Thermochemical Hydrogen Production", Gas Research Institute for the Institute of Gas Technology, Vols. 1-4, 1981, GRI-80/0023. Chicago, Illinois, USA.

[26] Rosen, M.A., Naterer, G.F., Sadhankar, R., Suppiah, S., "Nuclear-Based Hydrogen Production with a Thermochemical Copper-Chlorine Cycle and Supercritical Water Reactor", Canadian Hydrogen Association Workshop, 19-20 October 2006, Quebec, Canada.

[27] Wang, Z., Gabriel, K., Naterer, G.F., "Heat Analysis of Cu-Cl Thermocycle", Presentation at ORF Workshop, 28 May 2007, University of Ontario Institute of Technology, Oshawa, Ontario, Canada.

[28] Chukwu, C.C., Naterer, G.F., Rosen, M.A., "Process Simulation of Nuclear-based Thermochemical Hydrogen Production with Copper-Chlorine Cycle", Proceedings of 32nd Canadian Nuclear Society Conference. 1-4 June 2008.

[29] Li, J., Suppiah, S., "Recent Advances in Nuclear Hydrogen Research Activities at AECL", Presentation at ORF Workshop, 28 May 2007, University of Ontario Institute of Technology, Oshawa, Ontario, Canada.

[30] Law, V.J., Prindle, J.C., Lupulescu, A., "ASPEN PLUS Modeling of the Three-Reaction Version of the Cu-Cl Thermochemical Cycle for Hydrogen Production from Water", Summer Report for Argonne National Laboratory, 31 August 2007, Tulane, New Orleans, USA.

[31] Ferrandon, M.S., Lewis, M.A., Tatterson, D.F., Nankani, R.V., Kumar, M., Wedgewood, L.E., Nitsche, L.C., "The Hybrid Cu-Cl Thermochemical Cycle: Conceptual Process Design and H2A Cost Analysis; Limiting the Formation of CuCl during Hydrolysis", 2008, ANL Quarterly report (1) Argonne, Illinois, USA.

[32] Baykara, S.Z., "Hydrogen Production by Direct Solar Thermal Decomposition of Water, Possibilities for Improvement of Process Efficiency", Int. Journal of Hydrogen Energy, Vol. 29, 2004, pp. 1451-1458.

[33] Abanades, S., Charvin, P., Flamant, G., Neveu, P., "Screening of Water-Splitting Thermochemical Cycle Potentially Attractive for Hydrogen Production by Concentrated Solar Energy", Energy, Vol. 31, 2006, pp. 2805-2822.

[34] Suppiah, S., Li, J., Deschenes, L., "Direct Electro-Thermal Decomposition of SO_3 in S-I Process for H_2 Production", Proceedings of Second International Green Energy Conference, 25-29 June 2006, Oshawa, Ontario, Canada.

[35] Steimke, J., Steeper, T., "Generation of Hydrogen using Electrolyzer with Sulfur Dioxide Depolarized Anode", Proceedings of American Institute of Chemical Engineers (AICHE) Meeting, 4-9 Nov. 2007, Salt Lake City, Utah, USA

[36] Aspen Plus User Guide, 2006.5, Aspentech Inc., Houston, USA.

[37] Babu, B.V., "Process Plant Simulation", Fourth Impression, Oxford University Press, New Delhi, 2007.

[38] Gubbins, K.E., "Equations of State - New Theories", Fluid Phase Equilibrium, Vol. 13, 1983, pp. 35-57.

[39] Soave, G., "Equilibrium Constants for Modified Redlich-Kwong Equation-of-state", Chemical Engineering Science, Vol. 27, 1972, pp. 1196-1203.

[40] Peng, D.Y., Robinson, D.B., "A New Two-Constant Equation of State Fundamentals", Industrial and Engineering Chemistry, Vol. 15, 1976, pp. 59-64.

[41] Ramesh, K., Aziz, N., Abd Shukor, S.R., Ramasamy, N., "Dynamic Rate-Based and Equilibrium Model Approaches for Continuous Tray Distillation Column", Journal of Applied Sciences Research, Vol. 3, 2007, pp. 2030-2041.

[42] Twu, C.H., Coon, J.E., Kusch, M.G., Harvey, A.H., "Selection of Equations of States Models for Process Simulator", Simulation Science Inc. Workbook Meeting, 24 July 1994, California, USA.

[43] Huron, M.J., Vidal, J., "New Mixing Rules in Simple Equations of State for Representing Vapor-liquid Equilibria of Strongly Non-ideal Mixtures", Fluid Phase Equilibrium, Vol. 3, 1979, pp. 255-271.

[44] Onken, U., Rarey-Nies, J., Gmehling, J., "The Dortmund Data Bank: A Computerized System for Retrieval, Correlation, and Prediction of Thermodynamic Properties of Mixtures", Int. Journal of Thermophysics, Vol. 10, 1989, pp. 739-747

[45] Renon, H. Prausnitz, J.M., "Local Compositions in Thermodynamic Excess Functions for Liquid Mixtures", AIChE Journal, Vol. 14, 1968, pp. 135-144.

[46] Rackett, H.G., "Equation of State for Saturated Liquids", Journal of Chemical and Engineering Data. Vol. 15, 1970, p. 514.

[47] Chen, C.C., Evans, L.B., "A Local Composition Model for the Excess Gibbs Energy of Aqueous Electrolyte Systems", AIChE Journal, Vol. 32, 1986, pp. 444-459.

[48] Mock, B., Evans, L.B., Chen, C.C., "Thermodynamic Representation of Phase Equilibria of Mixed-Solvent Electrolyte Systems", AIChE Journal, Vol. 32, 1986, pp. 1655-1664.

[49] Mathias, P.M., "Aspen Plus Model for Solubilities in the $CuCl_2$-CuCl-HCl-H_2O System", Argonne National Laboratory Report, 20 May 2007, Argonne, Illinois, USA.

[50] Masin, J., Lewis, M.A., "Development of the ANL Low Temperature Copper Chloride Process", Presentation of ANL, 15 Nov. 2006, Chicago, USA.

[51] Department of Chemistry, Moscow State University "Thermodynamic Properties of Compounds", http://www.chem.msu.su/rus/weldept.html#lib, accessed on 10 May 2008.

[52] Novikov, G.I., Voropaev, L.E., Rud'ko, P.K., Zharskii, I.M., "Thermodynamic Properties", Russian Journal of Inorganic Chemistry (English translation), Vol. 24, 1979, pp. 811-813.

[53] Rennels, R.A., "Kinetics of the Decomposition of Cu_2OCl_2 (Melanothallite): The High Temperature Step in the Copper Chloride Thermochemical Water Splitting Cycle", presentation at the Solar 2008 Conference, paper 0149, 3-8 May 2008, San Diego, California, USA.

[54] Kreith, F., "CRC Handbook of Thermal Engineering", CRC Press LLC, 2000, Florida, USA.

[55] USA Department of Energy (DOE), "Hydrogen Analysis" www.energy.gov/h2a_analysis.html USA Department of Energy (DOE), www.energy.gov/h2a_analysis.html

[56] Levene, J., "Hydrogen Technology Analysis: H2A Production". Presentation at AICHE Annual Meeting, 12-17 November 2006, San Francisco, California, USA.

[57] Williams, R.B., Kornbluth, K., Erickson, P.A., Jenkins, B.M., Gildart, M.C., "Estimates of Hydrogen Production Potential and Cost from California Landfill Gas", 15th European Biomass Conference and Exhibition, 7-13 May 2007, Berlin, Germany.

[58] Schultz, K.R., "Use of the Modular Helium Reactor for Hydrogen Production", World Nuclear Association Annual Symposium, 3-5 September 2003, London England.

[59] Brown, L.C., Besenbruch, G.E., Lentsch, R.D. Schultz, K.R., Funk, J.F., Pickard, P.S., Marshall, A.C., Showalter, S.K., "High Efficiency Generation of Hydrogen Fuel using Nuclear Power", Technical Report GA-A24285, General Atomics, San Diego, California, 2003.

[60] Orhan, M.F., "Energy, Exergy and Cost Analyses of Nuclear-Based Hydrogen Production via Thermochemical Water Decomposition using a Copper-Chlorine (Cu-Cl) Cycle", MASc Thesis, Faculty of Engineering and Applied Science, University of Ontario Institute of Technology, April 2008, Oshawa, Canada.

[61] Turton, R., Baillie, R.C., Whiting, W.B., Shaeiwitz, J.A., "Analysis, Synthesis and Design of Chemical Processes", 2nd Edition, Prentice Hall, Upper Saddle River, New Jersey, 2003.

APPENDIX

Summary of Process Flow Diagram Shown in Figure 15

This table describes the block identifications, names and functions of the key unit operations used in the simulation flowsheet shown in figure 15.

Block Identification	Block Name	Function
B84	Flash	Separate steam
B11	RStoic	Reactor that produces hydrogen
B12	Sep	Separates gases from liquids
B33	Flash	Separate hydrogen from other gases
B61	RStoic	Electrolyzer
B62	RStoic	Hydrolyzer
B53	Sep	Separation of hydrolysis products
B71	RStoic	Oxy-decomposition
B72	Sep	Separates gases from liquids
B73	Flash	Separate oxygen from other gases
B90	Mixer	Combine components
B91	RStoic	Represents the dryer
B92	Flash	Separates steam from components
B10, B34	Mixer	Combine components
B31, B32, B41, B42, B61A, B61B, B64A, B64B, B70, B83	Heater and Cooler	Respectively supplies and removes heat at various stages
B1, B2, B51,B54, B65	Pump	Increase the pressure of components at various states

Input Summary for Cycle Shown in Figure 15

The following depicts the input data used in simulation for cycle flowheet shown in figure 15.

```
;Input Summary created by Aspen Plus Rel. 21.0 at 10:35:32 Sun Jul 27, 2008
;Directory C:\Documents and Settings\100333501\Desktop\ASPEN1\Thesis Results

TITLE 'Preliminary simulation of CuCl cycle- Dec 4, 2007'

IN-UNITS MET PRESSURE=bar TEMPERATURE=C DELTA-T=C PDROP=bar

DEF-STREAMS MIXCISLD ALL
```

```
DATABANKS ASPENPCD / AQUEOUS / SOLIDS / INORGANIC / &
      PURE13

PROP-SOURCES ASPENPCD / AQUEOUS / SOLIDS / INORGANIC / &
      PURE13

COMPONENTS
   WATER H2O /
   HCL HCL /
   CUCL CUCL /
   CUCL2 CUCL2 /
   "CUCL2(S)" CUCL2 /
   "CUO(S)" CUO /
   "CUCL(SC)" CUCL /
   "CUCL(SB)" CUCL /
   "CU(S)" CU /
   CU2OCL2S CU2OCL2 /
   H2 H2 /
   O2 O2 /
   CL2 CL2 /
   AR AR /
   H3O+ H3O+ /
   CL- CL- /
   CU++ CU+2

HENRY-COMPS GLOBAL H2 O2



FLOWSHEET
   BLOCK B33 IN=35 OUT=40 36
   BLOCK B92 IN=93 OUT=94 95
   BLOCK B41 IN=40 OUT=42 41
   BLOCK B90 IN=89 50 47 2 OUT=91
   BLOCK B83 IN=21 OUT=87 86
   BLOCK B84 IN=87 OUT=88 89
   BLOCK B71 IN=72 OUT=74
   BLOCK B70 IN=70 OUT=72 71
   BLOCK B73 IN=76 OUT=77 78
   BLOCK B62 IN=63 OUT=64
   BLOCK B51 IN=36 OUT=54 53
   BLOCK B31 IN=31 OUT=33 32
   BLOCK B12 IN=15 OUT=31 21
   BLOCK B11 IN=13 OUT=15
   BLOCK B10 IN=11 OUT=13
```

```
   BLOCK B72 IN=74 OUT=76 75
   BLOCK B91 IN=91 OUT=93 92
   BLOCK HCL IN=HCL-I OUT=HCL-O
   BLOCK O2 IN=O2-I OUT=O2-O
   BLOCK H2 IN=H2-I OUT=H2-O
   BLOCK B61 IN=61 OUT=63H 62
   BLOCK B62A IN=63B OUT=64A
   BLOCK B71A IN=72A OUT=74A
   BLOCK B62F IN=64A OUT=64V 64L
   BLOCK B32 IN=33 OUT=35 34
   BLOCK B42 IN=42 OUT=44 43
   BLOCK B34 IN=12 54 OUT=61
   BLOCK B65 IN=78 OUT=50 39
   BLOCK CUCL2-SO IN=CUCL2 CUCL2-SO OUT=CUCL2-L
   BLOCK 63M IN=63A OUT=63B
   BLOCK CUCL-AB IN=CUCL-0 OUT=CUCL-1
   BLOCK B54 IN=58 OUT=70
   BLOCK B53 IN=64 OUT=58 57
   BLOCK B61A IN=63H OUT=63I 63X
   BLOCK B61B IN=63I OUT=63 63Y
   BLOCK B64A IN=57 OUT=57A 57X
   BLOCK B64B IN=57A OUT=57B 57Y
   BLOCK B1 IN=44 OUT=2 45
   BLOCK B2 IN=57B OUT=47


STREAM 11
    IN-UNITS SI
   SUBSTREAM MIXED TEMP=25. <C> PRES=350. <psig>
   MOLE-FLOW WATER 10000.8 <kmol/hr> / HCL 800. <kmol/hr>
   SUBSTREAM CISOLID TEMP=25. <C> PRES=350. <psig>  &
      MOLE-FLOW=200. <kmol/hr>
   MOLE-FRAC "CUCL(SC)" 1.

STREAM 12
   IN-UNITS SI
   SUBSTREAM MIXED TEMP=25. <C> PRES=15. <psig>
   MOLE-FLOW WATER 100.2 <kmol/hr>

STREAM 63A
   IN-UNITS MET
   SUBSTREAM MIXED TEMP=420. <C> PRES=2.37 <bar>
   MOLE-FLOW WATER 1822. / HCL 65.
   SUBSTREAM CISOLID TEMP=510. <C> PRES=2.37 <bar>
   MOLE-FLOW "CUCL2(S)" 100.
```

```
STREAM 64
   IN-UNITS MET
   SUBSTREAM CISOLID TEMP=230. <C> PRES=35. MOLE-FLOW=49.99
   MOLE-FRAC "CUCL2(S)" 1. / "CUCL(SC)" 0. / "CU(S)" 0.

STREAM 72A
   IN-UNITS MET
   SUBSTREAM MIXED TEMP=550. <K> PRES=3.36 <bar>
   MOLE-FLOW WATER 47.4 / HCL 9.2
   SUBSTREAM CISOLID TEMP=550. <C> PRES=3.36 <bar>
   MOLE-FLOW CU2OCL2S 50.

STREAM CUCL-0
   SUBSTREAM MIXED TEMP=300. PRES=1.
   MOLE-FLOW CUCL 1.

STREAM CUCL2
   SUBSTREAM CISOLID TEMP=25. PRES=1.
   MOLE-FLOW "CUCL2(S)" 1.

STREAM CUCL2-SO
   SUBSTREAM MIXED TEMP=25. PRES=1.
   MASS-FLOW WATER 1000.

STREAM H2-I
   IN-UNITS MET
   SUBSTREAM MIXED TEMP=25. <C> PRES=1.
   MOLE-FLOW HCL 2.
   SUBSTREAM CISOLID TEMP=25. <C> PRES=1.
   MOLE-FLOW "CU(S)" 2.

STREAM HCL-I
   IN-UNITS MET
   SUBSTREAM MIXED TEMP=25. <C> PRES=1E-006
   MOLE-FLOW WATER 1.
   SUBSTREAM CISOLID TEMP=25. <C> PRES=1E-006
   MOLE-FLOW "CUCL2(S)" 1.

STREAM O2-I
   IN-UNITS MET
   SUBSTREAM MIXED TEMP=25. <C> PRES=1. MOLE-FLOW=1E-006
   MOLE-FRAC O2 1.
   SUBSTREAM CISOLID TEMP=25. <C> PRES=1.
   MOLE-FLOW "CUCL2(S)" 1. / "CUO(S)" 1.
```

```
BLOCK B10 MIXER
   IN-UNITS SI
   PARAM PRES=350. <psig> MAXIT=45 TOL=0.001 T-EST=25. <C>

BLOCK B34 MIXER
   PARAM PRES=0. <psia>

BLOCK B90 MIXER
   IN-UNITS MET
   PARAM PRES=25. <bar>

BLOCK B12 SEP
   IN-UNITS SI
   PARAM PRES=350. <psig>
   FRAC STREAM=31 SUBSTREAM=MIXED COMPS=WATER HCL CUCL  &
      CUCL2 "CUCL2(S)" "CUO(S)" "CUCL(SC)" "CUCL(SB)" "CU(S)"  &
      CU2OCL2S H2 H3O+ CL- CU++ FRACS=0.5 0.5 1. 1. 1.  &
      1. 1. 1. 1. 1. 0. 0.5 0.5 0.5
   FRAC STREAM=31 SUBSTREAM=CISOLID COMPS="CUCL2(S)"  &
      "CUCL(SC)" "CU(S)" FRACS=0. 0. 0.

BLOCK B53 SEP
   PARAM
   FRAC STREAM=58 SUBSTREAM=MIXED COMPS=WATER HCL CUCL  &
      CUCL2 "CUCL2(S)" "CUO(S)" "CUCL(SC)" "CUCL(SB)" "CU(S)"  &
      CU2OCL2S H2 O2 CL2 AR H3O+ FRACS=0. 0. 0. 0. 0.  &
      0. 0. 0. 0. 0. 0. 0. 0. 0. 0.
   FRAC STREAM=58 SUBSTREAM=CISOLID COMPS="CUCL2(S)" "CUO(S)"  &
      "CUCL(SC)" "CUCL(SB)" "CU(S)" CU2OCL2S FRACS=1. 1. 1.  &
      1. 1. 1.

BLOCK B31 HEATER
   IN-UNITS SI
   PARAM TEMP=100. <C> PRES=20. <psia>

BLOCK B32 HEATER
   PARAM PRES=0. <psia> VFRAC=0.35

BLOCK B41 HEATER
   IN-UNITS MET
   PARAM PRES=-5. <psia> VFRAC=0. NPHASE=2 T-EST=137. <C>
   PROPERTIES ELECNRTL HENRY-COMPS=GLOBAL CHEMISTRY=HCL  &
      TRUE-COMPS=NO
   BLOCK-OPTION FREE-WATER=NO

BLOCK B42 HEATER
```

```
   PARAM TEMP=25. PRES=-5. <psia>

BLOCK B61A HEATER
   PARAM PRES=-0.001 VFRAC=1.

BLOCK B61B HEATER
   PARAM TEMP=425. PRES=-0.001

BLOCK B64A HEATER
   PARAM PRES=0. VFRAC=1.

BLOCK B64B HEATER
   PARAM PRES=0. VFRAC=0.3

BLOCK B70 HEATER
   IN-UNITS MET
   PARAM TEMP=550. <C> PRES=-10. <psia>

BLOCK B83 HEATER
   IN-UNITS MET
   PARAM TEMP=25. <C> PRES=-5. <psia>

BLOCK B33 FLASH2
   IN-UNITS MET
   PARAM PRES=0. DUTY=0.

BLOCK B62F FLASH2
   PARAM PRES=0. DUTY=0. NPHASE=2
   PROPERTIES NRTL-RK HENRY-COMPS=GLOBAL
   BLOCK-OPTION FREE-WATER=NO

BLOCK B73 FLASH2
   IN-UNITS MET
   PARAM PRES=0. DUTY=0. NPHASE=2
   BLOCK-OPTION FREE-WATER=NO

BLOCK B84 FLASH2
   IN-UNITS MET
   PARAM PRES=-5. <psia> DUTY=0.

BLOCK B92 FLASH2
   IN-UNITS MET
   PARAM PRES=25. DUTY=0.

BLOCK B11 RSTOIC
   IN-UNITS SI
```

```
   PARAM TEMP=25. <C> PRES=0. <psig> HEAT-OF-REAC=NO
   STOIC 1 CISOLID "CUCL(SC)" -2. / MIXED H3O+ -2. / CL-  &
      -2. / "CUCL2(S)" 2. / H2 1. / WATER 2.
   CONV 1 CISOLID "CUCL(SC)" 1.
   REPORT COMPBAL

BLOCK B61 RSTOIC
   IN-UNITS MET
   PARAM TEMP=90. <C> PRES=-5. <psia>
   STOIC 1 MIXED CU++ -1. / CL- -2. / CISOLID "CUCL2(S)"  &
      1.
   CONV 1 MIXED CU++ 1.

BLOCK B62 RSTOIC
   IN-UNITS SI
   PARAM TEMP=400. <C> PRES=0.5 <atm> MAXIT=200
   STOIC 1 MIXED "CUCL2(S)" -1. / WATER -0.5 / CISOLID  &
      CU2OCL2S 0.5 / MIXED HCL 1.
   CONV 1 MIXED "CUCL2(S)" 1.

BLOCK B71 RSTOIC
   IN-UNITS MET
   PARAM TEMP=550. <C> PRES=-10. <psia> MAXIT=40
   STOIC 1 CISOLID CU2OCL2S -1. / MIXED CUCL 2. / O2 0.5
   CONV 1 CISOLID CU2OCL2S 1.
   BLOCK-OPTION PROP-LEVEL=4

BLOCK B72 RSTOIC
   IN-UNITS MET
   PARAM TEMP=25. <C> PRES=-10. <psia>
   STOIC 1 MIXED CUCL -1. / CISOLID "CUCL(SC)" 1.
   CONV 1 MIXED CUCL 1.

BLOCK B91 RSTOIC
   IN-UNITS MET
   PARAM TEMP=25. <C> PRES=-5. <psia>
   STOIC 1 MIXED CUCL -1. / CISOLID "CUCL(SC)" 1.
   CONV 1 MIXED CUCL 1.


BLOCK B71A RGIBBS
   IN-UNITS MET
   PARAM TEMP=550. <C> PRES=-10. <psia> NPHASE=2
   PROD CL2 M / CUCL / O2 / WATER / HCL

BLOCK CUCL-AB RGIBBS
```

```
   PARAM TEMP=700. <K> PRES=1. NPHASE=1 VAPOR=NO
   PROD CUCL / "CUCL(SC)" SS / "CUCL(SB)" SS

BLOCK B1 PUMP
   PARAM PRES=350. <psig>

BLOCK B2 PUMP
   PARAM PRES=350. <psig>

BLOCK B51 PUMP
   IN-UNITS SI
   PARAM PRES=1.3 <bar> EFF=0.8 DEFF=0.95

BLOCK B54 PUMP
   PARAM PRES=4.5

BLOCK B65 PUMP
   PARAM PRES=350. <psig>
```

Summary of Process Flow Diagram Shown in Figure 16

The following table describes the block identifications, names and functions of the key unit operations used in the simulation of the flowsheet shown in figure 16.

Block Identification	Block Name	Function
B1	Rstoic	Electrolyzer
B2	Sep	Separates gases from liquids
B3	Sep	Separates hydrogen from products
B4, B7, B19, B20, B25, B27, B28, B30	Heater and Cooler	Respectively supplies and removes heat at various stages
B5	Sep	Separates liquids from solids
B6	FSplit	Splits components into streams
B8	Mixer	Combine components
B10	Rstoic	Oxy-decomposition
B11	Sep	Separates oxygen from products
B12	Mixer	Combine CuCl2
B13	Rstoic	Represents the dryer
B14	Flash	Separates steam from components
B15	Mixer	Combine components
B16	Valve	Control the volume of components
B18	Mixer	Combine components
B21	Flash	Separates steam from components
B22	Rstoic	Hydrolyzer
B23	Sep	Separates hydrolysis products
B26	Compr	Isentropic compressor that supplies work
B29	Pump	Increase the pressure of components at various states

Input Summary for Cycle Shown in Figure 16

The following depicts the input data used in simulation for cycle flowsheet shown in figure 16.

```
;Input Summary created by Aspen Plus Rel. 21.0 at 11:54:32 Sun Jul 27, 2008
;Directory C:\Documents and Settings\100333501\Desktop\ASPEN1\Thesis Results


TITLE 'Aspen Plus Simulation of CuCl cycle - March 8, 2008'

IN-UNITS MET PRESSURE=bar TEMPERATURE=C DELTA-T=C PDROP=bar

DEF-STREAMS MIXCISLD ALL

DATABANKS PURE20  / ASPENPCD  / AQUEOUS  / SOLIDS  /  &
      INORGANIC  / PURE13

PROP-SOURCES PURE20  / ASPENPCD  / AQUEOUS  / SOLIDS  /  &
      INORGANIC  / PURE13

COMPONENTS
   WATER H2O /
   HCL HCL /
   CUCL CUCL /
   CUCL2 CUCL2 /
   "CUCL2(S)" CUCL2 /
   "CUO(S)" CUO /
   "CUCL(SC)" CUCL /
   "CUCL(SB)" CUCL /
   "CU(S)" CU /
   CU2OCL2S CU2OCL2 /
   "CUCL2.2W" "CUCL2*2W" /
   H2 H2 /
   O2 O2 /
   CL2 CL2 /
   AR AR /
   H3O+ H3O+ /
   CL- CL- /
   CU++ CU+2 /
   CUCL2- CUCL2- /
   CUCL3-- CUCL3-2 /
   CUCL+ CUCL+
```

```
HENRY-COMPS GLOBAL H2 O2 CL2 AR


FLOWSHEET
   BLOCK B35 IN=64 65 OUT=66 72
   BLOCK B36 IN=66 OUT=67 68
   BLOCK B37 IN=68 OUT=69 73
   BLOCK B38 IN=69 OUT=70 71
   BLOCK B40 IN=74 76 77 79 OUT=78
   BLOCK B9 IN=78 OUT=55
   BLOCK B33 IN=55 OUT=61
   BLOCK B24 IN=52 OUT=74
   BLOCK B1 IN=1 21 OUT=2
   BLOCK B2 IN=2 OUT=4 5
   BLOCK B3 IN=4 OUT=6 H2
   BLOCK B4 IN=5 OUT=8
   BLOCK B5 IN=8 OUT=9 10
   BLOCK B6 IN=10 OUT=11 12
   BLOCK B12 IN=9 11 OUT=14
   BLOCK B13 IN=13 OUT=15 19
   BLOCK B14 IN=15 OUT=16 17 18
   BLOCK B17 IN=6 OUT=23 24
   BLOCK B19 IN=25 30 OUT=26 28
   BLOCK B20 IN=26 OUT=27 29
   BLOCK B21 IN=24 OUT=30 25
   BLOCK B22 IN=16 17 27 OUT=31 3
   BLOCK B23 IN=31 OUT=32 33
   BLOCK B26 IN=32 OUT=36 49
   BLOCK B27 IN=36 OUT=37 45
   BLOCK B28 IN=37 OUT=38 46
   BLOCK B29 IN=7 OUT=21 48
   BLOCK B7 IN=33 OUT=22 39
   BLOCK B10 IN=22 OUT=34 44
   BLOCK B11 IN=34 OUT=35 O2
   BLOCK B15 IN=12 35 42 20 OUT=43
   BLOCK B16 IN=23 OUT=41
   BLOCK B18 IN=40 41 OUT=42
   BLOCK B25 IN=38 OUT=47 51
   BLOCK B30 IN=14 OUT=13
   BLOCK B34 IN=71 OUT=50 52
   BLOCK B39 IN=70 50 OUT=53
   BLOCK B8 IN=47 OUT=7 40

STREAM 1
   SUBSTREAM MIXED TEMP=105. PRES=24.
```

```
   MOLE-FLOW WATER 390. / HCL 42. / CUCL2 18.
   SUBSTREAM CISOLID TEMP=110. PRES=24.
   MOLE-FLOW "CUCL(SC)" 100.

STREAM 14
   SUBSTREAM MIXED TEMP=30 PRES=1
   MOLE-FLOW WATER 208.611644 / HCL 1.8338004 / H3O+  &
      0.267312845 / CL- 101.167313 / CUCL+ 100.9

STREAM 20
   SUBSTREAM MIXED TEMP=25. PRES=1.
   MOLE-FLOW WATER 50.

STREAM 64
   SUBSTREAM MIXED TEMP=105. PRES=24.
   MOLE-FLOW WATER 392. / HCL 42. / CUCL 20. / CUCL2 18.

STREAM 65
   SUBSTREAM MIXED TEMP=105. PRES=24.
   MOLE-FLOW WATER 240. / HCL 20.

STREAM 76
   SUBSTREAM MIXED TEMP=100. PRES=1.
   MOLE-FLOW WATER 30.

STREAM 77
   SUBSTREAM MIXED TEMP=25. PRES=1.
   MOLE-FLOW WATER 10.

STREAM 79
   SUBSTREAM MIXED TEMP=550. PRES=1.
   MOLE-FLOW CUCL 20.

BLOCK B6 FSPLIT
   FRAC 11 0.05

BLOCK B8 FSPLIT
   MOLE-FLOW 7 100. 1
   DEF-KEY KEYNO=1 SUBSTREAM=MIXED COMPS=CL-

BLOCK B17 FSPLIT
   MOLE-FLOW 23 139.2125984

BLOCK B34 FSPLIT
   FRAC 50 0.01
   PROPERTIES ELECNRTL CHEMISTRY=FULL
```

```
BLOCK B2 SEP
   PARAM
   MOLE-FLOW STREAM=4 SUBSTREAM=MIXED COMPS=WATER FLOWS= &
      1300.
   FRAC STREAM=4 SUBSTREAM=MIXED COMPS=HCL CUCL CUCL2  &
      "CUCL2(S)" "CUO(S)" "CUCL(SC)" "CUCL(SB)" "CU(S)"  &
      CU2OCL2S "CUCL2.2W" H2 O2 CL2 AR H3O+ CL- CU++  &
      CUCL2- CUCL+ FRACS=0. 0. 0. 0. 0. 0. 0. 0. 0. 0.  &
      1. 0. 0. 0. 0. 0. 0. 0. 0.
   FRAC STREAM=4 SUBSTREAM=CISOLID COMPS="CUCL2(S)" "CUO(S)"  &
      "CUCL(SC)" "CUCL(SB)" "CU(S)" CU2OCL2S "CUCL2.2W" FRACS= &
      0. 0. 0. 0. 0. 0. 0.
   PROPERTIES ELECNRTL CHEMISTRY=FULL

BLOCK B3 SEP
   PARAM
   FRAC STREAM=H2 SUBSTREAM=MIXED COMPS=WATER H2 FRACS=0.  &
      1.
   FRAC STREAM=H2 SUBSTREAM=CISOLID COMPS="CUCL2(S)" "CUO(S)"  &
      "CUCL(SC)" "CUCL(SB)" "CU(S)" CU2OCL2S "CUCL2.2W" FRACS= &
      0. 0. 0. 0. 0. 0. 0.

BLOCK B5 SEP
   PARAM
   FRAC STREAM=9 SUBSTREAM=MIXED COMPS=WATER HCL CUCL CUCL2
&
      "CUCL2(S)" "CUO(S)" "CUCL(SC)" "CUCL(SB)" "CU(S)"  &
      CU2OCL2S H2 O2 CL2 AR H3O+ CL- CU++ CUCL2- CUCL3--  &
      CUCL+ FRACS=0. 0. 0. 0. 0. 0. 0. 0. 0. 0. 0. 0.  &
      0. 0. 0. 0. 0. 0. 0. 0.
   MOLE-FLOW     STREAM=9     SUBSTREAM=MIXED     COMPS="CUCL2.2W"
FLOWS= &
      100.
   FRAC STREAM=9 SUBSTREAM=CISOLID COMPS="CUCL2(S)" "CUO(S)"  &
      "CUCL(SC)" "CUCL(SB)" "CU(S)" CU2OCL2S "CUCL2.2W" FRACS= &
      0. 0. 0. 0. 0. 0. 0.

BLOCK B11 SEP
   PARAM
   FRAC STREAM=O2 SUBSTREAM=MIXED COMPS=WATER HCL CUCL  &
      CUCL2 "CUCL2(S)" "CUO(S)" "CUCL(SC)" "CUCL(SB)" "CU(S)"  &
      CU2OCL2S "CUCL2.2W" H2 O2 CL2 AR H3O+ CL- CU++  &
      CUCL2- CUCL3-- CUCL+ FRACS=0. 0. 0. 0. 0. 0. 0. 0.  &
      0. 0. 0. 0. 1. 0. 0. 0. 0. 0. 0. 0. 0.
   FRAC STREAM=O2 SUBSTREAM=CISOLID COMPS="CUCL2(S)" "CUO(S)"  &
```

```
      "CUCL(SC)" "CUCL(SB)" "CU(S)" CU2OCL2S "CUCL2.2W" FRACS= &
      0. 0. 0. 0. 0. 0. 0.

BLOCK B23 SEP
   PARAM
   FRAC STREAM=33 SUBSTREAM=MIXED COMPS=WATER HCL CUCL  &
      CUCL2 "CUCL2(S)" "CUO(S)" "CUCL(SC)" "CUCL(SB)" "CU(S)"  &
      CU2OCL2S "CUCL2.2W" H2 O2 CL2 AR H3O+ CL- CU++  &
      CUCL2- CUCL3-- CUCL+ FRACS=0. 0. 0. 0. 0. 0. 0. 0.  &
      0. 0. 0. 0. 0. 0. 0. 0. 0. 0. 0. 0. 0.
   FRAC  STREAM=33  SUBSTREAM=CISOLID  COMPS="CUCL2(S)"  CU2OCL2S
&
      FRACS=1. 1.

BLOCK B36 SEP
   PARAM
   MOLE-FLOW STREAM=67 SUBSTREAM=MIXED COMPS=WATER FLOWS= &
      150.
   FRAC STREAM=67 SUBSTREAM=MIXED COMPS=HCL CUCL CUCL2  &
      "CUCL2(S)" "CUO(S)" "CUCL(SC)" "CUCL(SB)" "CU(S)"  &
      CU2OCL2S "CUCL2.2W" H2 O2 CL2 AR H3O+ CL- CU++  &
      CUCL2- CUCL3-- CUCL+ FRACS=0. 0. 0. 0. 0. 0. 0. 0.  &
      0. 0. 1. 0. 0. 0. 0. 0. 0. 0. 0. 0.
   FRAC STREAM=67 SUBSTREAM=CISOLID COMPS="CUCL2(S)" "CUO(S)"  &
      "CUCL(SC)" "CUCL(SB)" "CU(S)" CU2OCL2S "CUCL2.2W" FRACS= &
      0. 0. 0. 0. 0. 0. 0.
   PROPERTIES ELECNRTL CHEMISTRY=FULL

BLOCK B38 SEP
   PARAM
   FRAC STREAM=70 SUBSTREAM=MIXED COMPS=WATER HCL CUCL  &
      CUCL2 "CUCL2(S)" "CUO(S)" "CUCL(SC)" "CUCL(SB)" "CU(S)"  &
      CU2OCL2S "CUCL2.2W" H2 O2 CL2 AR H3O+ CL- CU++  &
      CUCL2- CUCL3-- CUCL+ FRACS=0. 0. 0. 0. 0. 0. 0. 0.  &
      0. 0. 1. 0. 0. 0. 0. 0. 0. 0. 0. 0.
   FRAC STREAM=70 SUBSTREAM=CISOLID COMPS="CUCL2(S)" "CUO(S)"  &
      "CUCL(SC)" "CUCL(SB)" "CU(S)" CU2OCL2S "CUCL2.2W" FRACS= &
      0. 0. 0. 0. 0. 0. 0.
   PROPERTIES ELECNRTL CHEMISTRY=FULL

BLOCK B4 HEATER
   PARAM TEMP=21.5 PRES=-5. <psia>
   PROPERTIES ELECNRTL CHEMISTRY=FULL

BLOCK B7 HEATER
   PARAM TEMP=540. PRES=0.
```

```
BLOCK B9 HEATER
   PARAM TEMP=100. PRES=0.

BLOCK B19 HEATER
   PARAM PRES=1. VFRAC=1.

BLOCK B20 HEATER
   PARAM TEMP=400. PRES=0.

BLOCK B25 HEATER
   PARAM TEMP=105. PRES=0.

BLOCK B27 HEATER
   PARAM TEMP=116. PRES=-5. <psia>

BLOCK B28 HEATER
   PARAM PRES=0. VFRAC=0.

BLOCK B30 HEATER
   PARAM TEMP=400. PRES=-5. <psia>
   PROPERTIES ELECNRTL CHEMISTRY=FULL

BLOCK B37 HEATER
   PARAM TEMP=22. PRES=-5. <psia>
   PROPERTIES ELECNRTL CHEMISTRY=FULL

BLOCK B14 FLASH2
   PARAM TEMP=400. PRES=1.

BLOCK B21 FLASH2
   PARAM PRES=1. DUTY=0.

BLOCK B1 RSTOIC
   PARAM TEMP=105. PRES=-5. <psia>
   STOIC 1 CISOLID "CUCL(SC)" -1. / MIXED H3O+ -1. / WATER  &
      -1. / CL- -1. / "CUCL2.2W" 1. / H2 0.5
   CONV 1 CISOLID "CUCL(SC)" 1.
   PROPERTIES ELECNRTL HENRY-COMPS=GLOBAL CHEMISTRY=FULL

BLOCK B10 RSTOIC
   PARAM TEMP=540. PRES=1.
   STOIC 1 CISOLID CU2OCL2S -1. / MIXED CUCL 2. / O2 0.5
   CONV 1 CISOLID CU2OCL2S 1.
   PROPERTIES NRTL HENRY-COMPS=GLOBAL CHEMISTRY=HCL  &
      FREE-WATER=STEAM-TA SOLU-WATER=3 TRUE-COMPS=YES
```

```
BLOCK B12 RSTOIC
   PARAM TEMP=30. PRES=1. NPHASE=1 PHASE=L
   STOIC 1 MIXED "CUCL2.2W" -1. / CUCL+ 1. / CL- 1. /  &
      WATER 2.
   CONV 1 MIXED "CUCL2.2W" 1.
   PROPERTIES  ELECNRTL  HENRY-COMPS=GLOBAL  CHEMISTRY=CUCL2W
&
      FREE-WATER=STEAM-TA SOLU-WATER=3 TRUE-COMPS=YES
   BLOCK-OPTION FREE-WATER=NO

BLOCK B13 RSTOIC
   PARAM TEMP=400. PRES=0.
   STOIC 1 MIXED CUCL+ -1. / CL- -1. / CISOLID "CUCL2(S)"  &
      1.
   CONV 1 MIXED CUCL+ 1.

BLOCK B22 RSTOIC
   PARAM TEMP=400. PRES=1.
   STOIC 1 CISOLID "CUCL2(S)" -2. / MIXED WATER -1. /  &
      CISOLID CU2OCL2S 1. / MIXED HCL 2.
   CONV 1 CISOLID "CUCL2(S)" 0.995024876

BLOCK B35 RSTOIC
   PARAM TEMP=105. PRES=-5. <psia>
   STOIC 1 MIXED CUCL2- -1. / H3O+ -1. / WATER 1. /  &
      CUCL+ 1. / CL- 1. / H2 0.5
   CONV 1 MIXED CUCL2- 1.
   PROPERTIES ELECNRTL HENRY-COMPS=GLOBAL CHEMISTRY=FULL

BLOCK B29 PUMP
   PARAM PRES=24.

BLOCK B33 PUMP
   PARAM PRES=24.

BLOCK B26 COMPR
   PARAM TYPE=ISENTROPIC PRES=1.5
   PERFOR-PARAM CALC-SPEED=NO

BLOCK B16 VALVE
   PARAM P-OUT=1.

BLOCK B24 VALVE
   PARAM P-OUT=1.
```